

Spring 2009

# Single-walled carbon nanotube device fabrication using spin coating of dispersions

Paul Jeremy Hummel  
*Louisiana Tech University*

Follow this and additional works at: <https://digitalcommons.latech.edu/dissertations>



Part of the [Electrical and Computer Engineering Commons](#)

---

## Recommended Citation

Hummel, Paul Jeremy, "" (2009). *Dissertation*. 482.  
<https://digitalcommons.latech.edu/dissertations/482>

This Dissertation is brought to you for free and open access by the Graduate School at Louisiana Tech Digital Commons. It has been accepted for inclusion in Doctoral Dissertations by an authorized administrator of Louisiana Tech Digital Commons. For more information, please contact [digitalcommons@latech.edu](mailto:digitalcommons@latech.edu).

**SINGLE-WALLED CARBON NANOTUBE DEVICE  
FABRICATION USING SPIN COATING  
OF DISPERSIONS**

by

Paul Jeremy Hummel, B.S.

A Dissertation Presented in Partial Fulfillment  
Of the Requirements for the Degree  
Doctor of Philosophy

COLLEGE OF ENGINEERING AND SCIENCE  
LOUISIANA TECH UNIVERSITY

May 2009

UMI Number: 3358252

### INFORMATION TO USERS

The quality of this reproduction is dependent upon the quality of the copy submitted. Broken or indistinct print, colored or poor quality illustrations and photographs, print bleed-through, substandard margins, and improper alignment can adversely affect reproduction.

In the unlikely event that the author did not send a complete manuscript and there are missing pages, these will be noted. Also, if unauthorized copyright material had to be removed, a note will indicate the deletion.

UMI<sup>®</sup>

---

UMI Microform 3358252  
Copyright 2009 by ProQuest LLC  
All rights reserved. This microform edition is protected against  
unauthorized copying under Title 17, United States Code.

---

ProQuest LLC  
789 East Eisenhower Parkway  
P.O. Box 1346  
Ann Arbor, MI 48106-1346

LOUISIANA TECH UNIVERSITY

THE GRADUATE SCHOOL

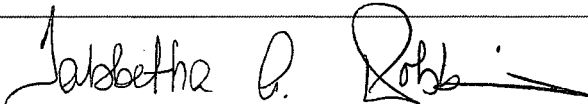
April 21, 2009

Date

We hereby recommend that the dissertation prepared under our supervision  
by Paul Jeremy Hummel

entitled Single-walled Carbon Nanotube Device Fabrication using Spin Coating  
Dispersions

be accepted in partial fulfillment of the requirements for the Degree of  
Doctor of Philosophy

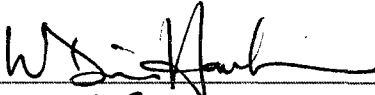
  
\_\_\_\_\_  
Supervisor of Dissertation Research

  
\_\_\_\_\_  
Head of Department  
College of Engineering and Science  
Department

Recommendation concurred in:

  
\_\_\_\_\_

  
\_\_\_\_\_

  
\_\_\_\_\_

  
\_\_\_\_\_

Advisory Committee

Approved:  
  
\_\_\_\_\_  
Director of Graduate Studies

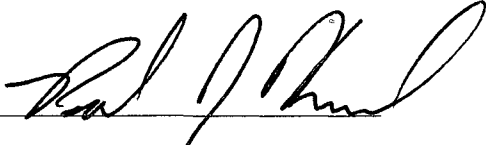
Approved:  
  
\_\_\_\_\_  
Dean of the Graduate School

  
\_\_\_\_\_  
Dean of the College

## APPROVAL FOR SCHOLARLY DISSEMINATION

The author grants to the Prescott Memorial Library of Louisiana Tech University the right to reproduce, by appropriate methods, upon request, any or all portions of this Dissertation. It is understood that "proper request" consists of the agreement, on the part of the requesting party, that said reproduction is for his personal use and that subsequent reproduction will not occur without written approval of the author of this Dissertation. Further, any portions of the Dissertation used in books, papers, and other works must be appropriately referenced to this Dissertation.

Finally, the author of this Dissertation reserves the right to publish freely, in the literature, at any time, any or all portions of this Dissertation.

Author   
Date 5/6/2009

## ABSTRACT

This research looks at ways to utilize already synthesized carbon nanotubes (CNT) to manufacture electrical connections using current tools and fabrication methods employed in the semiconductor industry. Purchased single-walled carbon nanotubes (SWNT) are separated and placed in suspension using poly(sodium styrene sulfonate) (PSS). The PSS non-covalently bonds to the SWNTs, causing them to repel each other due to the negative charge of the PSS. The suspension of SWNTs is spin coated over a processed silicon (Si) wafer with fabricated trenches. A Si wafer with a top silicon dioxide ( $\text{SiO}_2$ ) layer is spin coated with Shipley 1827 photoresist. UV light is used to expose areas to the photoresist, creating trench areas. After removal of the exposed areas of the photoresist, trenches are etched into the  $\text{SiO}_2$  layer with a buffered oxide etch (BOE) solution of hydrofluoric acid. The suspension of SWNTs is spin coated over the processed Si wafer. The wafer is placed on a hot plate at  $115^\circ\text{C}$  to slowly evaporate the water from the SWNT suspension. As the water evaporates, the SWNTs remain on the surface of the Si wafer or gather in the trenches. Finally, the photoresist is removed, lifting off all of the SWNTs that are not in the trenches. Several trenches have a sufficient fill rate to allow IV characteristics to be performed. A Keithley probe station is used to measure the resistance of the SWNT composite material in the trench. These results,  $47.3\text{ k}\Omega$ , are similar to

other fabricated SWNT/polyelectrolyte thin films, showing that the method presented can be used to simplify the process of fabricating SWNT composite wires. Raman spectroscopy is also used to determine if the SWNTs in the SWNT composite structure are aligned in any direction. There is no preferential orientation of the SWNTs in the structure, rather the SWNTs appeared to be randomly oriented in all directions.

You cannot go on 'explaining away' forever: you will find that you have explained explanation itself away. You cannot go on 'seeing through' things for ever. The whole point of seeing through something is to see something through it. ... If you see through everything, then everything is transparent. But a wholly transparent world is an invisible world. To "see through" all things is the same as not to see.

C.S. Lewis, "Abolition of Man"

## TABLE OF CONTENTS

ABSTRACT .....	iii
LIST OF TABLES .....	x
LIST OF FIGURES .....	xi
ACKNOWLEDGEMENTS.....	xiv
CHAPTER 1 INTRODUCTION .....	1
1.1 Background and Research Need.....	1
1.2 Objective and Scope of Research.....	3
CHAPTER 2 LITERATURE REVIEW.....	4
2.1 Carbon Nanotubes .....	5
2.1.1 Carbon Nanotube Structure .....	6
2.1.2 Electrical Properties.....	10
2.1.3 Mechanical Properties.....	18
2.1.4 Current Uses / Future Products .....	18
2.2 Synthesis.....	22
2.2.1 Electric Arc Discharge .....	23
2.2.2 Laser Ablation.....	24
2.2.3 Chemical Vapor Deposition.....	25
2.3 Device Fabrication .....	42
2.3.1 CNT Direct Manipulation.....	42

2.3.2 CNT Electronic Field Placement.....	43
2.3.3 CNT Layer-by-Layer Placement.....	45
2.4 Dispersion.....	48
2.4.1 Surfactants / Polymers.....	48
2.4.2 Electrical.....	49
CHAPTER 3 SWNT SUSPENSIONS.....	51
3.1 Layer-by-Layer Self Assembly.....	52
3.1.1 Alternating Polyelectrolytes.....	53
3.1.2 Single Polyelectrolyte.....	55
3.2 NEXAFS Study of Suspensions.....	56
3.2.1 SWNT Acid Treatment.....	57
3.3 Conclusion.....	64
CHAPTER 4 FABRICATION.....	66
4.1 Overview.....	67
4.1.1 Spin Coating into Wells of Photoresist.....	67
4.1.2 Spin Coating into SiO <sub>2</sub> .....	68
Trenches without Photoresist.....	68
4.1.3 Spin Coating into SiO <sub>2</sub> .....	69
Trenches with Lift-Off.....	69
4.2 Mask Design.....	71
4.2.1 Wells.....	73
4.2.2 Trenches.....	75

4.3 Procedure Specifications.....	77
4.3.1 Lithography .....	78
4.3.2 SiO <sub>2</sub> Etching.....	79
4.3.3 Spin Coat SWNT Solution .....	80
4.3.4 Evaporation.....	80
4.3.5 Lift-Off.....	81
4.4 Results .....	81
4.4.1 Photoresist Wells .....	81
4.4.2 SiO <sub>2</sub> Trenches without Photoresist .....	86
4.4.3 SiO <sub>2</sub> Trenches with Lift-Off.....	93
4.5 Conclusion.....	99
CHAPTER 5 CHARACTERIZATION.....	100
5.1 IV Characterization.....	100
5.1.1 Results .....	101
5.2 Raman Characterization .....	103
5.2.1 Equipment List.....	104
5.2.2 Results .....	104
5.3 Conclusion.....	107
CHAPTER 6 CONCLUSIONS AND FUTURE WORK SUGGESTIONS.....	108
6.1 Research Conclusion .....	108
6.2 Future Suggestions .....	109
6.2.1 Fabrication.....	109
6.2.2 Heat treatment.....	110

6.2.3 Raman Spectroscopy.....	111
6.2.4 Three or Four Probe Measurements .....	111
REFERENCES.....	112

## LIST OF TABLES

Table 3.1: MicrotechNano SWNT Specifications .....	51
Table 4.2: Spin Coating into Wells of Photoresist.....	68
Table 4.3: Spin Coating into SiO <sub>2</sub> Trenches without Photoresist.....	69
Table 4.4: Spin Coating into SiO <sub>2</sub> Trenches with Lift-Off .....	71
Table 4.5: Trench Dimensions in Mask Design .....	77
Table 4.6: SiO <sub>2</sub> Trench Measurements with AFM .....	92

## LIST OF FIGURES

Figure 2.1: Buckyball - $C_{60}$ .....	4
Figure 2.2: Graphene Sheet of Carbon Atoms.....	6
Figure 2.3: Construction of CNT from Graphene Sheet [6] .....	7
Figure 2.4: Rendered SWNT with a Wrapping Vector (5,5).....	8
Figure 2.5: Rendered SWNT with a Wrapping Vector (10,0).....	8
Figure 2.6: Rendered SWNT with a Wrapping Vector of (5,8).....	9
Figure 2.7: Atomically Resolved STM Images of Individual SWNTs [8].....	10
Figure 2.8: Parallel Connected Plastic and Metal with Equivalent Circuit Model .....	15
Figure 2.9: Series Connected Plastic and Metal with Equivalent Circuit Model .....	16
Figure 2.10: Al Gate CNT Transistor [44].....	21
Figure 2.11: Electric Arc Discharge Setup.....	24
Figure 2.12: Laser Ablation Setup.....	25
Figure 2.13: Purchased SWNT Powder.....	25
Figure 2.14: Chemical Vapor Deposition Setup .....	27
Figure 2.15: Base and Tip Growth Mechanisms .....	28
Figure 2.16: AFM Image of Catalyst Pad with SWNTS [6] .....	29
Figure 2.17: AFM of SWNT with 125 mL/min Co-Flow $H_2$ [56] .....	30
Figure 2.18: TEM Images of the Raw Unpurified SWNTs [61].....	32
Figure 2.19: TEM of Synthesized CNTs from Thermal CVD (a-c) and PECVD (d-f). Temperatures Increase Left to Right, 550°C, 700°C, and 850°C [54] .....	34

Figure 2.20: SEM Image of Vertically Aligned CNFs [55] .....	35
Figure 2.21: Image of SWNTs Produced by RF-PECVD [59] .....	36
Figure 2.22: SEM Image of High Density Growth of CNTs [67] .....	37
Figure 2.23: TEM Images of Resulting CNTs [57] .....	38
Figure 2.24: SEM Images of Y-Junction SWNT [68].....	39
Figure 2.25: TEM of CNT Bamboo Structure [69] .....	40
Figure 2.26: SEM of SWNT Aligned with AC Electric Field [80] .....	44
Figure 2.27: SWNT Bundle Across Two Electrodes [24].....	45
Figure 2.28: Controlled Placement of SWNTs [86].....	47
Figure 3.1: Molecular Structure of PSS (a) and PAH (b).....	52
Figure 3.2: SWNT Suspension with PSS / PAH. ....	54
Figure 3.3: SWNT Suspension with Single Polyelectrolyte, PSS.....	56
Figure 3.4: TEM of SWNT Suspension[96] .....	56
Figure 3.5: Carbon Atom NEXAFS After 2 Hour Acid Treatment.....	59
Figure 3.6: Carbon Atom NEXAFS After 10 Hour Acid Treatment .....	60
Figure 3.7: Oxygen Atom NEXAFS After 2 Hour Acid Treatment.....	62
Figure 3.8: Oxygen Atom NEXAFS After 10 Hour Acid Treatment.....	63
Figure 4.1: UV Lithography.....	72
Figure 4.2: LEdit Mask Marking Cells of 15 $\mu\text{m}^2$ Wells .....	74
Figure 4.3: LEdit Mask of Single Cell of 15 $\mu\text{m}$ Wells.....	74
Figure 4.4: Printed Thin Film Mask.....	75
Figure 4.5: LEdit Mask Marking Cells with Trenches .....	76
Figure 4.6: Trench Diagram with Dimensions Marked.....	77

Figure 4.7: 15 $\mu\text{m}^2$ Wells After Developing for 20 seconds .....	82
Figure 4.8: 15 $\mu\text{m}^2$ Wells After Developing for 60 seconds.....	83
Figure 4.9: SWNT Pad Structures.....	83
Figure 4.10: SWNT Pads with Incomplete Fill.....	84
Figure 4.11: SWNT Pad Structures with Incomplete Removal.....	84
Figure 4.12: SWNT Pads Removed During Lift-Off.....	85
Figure 4.13: Correlation of Well Locations and SWNT Material.....	85
Figure 4.14: Trenches in Photoresist.....	87
Figure 4.15: AFM Image of 170 $\mu\text{m}$ x 8 $\mu\text{m}$ Trench Etched for 3 Minutes.....	88
Figure 4.16: AFM Image of 30 $\mu\text{m}$ x 4 $\mu\text{m}$ Trench Etched for 3 Minutes.....	89
Figure 4.17: AFM Image of 50 $\mu\text{m}$ x 2 $\mu\text{m}$ Trench Etched for 5 Minutes.....	90
Figure 4.18: AFM Image of 20 $\mu\text{m}$ x 2 $\mu\text{m}$ Trench Etched for 5 Minutes.....	91
Figure 4.19: SWNT Structures in 8 $\mu\text{m}$ Width Trenches .....	95
Figure 4.20: SWNT Structures in 4 $\mu\text{m}$ Width Trenches .....	96
Figure 4.21: SWNT Structures in 2 $\mu\text{m}$ Width Trenches.....	97
Figure 4.22: Two Rows of SWNTs in Trenches.....	98
Figure 5.1: IV Characterization of SWNT Wire .....	102
Figure 5.2: Raman Spectroscopy of SWNT Sample .....	104
Figure 5.3: Optical and Raman Images Left to Right HV, VV, HH Mode.....	106

## **ACKNOWLEDGEMENTS**

I would like to thank first and foremost, the Savior of my life, Jesus Christ. Without Him, I can do nothing (John 15:5). Every good thing comes from Him (James 1:17), so any praise or worthiness in this work belongs foremost and fully to Him. I have also been blessed with a wonderful, patient wife who has been a constant support and aid. Without her I do not know if I would have ever been able to finish. I also must thank my advisor, Dr. Dobbins. Only with her support, advice, and time has this project been a success. I would have never been able to put everything together in the time frame I needed without her sacrifice. All of my committee members have also been a true encouragement and blessing. Their willingness to cooperate in every way to help this project come together (and especially come to an end) cannot be over appreciated. No individual is stronger than the family he comes from, and I must thank my family, both those in Pennsylvania and Mississippi. Without your constant encouragement, prayer, and understanding, this project would have been disastrous. I cannot leave out all the support and prayers from friends near and afar. The continuous prayers have truly made this paper happen. I do not want to imagine how difficult this process would have been without them. Only by the many prayers was I given the needed strength and energy to persevere and accomplish this significant undertaking. I am eternally grateful to all who have contributed, directly or indirectly, to me and

this project. Any achievement in this project truly belongs to all of you and not to me. As I look back at all that was accomplished, I see how little my part was compared to the whole. I cannot thank all of you enough, but know that you are all cherished and appreciated.

## CHAPTER 1

### INTRODUCTION

#### 1.1 Background and Research Need

Since their discovery in 1991 [1], carbon nanotubes (CNT) have been viewed as having great potential for development in a variety of fields. Research groups from across the globe have spent the last 18 years and millions of dollars trying to unlock the mysteries of the CNT and integrate them into new, smaller, faster, and better products. The greatest strength of the CNT, its near atomic size, has also been its greatest weakness. Their small size has made individual manipulation for device fabrication a challenge. CNTs have been fabricated by several methods, but none have been able to control the synthesis enough to allow for direct device fabrication. Devices have been demonstrated, but only by long, tedious, manual manipulation of the CNT onto prefabricated contact pads. This type of processing is costly as well as time consuming.

In the last 7 years, semiconductor manufacturing processes have reached the scales below 100 nm. The improved manufacturing processes have opened the door to feasible CNT device fabrication without increasing production costs beyond the range of profitability. This has led to several companies announcing new products incorporating CNTs. NEC predicts having a CNT transistor device as

early as 2010 [2]. Samsung demonstrated a color e-paper product that uses CNT electrodes at the Meeting on Information Display in October 2008. Several companies around the world have already claimed patents on CNTs, fabrication processes, and CNT devices. Companies holding patents on CNTs include NEC, IBM, Samsung, Intel, Fuji Xerox, General Electric, Canon, Philips Electronics, and Honeywell [3]. Most companies looking at CNTs are trying to integrate them into electrical devices. This is because CNTs have a unique conducting property; they can be metallic or semiconducting based on their size and structure. The two conduction types suggest that entire integrated circuits may be replaceable. Semiconducting CNTs can replace all of the transistor based components while the interconnects can be replaced by metallic CNT wires.

This possibility promises a continued reduction in size that silicon based products may not be able to achieve. With the current pace of shrinking circuits, the atomic size barrier is looming in the near future. Silicon based products may reach their limits at that barrier, and therefore, a new material will be needed. CNTs are continuing to look like that new material. Their electrical properties and nano scale size puts CNTs in the premier position to overtake and replace silicon as the next material to create the top of the line microelectronic devices. However, without a mass manufacturing process to allow devices to be batch processed, CNTs will be regulated to a niche market or remain in the arena of perpetual research.

## **1.2 Objective and Scope of Research**

This work is developed to help solve the problem of integrating SWNTs into devices using technologies that can be batch processed on a large scale. For CNTs to be realized in actual products and devices, a new manufacturing method must be developed to integrate CNTs into the fabrication process of the individual devices. The quickest way to integrate CNTs into current products is to use existing technologies, fabrication processes, and equipment. Several of the fabrication processes that have been developed to build CNT devices require process steps or equipment that does not integrate well with current fabrication setups in industry. Retooling a fabrication plant can be almost as expensive as building a new one. If current fabrication tools and methodologies can remain unchanged while allowing CNTs to be incorporated into the device, new devices can be developed and fabricated with minimum upstart costs.

This work is a study to develop such a technique. In this study, a methodology is devised to use current semiconductor fabrication technology and tooling to build CNT structures that can be incorporated into microelectronic devices. The simplest point of integration in a semiconductor device is as a metal contact between transistors or MEM devices. SWNTs have a high conductivity that makes them ideal for such nanowire connections. This study will also fabricate SWNT structures that could be used as metal contacts in a microelectronic device.

## CHAPTER 2

### LITERATURE REVIEW

Carbon is the basis of all life on earth. This is due to the remarkable capability of carbon atoms to concatenate. They can form long chains and become the backbone of many complex structures. Carbon's unique properties have placed it as the focal work of numerous researchers for countless years. With all of the research invested in carbon structures, it is partly surprising that the discovery of the carbon nanotubes (CNTs) took so long. The first step towards fabricating the CNT was not creating a tubular structure, but rather spherical clusters of carbon atoms referred to as  $C_{60}$  because they contain 60 carbon atoms. A diagram of  $C_{60}$  is shown in Figure 2.1 below.

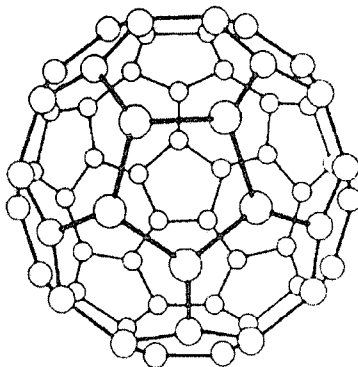


Figure 2.1: Buckyball -  $C_{60}$

These spheres later were given title Buckyballs by Richard Smalley and Harry Kroto, who discovered the Buckyball in 1985 [4]. However, no significant amount of  $C_{60}$  could be manufactured in a typical research lab using their process. Five years later, Wolfgang Krätschmer and Donald Huffman devised a method that could create macroscopic amounts of  $C_{60}$  in any basic laboratory. They used a carbon arc to vaporize graphite. The ease of producing large quantities of  $C_{60}$  set the stage for a surge of new research. CNTs were first discovered a year later, in 1991, by Sumio Iijima [1]. Iijima was working with Buckyballs when he observed some different graphite particles around the cathode during the arc-evaporation process [1]. Upon closer investigation, he found tiny closed cylinders of graphite forming carbon fibers. Since that time, CNTs have been researched for a variety of applications ranging from mechanical structures to chemical storage for hydrogen to electrical transistor devices. Their many unique properties make them ideal materials for new devices and replacements for others. Because carbon based materials are readily available, the material cost of creating CNTs is relatively inexpensive.

## **2.1 Carbon Nanotubes**

Carbon, with four valence electrons, can bond with itself in different configurations. The two most common bonding configurations create diamond and graphite. When the four valence bonds are shared equally, creating a  $sp^3$  hybridization, diamond is formed. If only three electrons are shared covalently and the fourth is shared among all atoms, graphite is formed [5]. Graphite forms a layered structure with very strong in plane bonds and very weak out of plane bonds

(van der Waals). The carbon atoms in an individual layer form a repeating hexagon pattern, as pictured in Figure 2.2 below.

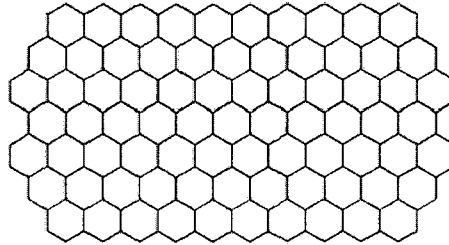


Figure 2.2: Graphene Sheet of Carbon Atoms

CNTs form when a sheet of the  $sp^2$  hybridized carbon graphene rolls together to form a cylinder. CNTs can be treated as a macromolecular system with a well defined architecture of graphene sheets. This perfectly defined lattice structure is what separates CNTs from other carbon based fibers.

### **2.1.1 Carbon Nanotube Structure**

Carbon nanotubes fall into two major classifications of multi-walled (MWNT) and single-walled nanotubes (SWNT). The difference between the two types is self-explanatory. The MWNTs are typically larger and consist of multiple shells similar to a tube shaped onion. These layers add complexity when trying to correlate theoretical calculations with experimental results. The electronic structure of the smallest inner tube is superimposed by the outer shells [5]. The overlay of these layers causes the conductive properties of all MWNTs to resemble a semi-metallic structure. SWNTs are smaller, simpler, and easier to analyze mathematically, and as such they have been the focus of much of the current research. SWNTs also have the unique property to vary from a metallic conductor

to a semiconductor. The key determining factor distinguishing metallic from semiconducting nanotubes is the nanotubes chirality. The chirality is more easily visualized in the concept of a sheet of rolled graphene. This sheet concept is used to study SWNTs theoretically. There are three sub-classifications, (zigzag, chiral, and armchair) of SWNTs depending on the angle at which the graphene is rolled up to form the SWNT. The graphene sheet must be rolled up so that two equivalent lattice sites coincide. In Figure 2.3, the wrapping vector  $C$  is defined by the two relative lattice sites.

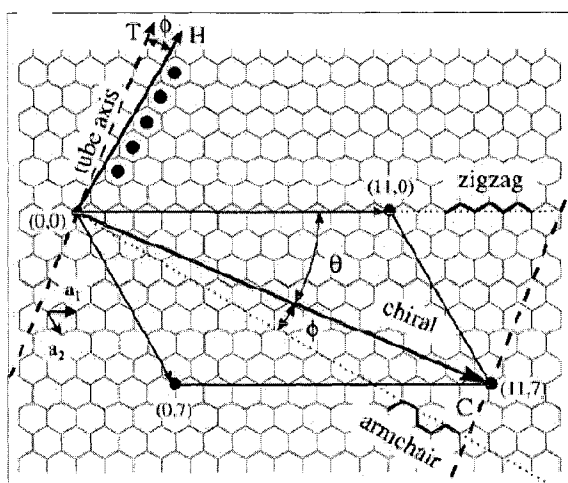


Figure 2.3: Construction of CNT from Graphene Sheet [6]

This vector can also be specified by a pair of integers  $(n,m)$  that define the magnitude of the unit vectors  $a_1$  and  $a_2$  respectively. Thus, the vector  $C$  is defined as  $C=na_1+ma_2$ . Armchair SWNTs are created when the magnitudes of  $a_1 = a_2$ . They are characterized by an armchair pattern in the carbon atoms on the length of the tube, as highlighted in Figure 2.3. Rendered images with Gabedit version 2.1.8 are shown below in Figure 2.4 of a SWNT with a wrapping vector of  $(5,5)$ .

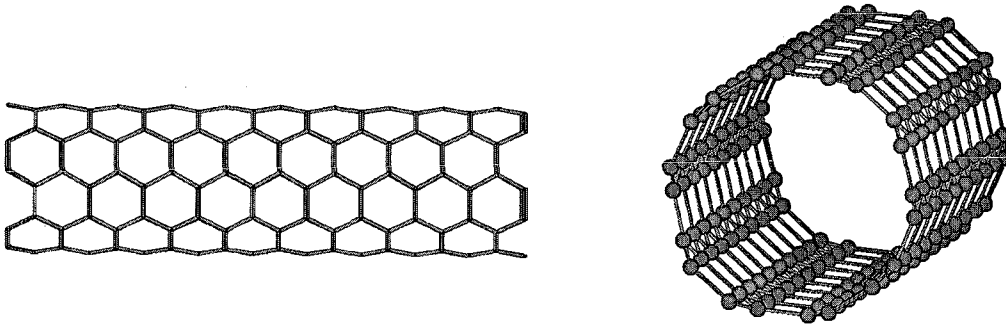


Figure 2.4: Rendered SWNT with a Wrapping Vector (5,5)

Zigzag SWNTs are created when the magnitude of  $a_2=0$ , creating a zig-zag pattern along the length of the tube, also highlighted in Figure 2.3. Rendered images with Gabedit are shown below in Figure 2.5 of a SWNT with a wrapping vector of (10,0).

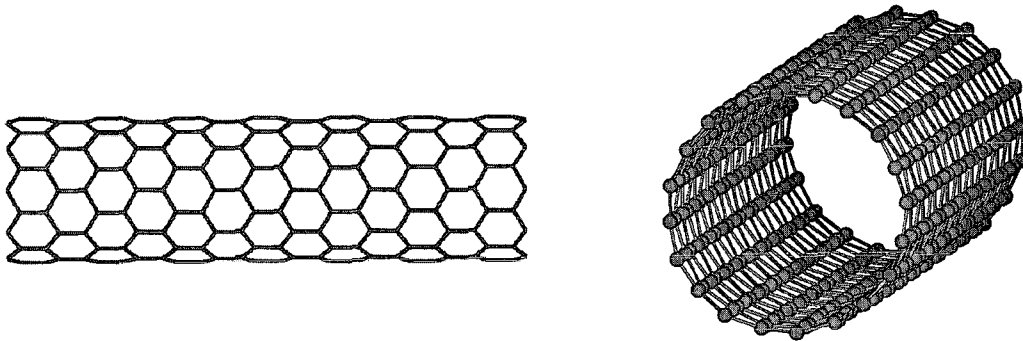


Figure 2.5: Rendered SWNT with a Wrapping Vector (10,0)

All other SWNTs are defined as chiral. They have a finite wrapping angle exclusively between  $0^\circ$  and  $30^\circ$  [7]. Rendered images with Gabedit are shown below in Figure 2.6 of a SWNT with a wrapping vector of (5,8).

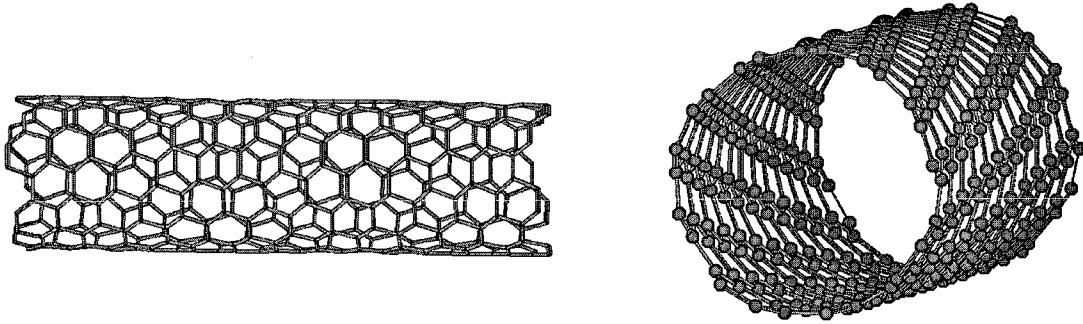


Figure 2.6: Rendered SWNT with a Wrapping Vector of (5,8)

Note the armchair and zigzag structures have a repeating pattern around the cylindrical surface of the SWNT so the pattern on the front side of the CNT can match the back side. The images above are 3-dimensional, but with the back half of the tube mirroring the front half, the image appears to be a flat 2-dimensional image. The chiral image shows how the pattern repeats in a rotating manner around the cylinder wall so the pattern on the front and back of the SWNT do not line up. That is why the side image in Figure 2.6 appears more cluttered than the others. All armchair SWNTs display metallic conduction because the valence and conduction bands always cross each other at the Fermi energy for a certain wave vector. The other two types can display metallic or semiconductor properties depending on the angle of chirality. When  $n+m = 3x$  ( $x$  being any integer value), tubes are expected to be metallic. All other combinations of  $(n,m)$  will exhibit semiconductor properties [8]. Figure 2.7 shows scanning tunneling microscope (STM) images of SWNTs of various types.

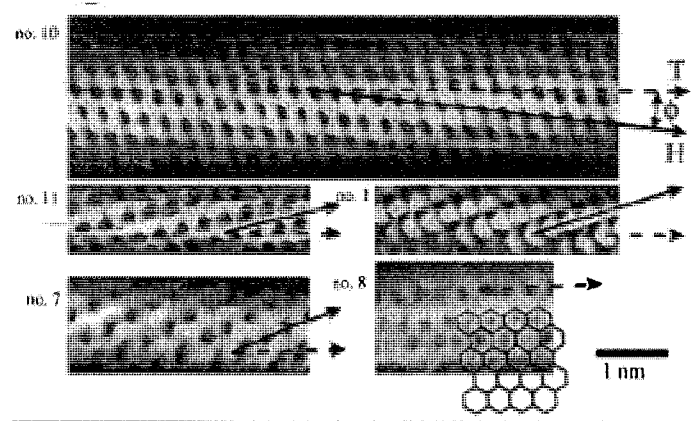


Figure 2.7: Atomically Resolved STM Images of Individual SWNTs [8]

Tubes number 1, 10, and 11 have a chiral structure. Tube number 7 has a zigzag structure, and tube number 8 has an armchair structure. These images are gathered from Wildoer's work [8].

### **2.1.2 Electrical Properties**

Understanding the electrical characteristics of CNTs begins with understanding graphene, the component structure of CNTs. Because graphene is made up of  $sp^2$  bonded carbon atoms, the band structure is unusual. A typical metallic material has more states that propagate through the material at the Fermi energy level ( $E_F$ ). A typical semiconducting material has a gap with no electron states near  $E_F$ . Graphene can have both characteristic band structures depending on the direction of the electrical field or the direction electrons are moving across the surface of the sheet of graphene. In most directions, electrons are backscattered at  $E_F$  due to the lattice structure resulting in a band structure with a gap of no electron states like a semiconductor. In some directions, the electron scattering interfere differently with the lattice, resulting in less backscatter and a

band structure more like a metal. Because of the repeating pattern of graphene, this direction of metallic nature repeats every 60° [9]. This is the root cause of why some CNTs have metallic properties and others have semiconducting properties.

One of the more interesting discoveries about the semiconductor properties of SWNTs, due to the fact that the entire structure is made of identical carbon atoms, is that the chemical bonding between the carbon atoms in metallic and semiconducting SWNTS is the same. This means that the only factor that affects the energy gap in semiconducting SWNTs, according to Equation 2.1, is the diameter of the tube.

$$E_{gap} = \frac{2\gamma_0 \cdot a_{c-c}}{d} \quad (2.1)$$

In Equation 2.1,  $\gamma_0$  is defined as the carbon to carbon tight binding overlap energy,  $a_{c-c}$  is the nearest neighbor distance (0.142 nm), and  $d$  is the diameter of the SWNT. This equation also demonstrates that the energy gap gets smaller as the diameter increases. These SWNT characteristics defined by Equation 2.1 have been correlated with experimental data [8]. This unique electrical characteristic has created a renewed interest in devising single molecule semiconductor devices. This process has not proven easy, but the rewards of such a realization have enticed many to try.

The largest problem in developing a single molecular device is the manufacturing. Because these structures are on the atomic level, synthesizing ideal structures and manipulating the structures has proven quite difficult. The

atomic scale necessary to characterize CNTs has caused two different classes of measurements to be performed. Some studies have used CNT manipulation techniques to measure the electrical characteristics of a single CNT [8, 10-14] while others have created micro sized CNT thin films to measure the characteristics of the film [15-17]. To electronically characterize a single CNT requires the fabrication of highly conducting contacts, typically gold (Au), to transition from the 2-10 nm size of a CNT to a contact pad on the scale of 1-2  $\mu\text{m}$ . These metal contacts can be pre-fabricated on a substrate before dropping a CNT onto them. A technique for precise deposition of a single CNT has not been discovered, so the deposition is typically followed up by manually pushing the CNT onto the contact pads using an AFM tip. Moving the CNT onto the contact pads can be tedious and time consuming.

The other method to connect contact pads to a single CNT is to basically reverse the process. First a CNT is deposited onto a clean substrate. The substrate is then scanned in an SEM to find the exact location of the CNT. Then standard lithography is used to fabricate contact leads exactly atop the CNT. This method avoids the tedious moving of the CNT. However, the methods of fabricating the contact pad can involve the expense of designing and building a custom chrome mask for standard UV lithography or require the slower and more expensive electron beam (e-beam) lithography. E-beam lithography has the added benefit of a smaller feature size. E-beam lithography has a feature size limit of 20-40 nm. Comparing that to UV lithography, the leaders in the semiconductor

industry have just recently achieved 32 nm feature size limits [18], although doing this requires very expensive lithography equipment and specialized mask designs.

Outside of industry, research centers are more typically capable of using UV lithography with a feature size of 50 nm – 1  $\mu\text{m}$ . This creates metal contacts that are significantly larger than the CNT they are used to testing, so the contacts and especially the interface junction between the contact and the CNT can affect the characterization results [19]. This must always be considered when looking at experimental electrical measurements of CNT devices. Measured resistance values for a single SWNT can vary from 20 k $\Omega$  [20] to 1 T $\Omega$  [21]. Both studies used Au contacts. Other studies have used palladium (Pd) and aluminum (Al) contacts that can create Schottky barriers in the junctions between the CNT and metal contacts [22-24]. Quantum theory suggests a SWNT should have a resistivity of about 6 k $\Omega$  [21]. This assumes CNTs behave as ideal one-dimensional quantized conductors [7]. Electrons in the  $\pi$ -states are involved in the conduction, so the resistance of the CNT for ballistic transport should be described as Equation 2.2.

$$R = \frac{h}{4 e^2} \quad (2.2)$$

The reason for such low conductivity for a SWNT is due to the small scale. Even though CNTs have a current density much higher than other materials, their nm size only allows for microampere currents. For larger diameter CNTs, the behavior of conductance changes from a one-dimensional conductor to a two-dimensional conductor. MWNT will have increased conductivity with each shell allowing electron transport along the length of the tube. A 10-walled, 15 nm diameter MWNT has a theoretical resistance of 65  $\Omega$  [25]. Measured resistances of

MWNTs using 2 and 4 probe techniques range from 2 k $\Omega$  to 14 k $\Omega$  [26]. To compare with current silicon devices, a 20 nm silicon transistor has a resistance of 1 k $\Omega$  and a 150 nm long copper wire interconnect with a width of 10 nm has a resistance of 800  $\Omega$  [27]. The seemingly high resistance of CNTs does not prevent them from being used as replacements for metal interconnects in silicon based devices because any conductor will increase in resistivity as the wire size approaches the size of the CNT.

Characterizing thin films of CNTs can avoid some of the contact and scaling issues because the CNT film is on the scale of several microns as opposed to a few nm for an individual CNT. CNT thin films, while easier to measure experimentally, are much more complex to study from a theoretical viewpoint. Thin films are typically created with a mixture of CNTs and polymers [15, 17, 28-32]. In the final film, the CNTs are not aligned in any particular direction, so conduction will not necessarily occur solely along the length of the CNT. Along the width of the CNT, conduction will not be the 1-dimensional transport, but 2-dimensional just like a sheet of graphene. The bonding agent in the thin film, typically a polyelectrolyte, has a different conductivity than the CNTs and usually does not exhibit good conduction. This random mixture and orientation of CNTs increases the complexity beyond the scope of a theoretical study. A simplified metal and plastic model can help visualize the mixture in the thin film. When a mixture of metal and plastic beads are equally distributed and then melted together to form a thin film, the conduction would be hard to calculate theoretically due to the random dispersion of metal in the film. Increasing the ratio of metal to plastic would

increase conductivity by reducing the amount of insulating plastic. How the plastic and metal are connected in relation to the direction of conduction also affects the total conductivity in the film. In the simplest unit, a metal bead can be connected to a plastic bead in parallel or series with the direction of conduction. Figure 2.8 depicts how the metal and plastic components can be connected in parallel along with the equivalent circuit schematic.

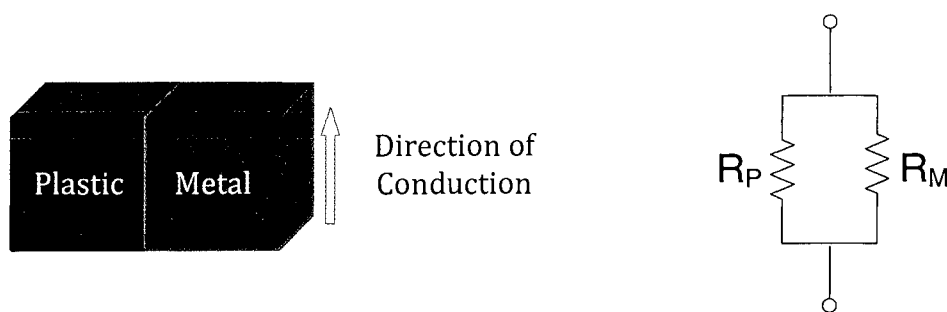


Figure 2.8: Parallel Connected Plastic and Metal with Equivalent Circuit Model

Resistance, as the inverse of conductivity, can be used to represent the conductivity of the metal and plastic. The resistance of the plastic bead should be much larger than the resistance of the metal bead, and therefore the total resistance for the two components can be calculated by combining the resistances of each individual component as shown in Equation 2.3. The resulting combined resistance, and hence conductivity, is very close to that of the metal bead.

$$R_T = \frac{R_P \cdot R_M}{R_P + R_M} \Big|_{R_P \gg R_M} \approx R_M \quad (2.3)$$

Similarly, Figure 2.9 depicts how the metal and plastic components can be connected in series along with the equivalent circuit schematic.



Figure 2.9: Series Connected Plastic and Metal with Equivalent Circuit Model

Equation 2.4 shows the combined resistance for the two beads connected in series is approximately the resistance of the plastic bead when the resistivity of the plastic much greater than that of the metal.

$$R_T = R_P + R_M \mid_{R_P \gg R_M} \approx R_P \quad (2.4)$$

Therefore increasing the concentration of metal not only reduces the insulating affect of plastic, but also reduces the likelihood of the metal and plastic being connected in series. Plastic beads connected in parallel have little affect on the conductivity. The best conductivity can be achieved by having a complete path of metal beads from one edge of the thin film to the other. Any plastic beads in series with this conduction path will significantly reduce the overall conductivity.

Applying these same principles to the CNT and polyelectrolyte film can give some general concept implications. The conductivity of the CNTs is much larger than the polyelectrolyte, so any series connections of polyelectrolyte with CNTs will hinder the conductivity of the film. An ideal film for high conductivity will have several paths of solely CNTs from edge to edge. In this regard, increasing the concentration of CNTs should improve conductivity. The nature and procedure of

fabricating the CNT thin film does not always allow the ratio of CNT and polyelectrolyte to be changed. There has not been a known parametric study on that aspect of CNT thin films. Research by M. Palumbo looked at a thin film of SWNT and polyelectrolyte poly(ethyleneimine) (PEI) with multiple Al contacts fabricated on top of the film. The measured conductance of the film was  $0.015 \mu\text{S}$ , giving a film resistance of  $66.67 \text{ M}\Omega$  [15]. This low conductivity would prevent any such film from being a usable option for any microelectronic devices. Another film in the same study was made with alternating layers of SWNTs dispersed with sodium dodecyl sulphate (SDS) and dodecyltrimethylammonium bromide (DTAB). This film, also with multiple Al contacts fabricated on top of the film, exhibited a conductance of  $5 \text{ mS}$  at a distance of  $0.5 \text{ mm}$  [15]. With an equivalent resistance of  $200 \Omega$ , this thin film composition could be an electrical alternative for microelectronics.

Another study by Wei Xue measured the conductivity of a SWNT and polyelectrolyte poly(dimethyldiallylammonium chloride) (PDDA) thin film. The size of the film studied was  $1 \text{ mm} \times 6 \text{ mm}$  connected on each side to a Au contact. The measured conductance at room temperature was  $0.045 \text{ mS}$  [17]. In comparison to the measured resistance values of individual CNTs above, this conductance is equivalent to  $22.2 \text{ k}\Omega$ . When the film was heat treated, the conductivity increased. At  $300^\circ \text{C}$ , the conductance peaked at  $2.29 \text{ mS}$ . Heating above this temperature caused the conductivity to decrease [17]. The conductance of  $2.29 \text{ mS}$  is equivalent to  $437 \Omega$  which makes this thin film a viable alternative for microelectronic devices.

### **2.1.3 Mechanical Properties**

CNTs have not only been studied for the unique electrical characteristics, but also for their mechanical properties. Theoretical studies of the mechanical properties of SWNTs have been performed to try to understand what expectations to have for mechanical studies of various CNTs [33]. SWNTs were studied rather than MWNTs due to the added complexity of the multiple shell like layers of MWNTs. In these studies, tensile strengths of 300 GPa have been predicted for SWNTs [33]. To utilize the superior mechanical strength of CNTs, they have been studied by integrating them into CNT / polymer composites [16, 28, 29, 34]. In order to measure the mechanical properties of these composites, thin films have been fabricated that can be tested in standard mechanical rigs. Various fabrication techniques have been employed recently to make a free standing thin film with one of the most common being layer-by-layer (lbl) self-assembly. Multiple studies investigating these types of CNT thin films have achieved similar stress-strain curves with failure occurring around 150 – 220 MPa [28, 29]. A more specific study of the mechanical properties of individual MWNTs was achieved by Min-Feng, by devising specialized loading devices that can operate entirely inside an SEM. The MWNTs were loaded until failure occurred. Tensile strengths for the outmost layer of a MWNT were determined to be in the range of 63 GPa [35].

### **2.1.4 Current Uses / Future Products**

CNTs have been shown to exhibit exceptional electrical, optical, thermal, and mechanical properties [36]. The nano-scale dimensions of CNTs and their length to diameter ratio makes them ideal for field emitters. Several studies have used

CNT films to demonstrate their field emission properties [37, 38]. They demonstrated CNT films were capable of emitting electron current densities of a few hundred  $\frac{mA}{cm^2}$  with a threshold voltage of only a few tens of volts [38]. CNTs are also being considered for electrochemical applications including fuel cells and batteries. CNTs have been shown to exhibit higher performance than amorphous carbon fibers [7, 39]. More recently, CNTs have been studied for hydrogen storage [40, 41]. With the increasing interest in hydrogen as a new energy storage and transport medium, it becomes imperative to find materials that can effectively, efficiently, and safely store hydrogen. One of the largest segments of research of CNTs revolves around the use of CNTs as semiconductors. There are several reasons for this. Semiconductor firms spend large amounts of money in R&D to find newer, faster, cheaper methods to produce products that are smaller, faster, and consume less power. The semiconductor industry moves at an incredible pace; new technology becomes outdated in months. For these reasons, the semiconductor industry stays on the leading edge of technology, and that edge is quickly approaching the realm of atomic sized structures like CNTs. If CNTs revolutionize the semiconductor industry, it will be because the semiconducting SWNTs can work as transistors. Applying a negative bias to the gate can make the SWNT conduct, or turn 'on'. In the same manner, applying a positive bias to the gate will make the SWNT behave like an insulator, or turn 'off', just like a p-type metal-oxide-silicon field effect transistor (MOSFET) [42]. Although substantial research has been done, the reason why a SWNT behaves like a p-type material instead of intrinsic silicon is not completely understood. The currently accepted

theory explains the doping properties coming from the connecting electrodes. The CNT and the electrode form a barrier at their junction. This barrier causes the CNT to behave as it does.

Groups at Stanford and Berkley have shown that changing the chemical environment of the SWNT can change its doping behavior. Exposure to certain chemicals can create SWNT transistors that behave like n-type MOSFETs [13]. The benefit of the CNT transistor is not only the small 1nm wide size, but how the CNT is able to avoid the problems that have plagued current bulk semiconductor materials from reaching such small scale sizes. 'Surface states' are electronic states that occur when a 3-D crystal is interrupted by a surface. These states cause an energy gap that typically degrade the performance of the electronic device. 'Surface states' have been the key factor hindering the continual reduction in size of bulk semiconductor devices. Because CNTs are composed of a sheet of graphene, a 2-D material, they never encounter a surface interrupting a 3-D surface [43]. CNTs instead behave more like a 1-D device. Their cylindrical shape also avoids any problems that occur due to edges in the material. Due to the inherent shape and material composition, the CNT is able to bypass some of the most prevalent barriers in current semiconductors. The uniqueness of CNTs allows them to be used to create transistors that are only a few nanometers in size by placing or growing a semiconducting CNT between two contact pads, source and drain, and applying a gate voltage on the Si wafer. More advanced manufacturing techniques include using Al to cover the CNT to replace the Si substrate as the gate terminal [44] (Figure 2.10).

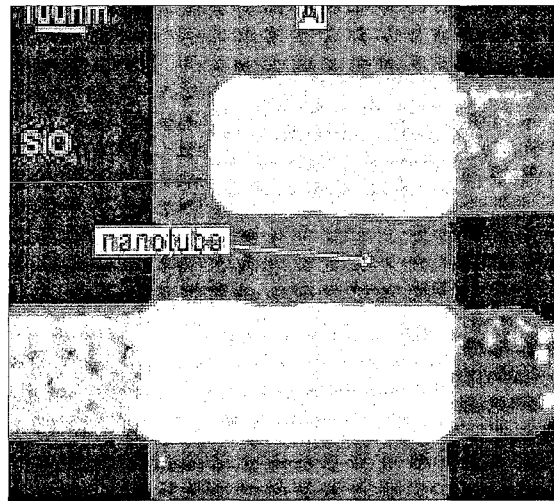


Figure 2.10: Al Gate CNT Transistor [44]

Currently, E-beam lithography can create a feature size of around 20nm x 20nm. The length of the CNT can be reduced without affecting performance. According to scanning tunneling spectroscopy measurements, the length of semiconducting CNTs has no effect on the band gap down to sizes of 50Å [45]. The gate field is also independent of the CNT length as long as the gate field is perpendicular to the axis of the CNT. The CNT transistor will have the same threshold voltage regardless of length. Therefore, carbon nanotubes can be reduced in size without reworking the voltage characteristics of the entire electrical device. These possibilities allow for continued size reduction with very little effects to the overall device design. The reason CNTs have not been incorporated into semiconductor devices is the lack of fabrication procedures that enable complex architectures required by the semiconductor industry [5].

## **2.2 Synthesis**

There have been several methods developed to manufacture CNTs. The first method was discovered by Sumio Iijima using arc vaporization with two graphite electrodes. This method will grow MWNTs [1, 46]. During an arc discharge between the two electrodes, the MWNT will grow on the cathode. To grow SWNTs, the electrodes in electric arc discharge setup were replaced with iron [47] or cobalt [48]. However, this method is not an efficient way to produce large quantities. Laser ablation and carbon arc techniques were developed to increase production rates. These newer methods are able to synthesis large quantities of high quality SWNTs. The next barrier to producing CNT devices involves manipulating the CNT from the material it was grown on to the final product. To further complicate this process, the above methods synthesize CNTs in large bundles of twisted tubes. The bundles have to be separated to extract a single CNT on the substrate. The bundles can be removed from the one base material and separated in a liquid solution before being deposited onto the final substrate, typically a silicon wafer. The CNT can then be manipulated with an atomic force microscope (AFM) to move it onto the premanufactured contact pads [49]. Instead of moving the CNT after it is deposited on the substrate, an alternative approach entails scanning the substrate after the CNT is deposited and then manufacturing contact pads around the CNT [9]. Neither of these processes, although acceptable in the laboratory, are suitable for mass manufacturing because they require too much direct individual human involvement to be profitable.

### **2.2.1 Electric Arc Discharge**

Electric arc discharge was the method used to first discover CNTs. Iijima was using the method devised to produce carbon fullerenes and Buckyballs. When he looked at the surface of the cathode in his experiment, he found that MWNTs had formed there [1]. The electric arc setup, shown in Figure 2.11 below, consists of two graphite electrodes, cathode and anode, inside a heat and pressure controlled chamber. MWNTs are generated when an electric arc is sparked across the two graphite rods. Typically a voltage of 20 V and currents less than 100 A are used. The chamber is usually filled with an inert gas like helium with a pressure around 500 Torr. Inside the interelectrode region, a plasma forms due to the high temperature, almost 3500° C. It is in this plasma where the MWNTs self assemble. The synthesis occurs very quickly. MWNT with 5 nm diameter can grow to 1 mm in length in 10 ms [5, 50]. The setup is modified slightly to produce SWNTs. A mixture of metal catalyst and graphite is packed into a hole that is drilled into the anode. A mixture of nickel (Ni), yttrium (Y), and graphite has given the best results [48, 51]. There are a few downsides to the electric arc discharge procedure. The biggest drawback, due to the size of the chamber and electrodes, is a small production of CNTs. The electric arc process cannot be easily scaled up to produce large quantities of either MWNTs or SWNTs. The other drawback in electric arc is the quality of the produced CNTs. Carbon soot is also created in the process which creates impurities in the synthesized CNTs. Therefore the CNTs will need to be further processed for purification. Other fabrication processes which can produce high quantities with fewer impurities have been developed.

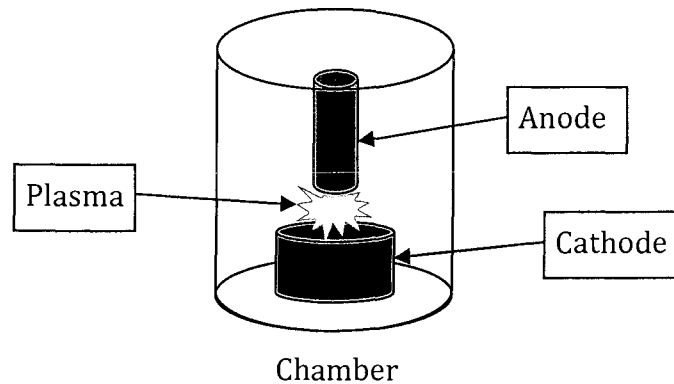


Figure 2.11: Electric Arc Discharge Setup

### 2.2.2 Laser Ablation

Laser ablation was devised to synthesize CNTs by creating similar conditions to the electric arc discharge using a more controllable energy source. The chamber is replaced with a tube furnace to supply heat. An inert gas, He or Ar, is pumped through the tube furnace at a similar pressure of 500 Torr as in electric arc discharge. A metal mixture target is placed in the furnace. Ni and Co have shown to give good results. The metal target is ablated with a strong laser. Pulsing the laser has shown to improve the yield of CNTs. Carbon deposits gather on an water cooled collector. The rapid cooling causes the deposits to form into CNTs [52, 53]. Figure 2.12 shows a typical laser ablation setup.

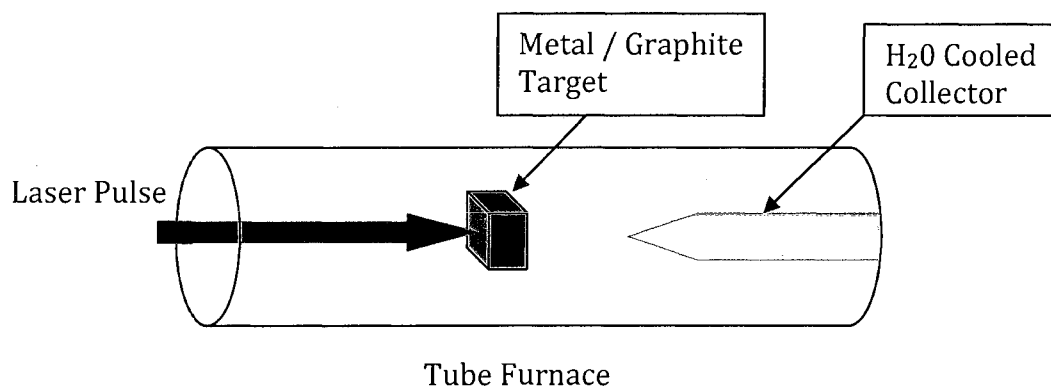


Figure 2.12: Laser Ablation Setup

Laser ablation is more controllable and can produce a higher quality SWNT. However, it suffers from the same batch processing limitations as electric arc discharge. The process does not scale up to allow for the synthesis of mass quantities of CNTs. The resulting SWNTs are bundled and tangled together to form black powder of carbon soot. An image of the resulting SWNT powder is shown below in Figure 2.13.



Figure 2.13: Purchased SWNT Powder

### **2.2.3 Chemical Vapor Deposition**

Although chemical vapor deposition (CVD) was not the first method developed to fabricate CNTs, this method has been increasingly researched due to

the ease and ability to grow individual SWNTs over the more commonly produced MWNTs. The CVD process was historically plagued by low yields and impurities due to amorphous carbon deposits. More recently, the CVD parameters have been adjusted to overcome these difficulties to produce very high quality SWNT. The process adjustability, simplicity of equipment, and high quality yields has made CVD the most common setup to synthesis SWNTs today. In the general CVD process, a substrate, typically silicon (Si), is thoroughly cleaned. An oxide layer is sometimes grown on the substrate. On the clean substrate, a catalyst material is evenly deposited. Catalysts can be evaporated [54] or sputtered [55] as a thin film, spin coated in an aqueous solution [6, 10, 56], spin coated powder [57, 58], deposited with ion implantation [59], or self-assembled with lbl [60]. Catalysts vary in chemical composition, but typically consist mostly of heavy metals and nanoparticles. The processed substrate is then loaded into a tube furnace. The furnace size can range in diameter from 1 to 4 inches. The furnace is set up to allow gas to flow through the quartz tube while operating at high temperatures. The sample is heated in the presence of an inert gas, typically argon. When the sample reaches the desired growth temperature, which can vary from 150° C to 1000° C, the neutral gas is replaced with a carbon feeding gas. At the high growth temperature, the feeding gas releases the carbon which attaches to the metal and nanoparticle catalyst and begins to concatenate. Feeding gases that have been used to produce CNTS include benzene, ethylene, methane, and carbon monoxide [61]. The growth process can occur at atmospheric pressure or low pressure and can vary in time from 5 minutes to 30 minutes. After the growth period, the

feeding gas is replaced with a neutral gas as the furnace cools. The CVD fabrication process can result in horizontally and vertically grown CNTs. A typical horizontal CVD setup is shown below in Figure 2.14.

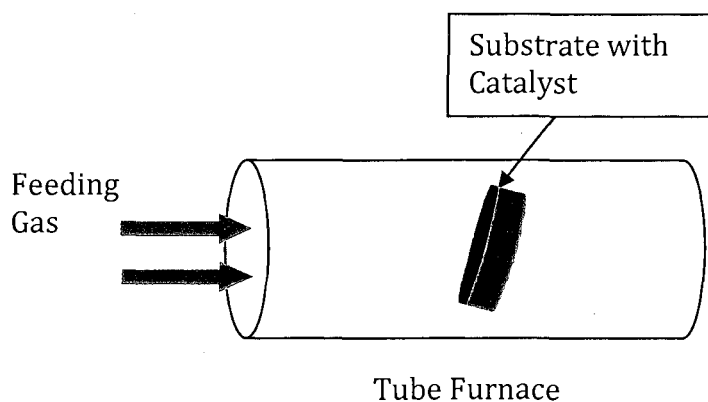


Figure 2.14: Chemical Vapor Deposition Setup

Due to the large number of variables in differing CVD growth processes, direct comparison of the resulting CNTs is difficult. The exact physical interactions occurring to cause the growth process have not yet been determined. The nature of the CVD process prevents any real time observation on the atomic level during the actual growth. Unfortunately, no single theory has been proposed that can explain or model the growth mechanism for CNTs completely. Baker *et al.* are generally given credit for proposing the first and foundational model of CNT growth [62]. This model has branched into two main growth mechanism hypotheses, base growth and tip growth [63-65]. The base growth model describes the growth of CNTs as originating from the base catalyst. The carbon from the feeding gas attaches at the base and pushes the nanotube further away from the catalyst. Tip growth model explains the growth occurring at the other

end of the nanotube, at the tip. A catalytic particle is attached at the tip of the nanotube at the beginning of the formation of the CNT, and as more carbon atoms attach at the tip, the catalytic particle is carried along. (Figure 2.15)

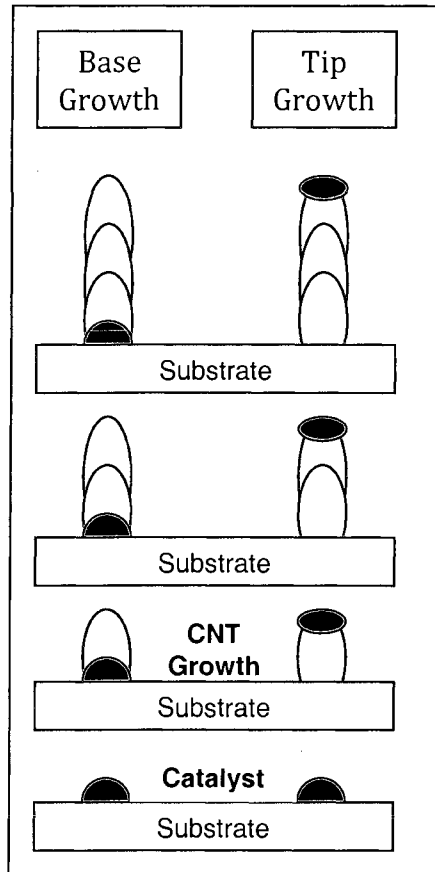


Figure 2.15: Base and Tip Growth Mechanisms

Growing CNTs using CVD depends on trial and error procedure to achieve good results for differing setups. However, a look at a multitude of differing processes and the accompanying results provides some generalizations about the effects of some parameters on the resulting CNTs produced.

J. Kong, *et al.* patterned  $3\mu\text{m}$  and  $5\mu\text{m}$  square catalyst pads by spin coating the aqueous catalyst suspension into wells created in a PMMA photoresist [6].

After evaporating the catalyst solvent, the PMMA was lifted off to leave only micro sized catalyst pads. The catalyst used was a solution of  $\text{Fe}(\text{NO}_3)_3 \cdot 9\text{H}_2\text{O}$ ,  $\text{MoO}_2(\text{acac})_2$ , and alumina nanoparticles in methanol. The CVD process was performed at  $1000^\circ\text{C}$  for 10 minutes with a feeding gas of methane at a flow rate of 1000 to  $6000 \text{ cm}^3/\text{min}$ . The resulting CNTs consisted of very straight, high quality SWNTs. Refer to Figure 2.16 below [6].

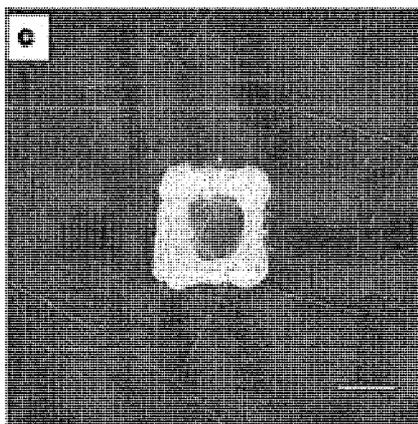


Figure 2.16: AFM Image of Catalyst Pad with SWNTS [6]

The SWNTs had diameters of 1-3nm and lengths up to  $20\mu\text{m}$ . TEM images show the SWNTs to have no amorphous carbon particles attached. These are very good results for device integration. The location of growth can be precisely controlled by exact placement of the catalyst pads. The SWNTs are very straight with little or no amorphous carbon attached. Other processes require an extra purification process after the CVD growth to remove particulates. In later publications [10, 20], this CVD procedure produced SWNTs in order to study their electrical characteristics. It is noteworthy that there was no mention of which flow rate of

methane produced the best results or any comparative analysis done. However, this is not a good process for growing large quantities. This process only resulted in a few scattered SWNTs instead of larger bundles as other procedures do. Before this CVD process can be integrated with device micromanufacturing, a further degree of control must be obtained. The SWNTs grow out radially from the catalyst pad. To reliably manufacture a device, the SWNT must be controlled to grow out from the catalyst pad in a single direction.

N. R. Franklin, *et al.* used the same catalyst as Kong above [56]. The major difference is that their tube furnace was able to accommodate an entire 4 in wafer. Most CVD furnaces are only able to process a 1 in<sup>2</sup> sample, so expanding to allow a 4 in wafer can significantly increase the throughput of the CVD process. The growth temperature was reduced to 900°C for 7 minutes. Methane was used as the feeding gas at a flow rate of 1500 ml/min. H<sub>2</sub> was co-flown with the methane at a rate ranging from 50 to 150 ml/min. The best results, shown in Figure 2.17 [56], was obtained with an H<sub>2</sub> co-flow rate of 125 ml/min.

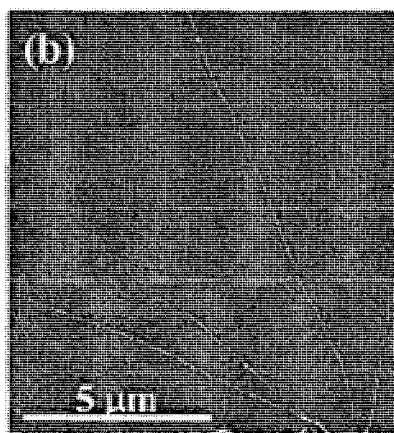


Figure 2.17: AFM of SWNT with 125 mL/min Co-Flow H<sub>2</sub> [56]

The resulting SWNTs were similar to those obtained from Kong, but these were only  $\sim 10\mu\text{m}$  in length. At an  $\text{H}_2$  co-flow rate of 50 ml/min, significant amounts of amorphous carbon are deposited on the wafer. At a co-flow rate of 150 ml/min, there is no growth of SWNTs. The reason for the variation in growth is due to the reactions between  $\text{H}_2$  and methane ( $\text{CH}_4$ ).  $\text{H}_2$  decreases the rate at which  $\text{CH}_4$  can decompose, thereby reducing the amount of carbon available for growth, and causing a slower growth mechanism [56]. The lower temperature and shorter growth time added with the  $\text{H}_2$  produced SWNTs half as long as those produced by Kong. The growth time could be lengthened, but the longer time could also increase the amount of amorphous carbon deposited. The resulting SWNTs are very similar to those obtained by Kong. The ability to process entire wafers is a progression towards integrating the CVD growth process with micromanufacturing techniques for device creation, and the long, straight, high quality SWNTs are ideal for use in a nano device.

B. Zheng, *et al.* used a similar catalyst as the above two, but applied with a sol-gel technique [61, 66].  $\text{Fe}(\text{NO}_3)_3 \cdot 9\text{H}_2\text{O}$ ,  $\text{MoO}_2(\text{acac})_2$ , and aluminum tri-sec-butoxide were dispersed in ethanol was used to create the aerogel. Processing the aerogel creates a fine powder that was finally used as the catalyst in the CVD furnace. The powder was placed directly in an alumina boat before going into the CVD furnace. The furnace was heated to  $860^\circ\text{C}$  before flowing carbon monoxide ( $\text{CO}$ ) at 1000 sccm for 15 to 120 minutes. The temperature was optimized at  $860^\circ\text{C}$  because at  $880^\circ\text{C}$ , the yield is reduced, and at  $820^\circ\text{C}$ , the amorphous carbon on the SWNTs increases. The flow rate of  $\text{CO}$  was also studied. At flow rates less

than 500 sccm, MWNTs begin to form, and flow rates higher than 1000 sccm resulted in the best quality SWNTs. Even at the best quality, the product after the CVD process contains impurities of amorphous carbon and aerogel support as shown in Figure 2.18 [61].

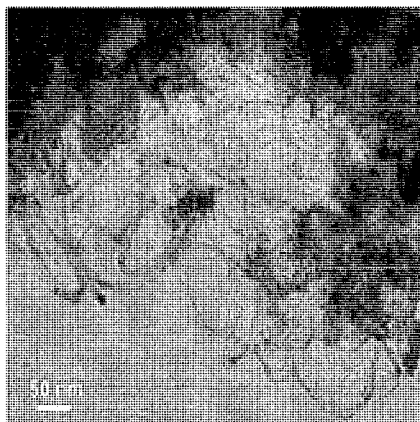


Figure 2.18: TEM Images of the Raw Unpurified SWNTs [61]

A purification process of washing in HF followed by a two-stage oxidation procedure with rinsing in HCl after each stage is needed to remove most of the metal impurities, although a negligible amount of metal oxide still remains on the SWNTs [61]. As shown in Figure 2.18, the resulting yield of SWNTs is much larger than either of the previous methods. The high yield comes at the cost of the extra purification processing that still does not result in the same high quality as the previous methods. The SWNTs are also bundled and twisted together. To do any characterization of an individual nanotube would require further processing to separate and disperse the clumps of nanotubes. This CVD procedure is better

suitable for producing SWNTs for projects where the location and orientation of growth is not critical and higher quantities are needed.

C. Ducati, *et al.* used a 3 nm thin film of Ni on top of a silicon dioxide ( $\text{SiO}_2$ ) layer for the catalyst material [54]. The  $\text{SiO}_2$  layer prevents the Ni from diffusing into the Si wafer and creating nickel silicide. After the wafer is coated with the Ni, it is annealed at  $700^\circ\text{C}$  for 15 minutes to cause the Ni layer to break into small nano islands. The CVD process was performed at temperatures ranging from  $550^\circ\text{C}$  to  $850^\circ\text{C}$  for 15 minutes with a feeding gas of  $\text{C}_2\text{H}_2$ . A plasma enhanced CVD (PECVD) process was also performed at each temperature. The thermal CVD (non PECVD) resulted in bundles of CNTs similar to Zheng above except the resulting CNTs in this procedure were MWNTs instead of SWNTs. As the growth temperature was increased, the size of the CNTs increased as well as the number of walls or shells of the MWNTs. The CNTs synthesized by PECVD were vertically aligned. At  $550^\circ\text{C}$ , the outer diameter of the MWNTs from the PECVD were 2 times the size of the thermal CVD. That factor decreased to 1.3 times at  $850^\circ\text{C}$ . Figure 2.19 shows an overview of both thermal and PECVD results at various temperatures [54].

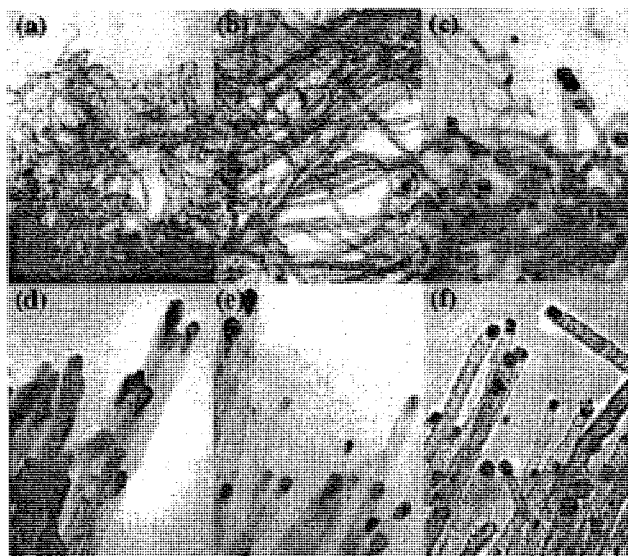


Figure 2.19: TEM of Synthesized CNTs from Thermal CVD (a-c) and PECVD (d-f). Temperatures Increase Left to Right, 550°C, 700°C, and 850°C [54]

Both the thermal and PECVD results have Ni particles at the tips of the CNTs suggesting a tip growth mechanism. The MWNT formation over SWNT formation is probably due to the grain boundaries and large size of the Ni islands used as a catalyst [54]. This CVD procedure shows the importance of the size and crystalline nature of the catalyst to the resulting CNTs produced.

S. Hofmann, *et al.* further studied PECVD for synthesizing CNTs [55]. After a 6 nm layer of Ni was sputtered on the oxidized Si wafer, the Ni layer was patterned using traditional lithography techniques. The patterned wafers were first processed for 10 minutes at 450°C with methane, ethylene, and acetylene plasma, each diluted with ammonia. The methane produced no growth. The ethylene had minimal growth. Finally, the acetylene plasma resulted in vertically aligned film of carbon nanofibers (CNF). The acetylene plasma was then used for PECVD

processing at 500°C, 270°C, and 120°C. At 120°C, there is minimal growth. The resulting growth at 500°C is shown in Figure 2.20 [55].

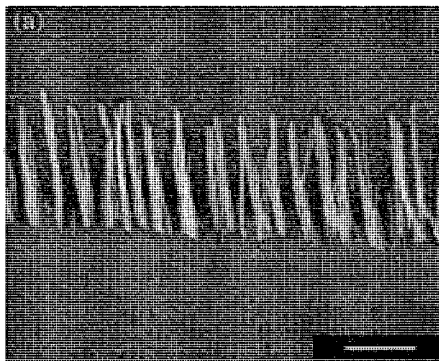


Figure 2.20: SEM Image of Vertically Aligned CNFs [55]

The low temperatures at which synthesis of carbon nano structures was demonstrated shows promise that a CVD process can be combined with traditional manufactured semiconductors without damaging them with high temperatures. However, CNFs are not as promising as CNTs because the fibers do not have a crystalline lattice structure and do not demonstrate the same electrical and mechanical characteristics of CNTs. The same growth mechanisms that govern CNT synthesis apply to growing CNFs, so, possibly with further research, a low temperature CVD process could produce CNTs.

T. Kato, *et al.* applied a radio frequency to PECVD techniques. Two substrate materials were used to grow CNTs on simultaneously [59]. A Ni substrate was prepared by exposing to plasma gas discharges of H<sub>2</sub>, He, and Ar. The H, He, and Ar ions implanted on the surface acted as the catalyst material. The Ni substrate was attached to the RF electrode in the CVD furnace. Another

substrate used zeolite as a support material for a Fe/Co catalyst. The PECVD was operated for 15 minutes at temperatures ranging from 550°C to 850°C with a mixture of methane and hydrogen as the feeding gas. On the Ni substrate, hydrogen showed little growth. Helium also produced little growth, but more than hydrogen. Argon produced a high density of MWNTs. The substrate located on the heater of the PECVD formed bundles of SWNTs even at temperatures of 550°C as shown in Figure 2.21 [59].

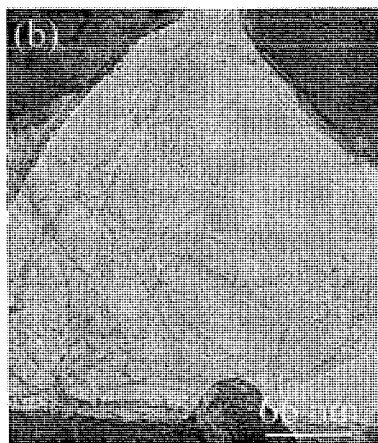


Figure 2.21: Image of SWNTs Produced by RF-PECVD [59]

This was the first time PECVD was used to form SWNTs. The SWNTs appear to have some impurities, but the quality appears comparable to purified SWNTs produced by Zheng. The main advantage of this process is the 330°C drop in processing temperature. This shows more possibility of a CVD process that can be integrated with current semiconductor manufacturing.

Z. Y. Juang, *et al.* studied the effect of ammonia ( $\text{NH}_3$ ) on CVD growth of CNTs [67]. Ni catalyst pads,  $10\mu\text{m}^2$ , were fabricated using typical lithography

techniques. The CVD process was performed at 900°C for 5 minutes with CH<sub>4</sub> or a mixture of CH<sub>4</sub> and NH<sub>3</sub> at a flow rate of 500 sccm. With Ar used as a diluting gas and the flow rate of CH<sub>4</sub> fixed, as the flow of NH<sub>3</sub> decreases, growth slows and the vertical alignment of the CNTs disappears. When the flow rate of CH<sub>4</sub> is not fixed and no diluting gas is used, the introduction of NH<sub>3</sub> has the opposite effect. As the flow of NH<sub>3</sub> is increased, the density of CNTs and vertical alignment both deteriorate. Figure 2.22 [67] shows the highest density growth with CH<sub>4</sub> = 3 x NH<sub>3</sub>. A further study delays introducing NH<sub>3</sub> at the beginning of the growth process.

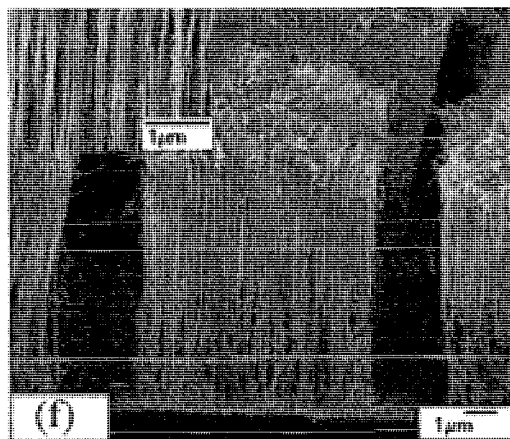


Figure 2.22: SEM Image of High Density Growth of CNTs [67]

The longer the NH<sub>3</sub> is delayed from being introduced reduces the density of CNTs produced [67]. A thorough study of one specific parameter in the CVD process can give a good picture of kinematics of the chemical interactions that are occurring during growth to help better model the process. This study was able to reveal that not only is the density of CNTs produced directly affected by the amount of carbon

available, but the vertical alignment is as well. With the right mixture of  $\text{CH}_4$  and  $\text{NH}_3$ , the density of CNTs produced was very high, which can be useful for any project requiring large quantities of CNTs. Hydrogen storage, creating hybrid cements and polymers for strength and rigidity, and fuel cell membranes can all use this type of CVD process to produce the necessary CNTs where quantity and density can be an issue.

J. Chen, *et al.* performed a parametric study of  $\text{CaCO}_3$  for growing MWNTs with CVD [57]. The  $\text{CaCO}_3$  catalyst was processed to give specific concentration ratio with Co, with the end product being a fine powder that was uniformly spread onto a quartz boat to go into the CVD furnace. The CVD process was performed at  $750^\circ\text{C}$  for 20 minutes with acetylene as the feeding gas with a flow rate of 100 ml/min. The CNTs produced were then purified by washing in nitric or hydrochloric acid. (Figure 2.23) [57]

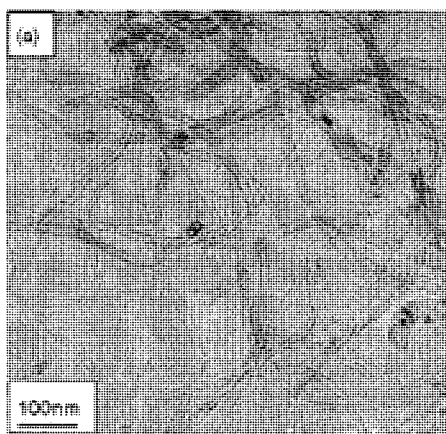


Figure 2.23: TEM Images of Resulting CNTs [57]

The  $\text{CaCO}_3$  catalyst worked best when used as a support for Fe-Co. The  $\text{CaCO}_3$  support reduces the amorphous carbon impurities on the resulting CNTs [57]. The  $\text{CaCO}_3$  catalyst support was investigated from several viewpoints to get a better idea of interactions that occur during the growth process.

S. Li, *et al.* adapted the CVD process of Kong above to work in a water based solution instead of a methanol suspension [68]. Standard lithography could be used instead of the more expensive e-beam lithography. The only change made the catalyst was the addition of ammonia to prevent the Fe from becoming soluble in water. The CVD parameters were slightly adjusted, dropping the temperature to  $900^\circ\text{C}$ , adding a co-flow of hydrogen (200 sccm) to the methane (1000 sccm) feeding gas, and extending the growth time to 12 minutes. The resulting SWNTs contained some Y-junctions as shown in Figure 2.24 [68].

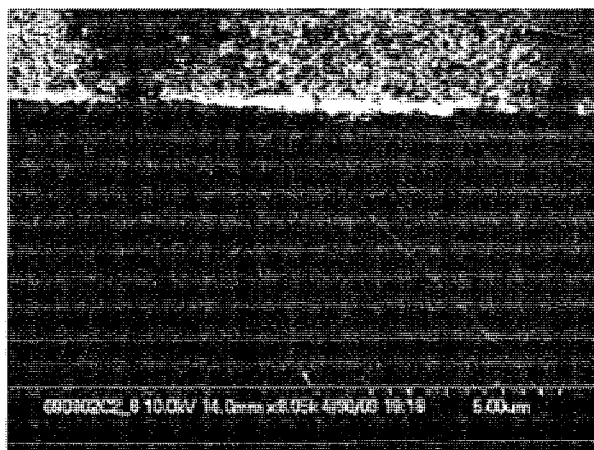


Figure 2.24: SEM Images of Y-Junction SWNT [68]

The Y-junctions are interesting because they may point to a method to connect different SWNTs together. They provide a better study of the electron

transport through a SWNT, or add a missing element to growth mechanism model. The cheaper lithography techniques used in this study allows more research to be done with SWNTs without requiring large funding grants or access to expensive equipment.

Z. Y. Juang, *et al.* performed further research on the effect of adding ammonia as a co-flow reagent with the carbon feedstock gas [69]. Instead of looking at the effect with a CH<sub>4</sub> feeding gas, C<sub>2</sub>H<sub>4</sub> is looked at. The same 10 nm thick 10μm<sup>2</sup> Ni catalyst pads were fabricated on a Si wafer with a SiO<sub>2</sub> layer. The temperature of the CVD process was varied from 800°C to 950°C. The flow rates of C<sub>2</sub>H<sub>2</sub> and NH<sub>3</sub> were also varied to determine what impact NH<sub>3</sub> had on the overall CNT produced. The resulting CNTs had a bamboo structure as show below in Figure 2.25 [69].



Figure 2.25: TEM of CNT Bamboo Structure [69]

This bamboo structure varies in diameter and length as the amount of carbon stock for growth changes with the amount of NH<sub>3</sub> that is added.

Each of the above studies researched one aspect of the CVD process for growing CNTs. While many of the papers varied in too many parameters to make a direct correlation about a single aspect of the process, an examination of the entire scope of CVD synthesis of CNTs shows how varied and adjustable the process is to get a specific type of result. SWNTs, MWNTs, and CNFs can all be produced in varying amounts and qualities. However, looking at the different setups and

resulting CNTs produced provides generalizations about the current state of synthesis. Thin films tend to produce large quantities of MWNTs or CNFs, but have too large of grain boundaries and particulate size to grow smaller SWNTs. Aqueous solutions of catalyst materials with very small nanoparticles that are spin coated onto the substrate produce higher quality SWNTs, but at the cost of lower quantities of production. PECVD is able to synthesis CNTs at lower temperatures than thermal CVD, but at the cost of creating more amorphous carbon and CNTs of a lower quality. Looking at the larger scope of all CVD processes, the progression and refinement of the CVD technique to synthesis CNTs becomes clear as larger quantities of CNTs can now be produced with more control over their location, orientation, and physical characteristics. CVD fabrication has shown an ability to grow large quantities of high quality SWNTs in generalized locations. Bundles of SWNTs can be synthesized in patterned arrangements by controlling the location and pattern of the catalyst material. The CVD process unfortunately does not integrate well with fabrication of microelectronic devices. CVD requires high temperatures, typically greater than 800°C. Semiconductor devices are not stable at such high temperatures. The doping of P-type and N-type regions in the semiconductor must remain inside strict specified boundaries. High temperatures cause the doped atoms to migrate through the substrate, thereby hindering performance or possibly causing device failure.

## **2.3 Device Fabrication**

With all of the unique and advantageous properties of CNTs, there has been a lot of research on how to incorporate CNTs into devices. NEC and IBM have both been leading the way with producing CNT devices. Both companies have demonstrated CNT transistor devices. NEC recently concluded a patent agreement to license their CNT patents with a U.S. company, SouthWest Nanotechnologies [70]. Although several companies have made press releases about future products incorporating CNTs [2, 71], few devices have been produced for mass manufacturing. According to Zhihong Chen, a research member at IBM, the two biggest hurdles to fabricating CNT electrical circuits are producing CNTs with precise characteristics and being able to place and align CNTs at the desired positions [72]. Incorporating CNTs into devices requires CNTs with specific parameters to be synthesized and then precisely placed into the device architecture. There has been much progress with manufacturing CNTs with specific characteristics as can be seen from the previous section. Controlling how to physically integrate the CNT into the electrical device is still a difficult challenge that has not been solved in a manner adequate for mass manufacturing. There have been several methods devised to control the placement of CNTs, direct manipulation, electric field, and lbl.

### **2.3.1 CNT Direct Manipulation**

The most common method for building CNT devices involves manipulating CNTs to prefabricated contacts. Manipulating CNTs can prove to be difficult due to their near atomic size. The first and still most common method for manipulating

CNTs is by using an AFM tip [21, 73-76]. CNTs manufactured by any of the methods mentioned above can result in bundles of CNTs that need to be separated and dispersed on a substrate. This will randomly place the CNTs on the surface. Using the AFM to manipulate and move the CNT adds an extra benefit by being able to image the surface with the same AFM equipment. The AFM can first run in non-contact mode to image the surface and find where the CNTs are located. After the CNTs have been located, the AFM can be run in contact mode to use the AFM tip to make contact with the CNT and manipulate it to move it where it is needed. A contact force of 20 nN is strong enough to bend and displace CNTs [73]. This procedure has been used to build and characterize CNT wires [21, 74, 75] and transistors [21, 76]. The AFM provides a very flexible method to manipulate and precisely position CNTs into device architectures. The flexibility of this method has the disadvantage of being a tedious, labor intensive task. Building single devices for testing and research purposes are ideal uses for AFM manipulation. For mass manufacturing CNT devices, a more automated system must be developed.

### **2.3.2 CNT Electronic Field Placement**

One of the first techniques tried to control the placement of CNTs on a substrate or device utilized an electric field [77, 78]. Those first experiments showed that an AC electric field could be used to align CNTs. Zhang, *et al.* proposed the SWNT is aligned in a DC electric field due to a dipole moment along the tube axis caused by static polarization [79]. This idea assumed one end of the SWNT was fixed to the surface as during CVD synthesis. Chen, *et al.* suggested the SWNT alignment was due to electrostatic force when both ends of the SWNT are

free [80]. His work was able to place SWNTs across a gap of 25  $\mu\text{m}$  as shown in Figure 2.26 below [80].

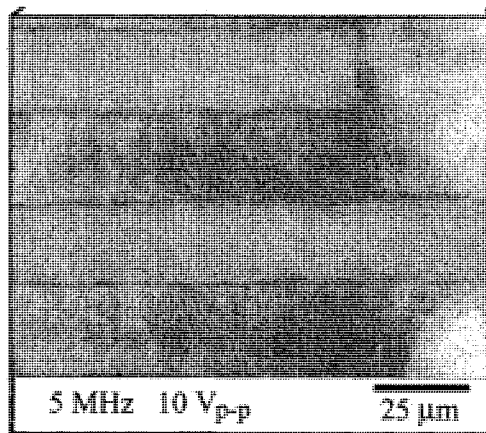


Figure 2.26: SEM of SWNT Aligned with AC Electric Field [80]

The electrodes were fabricated with standard lithography process. Those electrodes were then submerged in an ethanol solution of suspended SWNTs. An AC signal of 10  $V_{pp}$  was applied at a frequency of 5 MHz for 15 minutes. The AC electric field was able to align and attract SWNTs to the electrodes. Lower applied voltages resulted in fewer SWNTs being attracted to the electrodes. Lower frequencies resulted in decreased alignment of the SWNTs [80]. This study demonstrates that an AC electric field can be used to attach SWNTs to electrodes. However, large quantities of SWNTs were grouped around the electrodes, and no individual SWNT or bundle of SWNTs could be precisely placed. Changing the electrode configuration can improve the results. Dipasquale, *et al.* achieve a few nanotube ropes across a 3  $\mu\text{m}$  gap using a 1 MHz AC signal with a voltage of 5  $V_{pp}$  and 2 V DC bias for 30 seconds [81]. With a 1  $\mu\text{m}$  gap, Chen, *et al.* was able to get a

single SWNT bundle to align suspended across Au electrodes using an AC signal of 20 V<sub>pp</sub> at 2 MHz for 10 minutes [24]. These results are pictured below in Figure 2.27 [24].

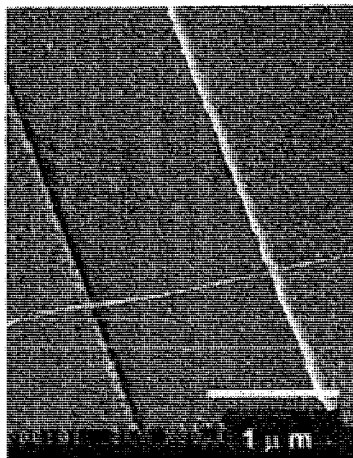


Figure 2.27: SWNT Bundle Across Two Electrodes [24]

Using an electric field, particularly with an AC signal, has been demonstrated to align and attach CNTs to electrodes. To achieve control over individual CNTs, the electrodes must be designed to achieve higher electric fields with smaller gaps. These requirements may prevent this technique from use in fabricating electronic devices. Specific electronic device architectures may not have electrodes that allow for good alignment and attachment. The small gap size also limits the use of CNTs for connecting nanowires.

### **2.3.3 CNT Layer-by-Layer Placement**

Lbl is a self-assembly mechanism to build structures from electrostatic forces [82]. This new technique is a bottom-up approach to building nano-sized devices. Polyelectrolytes can have different electrostatic charges depending on their

respective pH. Polyelectrolytes that have a positive charge in a neutral solution (pH 7) include poly(allylamine hydrochloride) (PAH), poly(ethylenimine) (PEI), and poly(diallyldimethylammonium chloride) (PDDA). Other polyelectrolytes, poly(sodium styrenesulfonate) (PSS) and poly(acrylic acid) (PAA), have a negative charge at pH 7. When polyelectrolytes with different charges are placed in a common solution, they will repel those with the same charge and attract those with the opposite charge. When these polyelectrolytes are added to aqueous solutions of CNTs, they are attracted to the CNTs and noncovalently “bond”. The bonding energy is not a true chemical bond. Rather they are attached by electrostatic forces [83]. After the CNTs have been functionalized with a polyelectrolyte, they can be self-assembled to a substrate using the same electrostatic forces with lbl. A similar process is used to fabricate CNT thin films [28-31, 84]. To control precise placement, films with a specific charge can be patterned on the substrate to create connection pads where the CNTs can be connected. The patterned film is commonly made of self-assembled monolayers (SAMs) [85, 86]. The SAMs layer can be patterned using standard lithography techniques. The substrate is then submerged in a solution of CNTs. The CNTs will then self-assemble on the substrate in the patterned SAMs layer with electrostatic forces. This process is very accurate at building specific CNT architectures as demonstrated in Figure 2.28 below where Wang, *et al* were able to fabricate complex line structures with linked SWNTs [86].

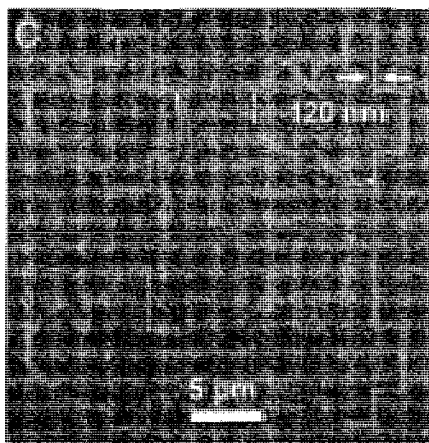


Figure 2.28: Controlled Placement of SWNTs [86]

This technique allows for good control over the placement of CNTs. The downside to this technique is the fabrication and stability of the SAM film. To form a SAM film with low defects can take from 12 hours to 2 days [87]. SAM production also requires a high purity level in the materials. A small 1% impurity can significantly reduce the order of the final film [87]. The surface attraction of the SAM layer to the substrate is also weak when outside of the aqueous environment. The interaction of sulfur-gold is around 45 kcal/mol compared to 83 kcal/mol for a C-C bond [87]. The process to fabricate a SAM film is also reversible. While this is useful to make corrections in a laboratory to fix a non-functional device, protection measures would have to be taken to prevent a working device from breaking apart in a working environment. These issues with SAM films have prevented them from being incorporated into mass manufactured nano devices.

## **2.4 Dispersion**

One of the largest tradeoffs in manufacturing CNTs is quantity and control. CNTs can be made in large quantities, but the results are large bundles of intermixed CNTs. When all of the CNT material is collected, it appears as black powder soot. The bundles are unusable for controlled placement or individual manipulation. To further complicate the situation, CNTs are not dissolvable in water. They remain as clumps and bundles. The synthesis of small quantities of CNTs can be costly and time consuming. Producing them in larger quantities can make them financially feasible for device fabrication. There have been several methods devised to separate bundles of CNTs into usable solutions.

### **2.4.1 Surfactants / Polymers**

The most common method for dispersing CNTs in water involves adding some surfactant to the solution and sonicating for an extended period of time. Surfactants can bond to CNTs covalently or noncovalently depending on the process of dispersion. Some surfactants that bond covalently require the CNT to be acid treated to break some of the C-C bonds or functionalize the CNT [88, 89]. As the literature shows, the issue is further complicated by some differing studies; some claim the bonding of polymer surfactants to CNTs is covalent while others claim the bonding is noncovalent [90]. Common surfactants include sodium octylbenzene sulfonate (NaDDBS) [91], dodecyltrimethylammonium bromide (DTAB) [92], and Triton X-100 [91], sodium dodecyl sulfate (SDS) [93]. The quality of the dispersion is dependent on the ratio of surfactant to CNTs in the suspension. Typical ratios of surfactants to CNTs varied for the above list of surfactants from 1:5

to 1:10 by weight [91]. Suspensions of CNTs can last up to 2 months without coagulating using the above mentioned surfactants [91]. A second group of surfactants used in dispersing CNTs in solution include polyelectrolytes. Dispersions have been made with PSS [30, 83], PDADMA [32], PAA [30], and PAH [32, 83]. The polyelectrolytes self-assemble on the sidewall of the CNTs with 1:1 electrostatic force. Some methods use a single polyelectrolyte to functionalize the sidewall of the CNTs. Because all the CNTs have the same external charge, they repel each other, causing the dispersion. Another method repeats the 1:1 process with polyelectrolytes of alternating charge [83]. The quality of polyelectrolyte layers improves as more layers are added using 1:1 self-assembly. Larger layers also increase the surface area, allowing a greater total charge to accumulate on the CNT. With each layer, the charge of the functionalized CNTs increases, causing a greater repelling force and a better suspension. Because the polymer surfactants only bond to the CNT by electrostatic force, the chemical structure of the CNT remains unchanged. This allows the CNT to keep the same mechanical and electrical properties. However, the polymers can affect device properties when connected into a device as explained previously with electrical properties.

#### **2.4.2 Electrical**

Other dispersion techniques have been devised to avoid some of the issues caused by chemically functionalizing CNTs. Electric fields have been used to create suspensions of CNTs. Both DC [94] and AC [95] fields have been shown to create a dispersion with CNTs in water. Acid treated CNTs are placed in a water solution and sonicated for a short time of 20 minutes. Two Al electrodes are

placed in the solution and an AC signal is applied. After 4 hours, the AC field is able to separate and disperse the CNTs [94].

## CHAPTER 3

### SWNT SUSPENSIONS

The fabrication methodology devised in this work builds from and utilizes research occurring in the Institute for Micromanufacturing (IfM) at Louisiana Tech University. The expertise of Dr. Yuri Lvov in lbl self-assembly has provided many research projects to employ the useful technique. This section will outline two procedures that were devised to disperse SWNTs using lbl. The dispersions were all performed with commercially purchased SWNTs from MicrotechNano with the specifications listed in Table 3.1 below.

Table 3.1: MicrotechNano SWNT Specifications

<b>External Diameter</b>	< 2 nm
<b>Length</b>	1-5 $\mu\text{m}$
<b>Purity</b>	CNT > 90% SWNT > 50%
<b>Amorphous Carbon</b>	< 5%
<b>Ash</b>	< 2 wt %
<b>Specific Surface Area</b>	500 - 700 $\text{m}^2/\text{g}$
<b>Thermal Conductivity</b>	$3235 \pm 400 \text{ W/m-K}$
<b>Ablating Temperature</b>	520 - 610° C (in air)
<b>IG / ID (Raman Data)</b>	> 9

An image of the SWNT powder from MicrotechNano is shown previously in Figure 2.13. At the end of this section, there is a discussion of near-edge x-ray absorption fine structure spectroscopy (NEXAFS) to characterize the commercial SWNTs after

being acid treated. The results demonstrate how much molecular damage can be done to the SWNT when performing dispersions with acid treatments.

### 3.1 Layer-by-Layer Self Assembly

The dispersion techniques described in this study use PSS and PAH to achieve a high quality suspension of SWNTs in water. The molecular structure of both polyelectrolytes is shown below in Figure 3.1.

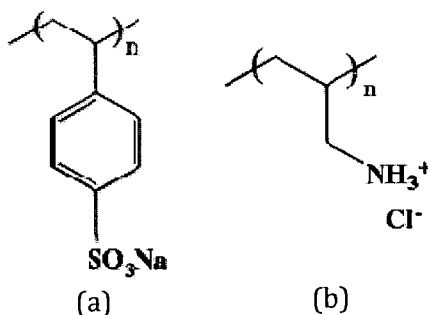


Figure 3.1: Molecular Structure of PSS (a) and PAH (b)

The PSS and PAH were both purchased from Sigma-Aldrich, with the PSS having a molecular weight of 70,000 and PAH having molecular weight of 56,000. Polyelectrolytes are defined as cationic or anionic based on their charge when fully ionized. Polycations have a positive charge while polyanions have a negative charge. Different polyelectrolytes become ionized at different pH. What pH ionization occurs at is defined as the pKa or acid-ionization constant. The pKa for a generic acid  $HA$  is defined below in Equation 3.1.

$$\text{pKa} = -\log_{10} \left( \frac{H^+ \cdot A^-}{HA} \right) \quad (3.1)$$

The same equation can be applied to a base  $BH^+$  by replacing  $A^-$  with  $B$ . The pKa describes the pH at which the polyelectrolyte is 50% ionized. So increasing the pH above the pKa for an acid (polyanion) will increase the ionization while decreasing the pH below the pKa for a base (polycation) will do the same. The pKa for PSS is 0.5 and the pKa for PAH is 8.5. A common solution with a pH between 0.5 and 8.5 will cause both PAH and PSS to be fully ionized, giving PAH a positive charge and PSS a negative charge.

Lbl is a flexible technique to build layers of polymers or nano-particles on a surface a few nm at a time. The same technique can be used to build layers of larger particles by first coating them with a layer of polyelectrolytes to give their surfaces a strong and distinct charge. For multiple layers to be built, the layers must alternate charges. If the surface originally has a negative charge, a cationic (positively charged) polyelectrolyte layer can be self-assembled, creating a surface with a positive charge. An anionic (negatively charged) polyelectrolyte layer can then be self-assembled, creating a negatively charged outer surface. This basic process is used to build layers of polyelectrolytes on the surface of SWNTs, causing them to disperse in an aqueous solution.

### **3.1.1 Alternating Polyelectrolytes**

The first method of dispersion devised by Dhullipudi, *et al.* involved building multiple layers of PSS and PAH on the surface of SWNTs [83]. Solutions of PSS and PAH were created in deionized water with a concentration of 2 mg/ml. SWNTs were added to a solution of deionized water in a concentration of 0.5 mg/ml. The pH of each solution was adjusted by adding HCl until a pH of 3 was achieved. At

this pH, both PSS and PAH will be ionized, giving them opposite charges. At a pH of 3, SWNTs become positively charged according to Zeta potential measurements [83]. The positive charge on the surface of the SWNTs will attract negatively charged polyions to self-assemble around the SWNT. The SWNTs were centrifuged out of the water solution and added to a PSS solution. After sitting for 10 minutes, the PSS self-assembled onto the surface of the SWNTs, changing the Zeta potential from positive to negative. The SWNTs were then centrifuged out of the PSS solution and rinsed in deionized water adjusted to a pH of 3. The rinsing procedure was repeated 3 times with the SWNTs be centrifuged out each time. After the final rinsing, the SWNTs were added to a PAH solution. The positively charged PAH self-assembled onto the PSS layer already built on the SWNT surface when allowed to sit for 10 minutes. The process can be repeated by alternating the polyions between positive and negative charges with a rinsing process between each stage. Repeating the process and building more layers onto the SWNT will improve the dispersion. An image of the SWNTs with two bilayers of PSS / PAH in suspension are pictured below in Figure 3.2 [83].

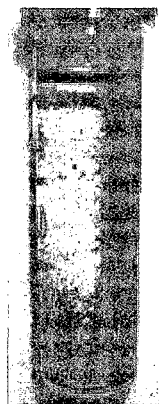


Figure 3.2: SWNT Suspension with PSS / PAH.

The SWNT suspension with 2 bilayers of PSS / PAH was stable for 5 hours before settling [83]. This process was used to make SWNT suspensions used for different fabrication testing.

### **3.1.2 Single Polyelectrolyte**

A simplified method of dispersing SWNTs was also developed by R. Chevious, *et al.* using only a single polyelectrolyte, PSS [96]. This process uses a single electrolyte, PSS, to create a suspension of SWNTs. Chevious was able to determine the minimum ratio, by mass, of PSS and SWNT of 1:8 was required to create a stable suspension [96]. Solutions of PSS were created in concentrations of 4 mg/ml in deionized water. HCl was again added to adjust the solution to a pH of 3. Purchased SWNTs were added to the PSS solution to create a concentration of 1 mg/ml. The solution was then sonicated for at least 5 hours. By varying the ratios of PSS to SWNT and the concentrations of each of their respective solutions, an ideal recipe was established. The ratio of PSS to SWNT of 5:1 results in the most stable suspension. Increased sonication, up to 20 hours, improves the suspension. The SWNT / PSS suspensions remained stable for more than 24 hours. A SWNT / PSS suspension produced using this method is picture below in Figure 3.3.

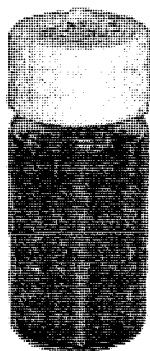


Figure 3.3: SWNT Suspension with Single Polyelectrolyte, PSS.

The suspension in Figure 3.3 is homogeneous with no visible conglomerates of SWNT bundles. TEM studies on samples made with 4 mg/ml PSS and sonicated for 5 hours, shown in Figure 3.4 below, also reveal reduced bundling of SWNTs as sonication time is increased [96].

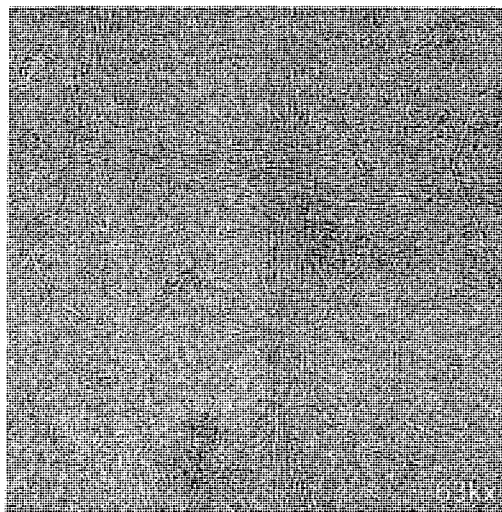


Figure 3.4: TEM of SWNT Suspension[96]

### **3.2 NEXAFS Study of Suspensions**

In NEXAFS, a sample is assailed by a beam of tunable X-ray photons beginning at an energy level below the core-level binding energy of the target atom.

The energy level increased beyond the target binding energy, giving a range of  $\approx 70$  eV. X-ray energies below the core-level binding energy cannot be absorbed by the target atom. When the X-ray energies reach the level of the core-binding electron, there is a sharp peak in the absorption because the X-rays have sufficient energy to excite a core electron which then emits a photo-electron and/or an Auger electron. This photo-electron can hit a neighboring atom with enough energy to excite its core-level electron. The process is repeated, creating an oscillation in the absorption pattern detected due to interference from the photo-electron emissions from the target and neighboring atoms.

The peaks and oscillations in the NEXAFS spectra allows specific bonds in molecules, ie C=C, C-C, and C-O bonds, to be detected with high accuracy. The spectra measurements in NEXAFS can be detected in three different modes, Auger electron yield (AEY), partial electron yield (PEY), or total electron yield (TEY) [97]. Taken in the above order, each method has higher sensitivities to bulk or surface effects in the sample. The experiments were performed in PEY mode. All of the NEXAFS experiments were conducted at National Synchrotron Light Source (NSLS) at Brookhaven National Laboratory in the end station along the U7A beamline.

### **3.2.1 SWNT Acid Treatment**

Some dispersion techniques use an acid treatment to functionalize the CNT. This process is often referred to as digestion because the acid breaks down the CNT. Because the structure of a CNT, especially a SWNT, is critical to its electrical and mechanical properties, this study compares different acids that are used to functionalize SWNTs in varying concentrations to see how each acid affects the

structure of a SWNT. To determine the functionalization of the SWNTs, NEXAFS was employed because it can provide physical and chemical information, including structural properties and local chemical functionalities [98].

The SWNT samples were prepared by sonicating 50 mg of purchased SWNTs in solutions of  $\text{HNO}_3$  or  $\text{HCl}$  for 2 and 10 hours. Samples were made with concentrations of 5 and 10% of  $\text{HNO}_3$  and 5%  $\text{HCl}$ . These samples were also compared with a plain sample of SWNTs. The solutions were smeared onto a Cu tape and attached to the sample bar in the UHV chamber end station. The light spectrum gathered was processed through pre-edge and post-edge normalization scripts. The pre-edge was first subtracted to zero. The post-edge was normalized by dividing the pre-edge normalization by the post-edge jump. This eliminates any intensity changes due to changes in total carbon content of the sample [99]. The resulting spectra at energies near the bonding energy of carbon are shown below in Figure 3.5 and Figure 3.6 [98].

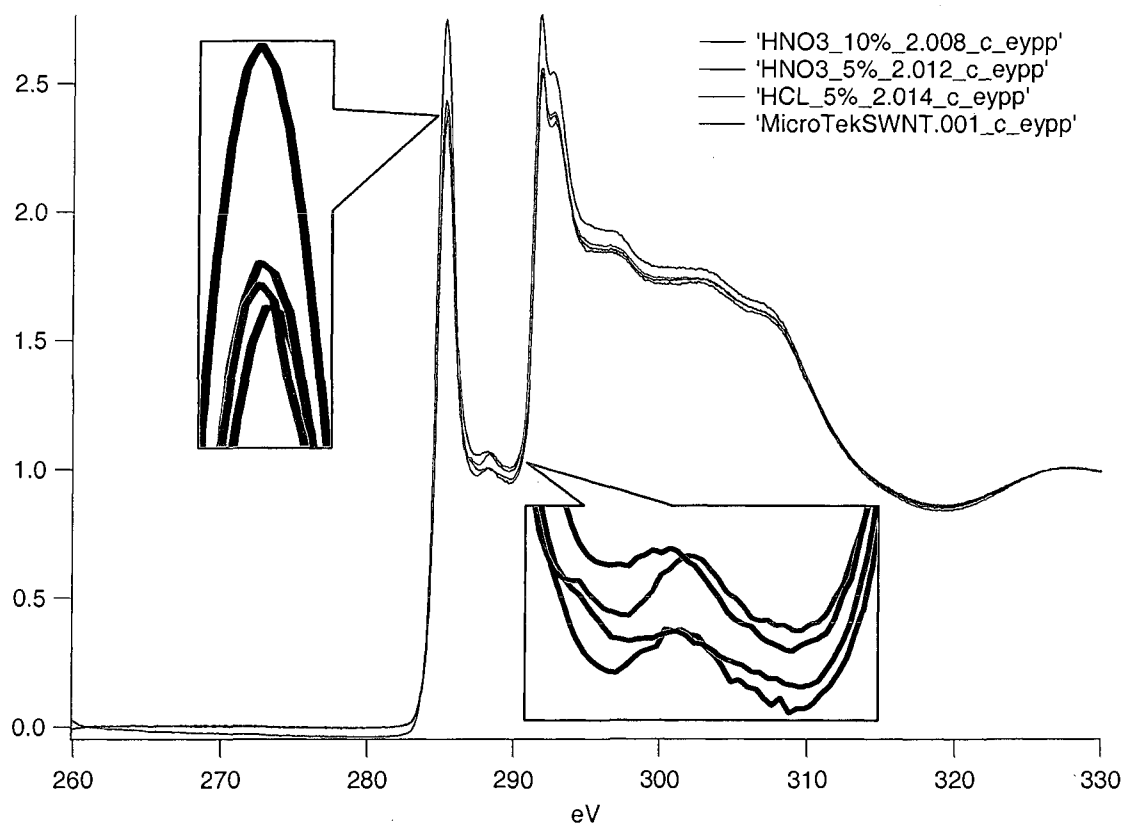


Figure 3.5: Carbon Atom NEXAFS After 2 Hour Acid Treatment

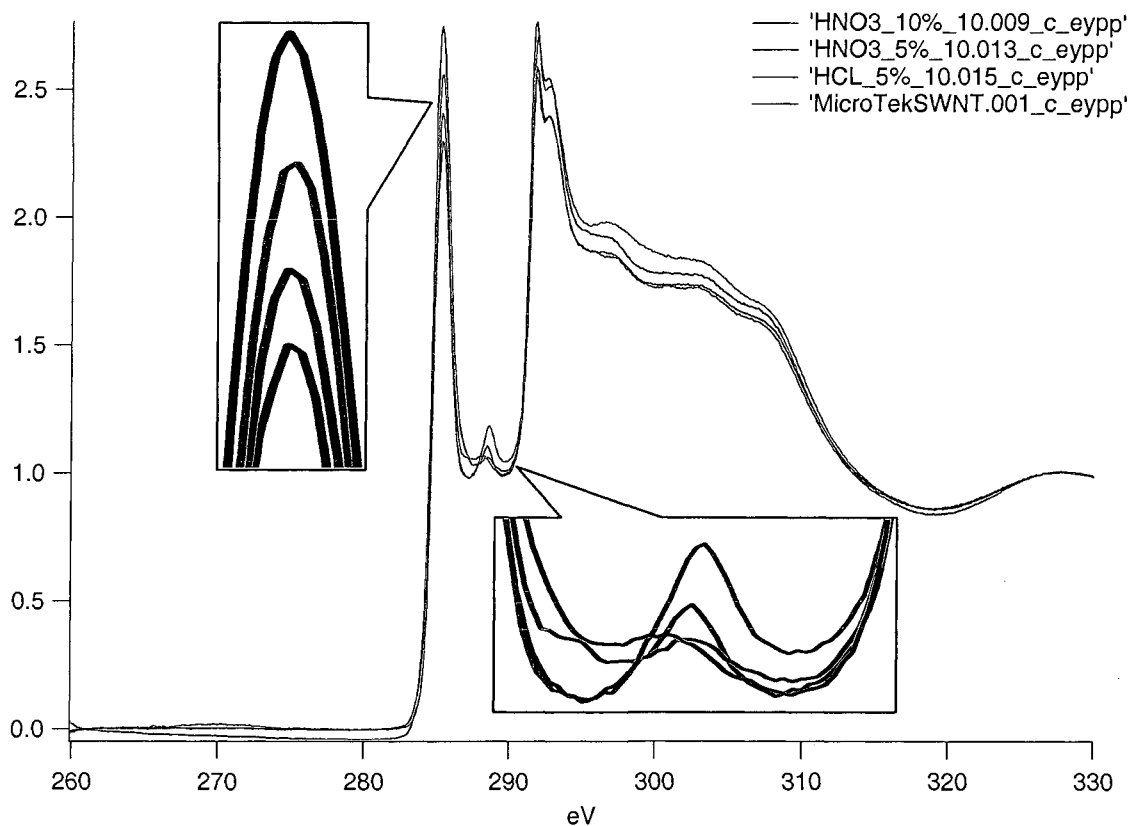


Figure 3.6: Carbon Atom NEXAFS After 10 Hour Acid Treatment

Carboxylate groups have characteristic peaks at 288-289 eV (C=O  $\pi^*$  resonance), 296 eV ( $\sigma^*$  resonance), and 302 eV (C=O  $\sigma^*$  resonance) [97]. Similar NEXAFS studies on CNTS have shown characteristic sharp C-C  $\pi^*$  transitions at 285 eV,  $\sigma^*$  C=C bond excitation at 292 eV, small peaks in the 287 - 290 eV due to  $\pi^*$  C=O and  $\sigma^*$  C-O resonances [99].

The NEXAFS spectra results from this investigation also fit in with the above characteristic peaks. A study of the above two graphs (Figure 3.5 and Figure 3.6), reveals that HCl has a higher peak at 288 eV, showing a higher concentration of  $\pi^*$  C=O bonding. Also interesting to note is that in Figure 3.6, the HCl has the highest peak at 285 eV, showing a higher concentration of C-C  $\pi^*$  bonding. It would seem

that the HCl is able to functionalize a higher percentage of the C-C bonds broken to C=O or C-O while the HNO<sub>3</sub> may break more C-C bonds without functionalizing the loose bond with a C=O. As the concentration of HNO<sub>3</sub> is increased, C=C bonding decreases. HCl is able to attack more of the C=C bonds after two hours, but HNO<sub>3</sub> attacks more after a longer period of 10 hours. Unlike the C=C bonds, the C-O and C=O bonds increase as the concentration of HNO<sub>3</sub> increases. However HCl solutions appear to have greater C-O and C=O bonding

To corroborate the data from the carbon atom NEXAFS, data was also taken at energy levels near the binding energy of oxygen. The oxygen spectra should have peaks at C-O and C=O binding energies to verify the results from above. Previous studies of SWNTs with NEXAFS showed characteristic peaks at 532 eV for C=O  $\pi^*$  transitions and broader peaks in the 538 - 542 eV range attributed to C-O  $\sigma^*$  transitions [100]. The gathered spectra for the oxygen binding energies, shown in Figure 3.7 and Figure 3.8 below, had very similar characteristics [98].

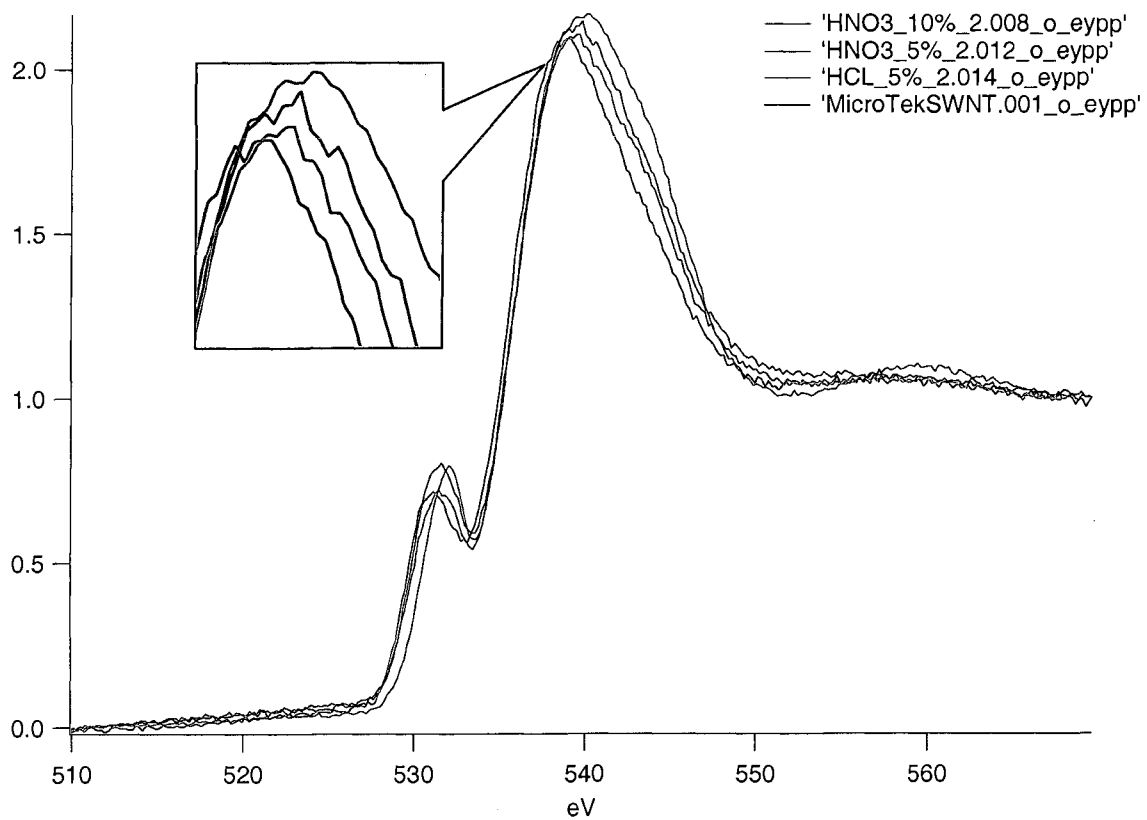


Figure 3.7: Oxygen Atom NEXAFS After 2 Hour Acid Treatment

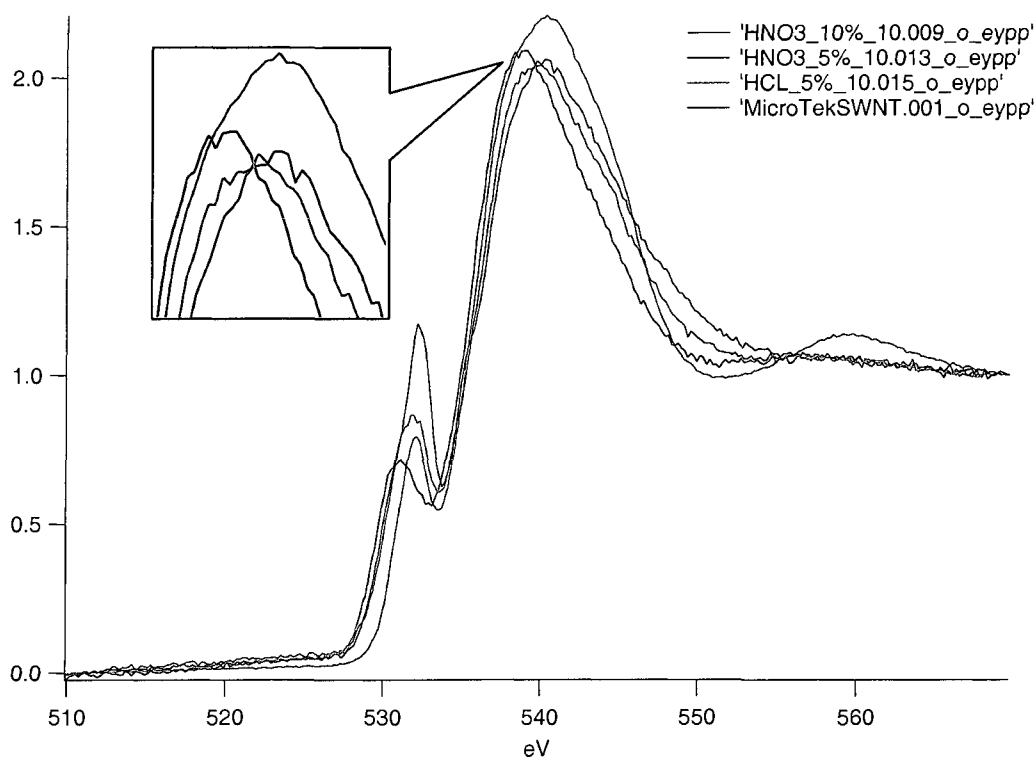


Figure 3.8: Oxygen Atom NEXAFS After 10 Hour Acid Treatment

The data in Figure 3.7 and Figure 3.8 above does not appear to corroborate the conclusions from the carbon energy graphs. After 2 and 10 hours, the HCl has one of the lowest peaks at 532 eV. After 10 hours, HCl does have the highest peak around 541 eV. Interestingly the 5% and 10% HNO<sub>3</sub> trade spots as the highest peak at 532 eV. Also worth noting is the extra peak in the HCl spectra around 559 eV. What appears to happen in the HCl solutions is that between 2 hours and 10 hours, the C=O transitions to C-O, but this does not occur in the HNO<sub>3</sub> acid treatments. These graphs corroborate the conclusions reached from the carbon target NEXAFS while adding distinctions between the C=O and C-O bonding that was not distinguishable in the carbon edge data. After 2 hours, HCl has the largest

peak followed by the 10% HNO<sub>3</sub> at 540 eV. After 10 hours, HCl is followed by 5% HNO<sub>3</sub> at 540 eV. At 288.5 eV, the same flip-flop occurs in Figure 3.5 and Figure 3.6.

The results from the NEXAFS data reveal that even lower concentrations of acid can functionalize a SWNT in a relatively short time period. Specifically, the data shows that lower concentrations of HCl can functionalize SWNTs in a shorter period of time compared to HNO<sub>3</sub>. Both HCl and HNO<sub>3</sub> cause breakage in C-C and C=C bonds. How much these broken bonds affect the electrical or mechanical characteristics of the SWNTs cannot be determined with NEXAFS. More detailed studies would need to be performed to determine where the majority of the broken carbon bonds are located on the surface of the SWNT. Most functionalization studies suggest the bonds on the end caps of the CNT break at a lower energy level [52, 101].

### **3.3 Conclusion**

This study was able to build from simultaneously occurring research at the IfM to produce SWNT suspensions. Utilizing lbl self-assembly to create suspensions of SWNTs avoids acid treatments that damage the SWNT structure that can lead to degraded performance. The Lbl technique is very robust, allowing the possibility of creating similar suspensions with different polyelectrolytes or nanoparticles that may have superior characteristics for the individual application. If the SWNT suspension is going to be incorporated into an electrical device, polyelectrolytes with better electrical properties could be interchanged with PSS or PAH without having to change any processing procedures. Because the

polyelectrolytes bond to the SWNT noncovalently, the PSS and PAH can be removed with thermal treatment, burning off the unneeded or unwanted polyelectrolyte. These suspensions allow for the mass manufacturing of a pure SWNT device, comprised of pure SWNTs without defectives or other additives.

## **CHAPTER 4**

### **FABRICATION**

The quickest route to implement a mass produced CNT device must utilize existing fabrication technology and tooling. The semiconductor industry revenues in 2008 topped out at \$266.5 billion according to iSuppli Corp [102]. An industry that large cannot make sweeping, large scale changes immediately. Before devices can be produced, fabs must be built. Before fabs can be built, the manufacturing equipment in the fab must first be manufactured. There has been extensive research on CNTs and CNT devices as exemplified by the long list of references. However, no manufacturing methodology has been devised to incorporate CNTs into semiconductor devices or fabricate CNT devices on a scale that is economically expedient. No device can be designed without consideration of the fabrication methodology. This study will look at a fabrication methodology that utilizes existing lithography technology, processes, and tooling to incorporate SWNTs into existing devices. The simplest first step to add SWNTs into microelectronic devices is to replace existing metal conduction paths and wires with SWNTs. Ideally, an individual SWNT could be utilized as a nanowire. However, current fabrication technology does not have the capability to efficiently and controllably build nanowires with an individual SWNT. This study will instead build wires

from bundles of SWNTs. While the fabrication demonstrated in this study is on a  $\mu\text{m}$  scale, the technology and processing is principally unchanged when transitioning to sub  $\mu\text{m}$  scales.

## **4.1 Overview**

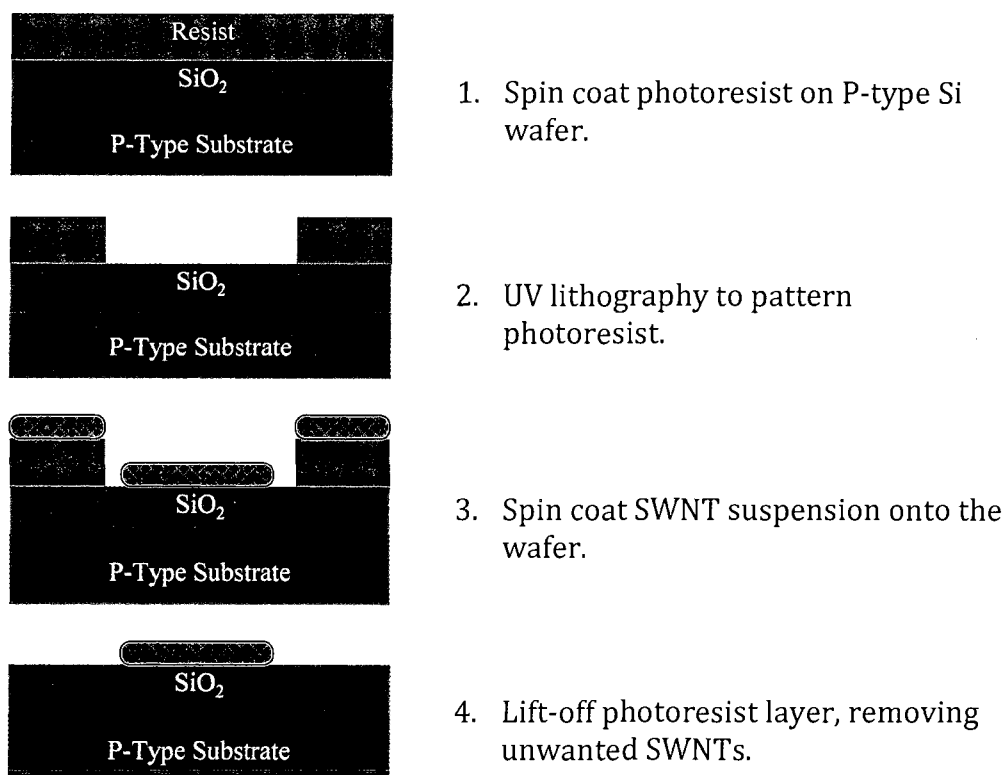
This study investigates three different manufacturing methodologies to produce SWNT wires for incorporation in microelectronic devices. The wires are comprised of bundles of SWNTs and polyelectrolytes in the form of a long rectangular shaped thin film. The shape, size, and location of the wire film can be controlled with standard UV lithography. This chapter will start with an overview of the processing procedures, followed by detailed fabrication parameters, and finally a comparison of the results from the three different procedures.

### **4.1.1 Spin Coating into Wells of Photoresist**

The first procedure tested was the simplest. A photoresist layer is spin coated on top of a Si wafer, although any substrate could work. The photoresist layer is patterned to remove small wells. A suspension of SWNTs is spin coated on top of the photoresist. The aqueous solution covered the entire wafer with a small layer of suspended SWNTs. The water from the suspension is then evaporated out, leaving only aggregated SWNTs. Because the wells are deeper than the flat surface and contain more SWNT solution, the water in the wells should take longer to evaporate out. The water will pull radially from outside the well towards the well during evaporation, causing the SWNTs around the well to be accumulated inside the well. After evaporation, the wafer is placed in acetone and agitated to

remove the photoresist in a lift-off procedure. The photoresist removes the unwanted SWNTs located outside of the wells [103]. The process is detailed in Table 4.2.

Table 4.2: Spin Coating into Wells of Photoresist

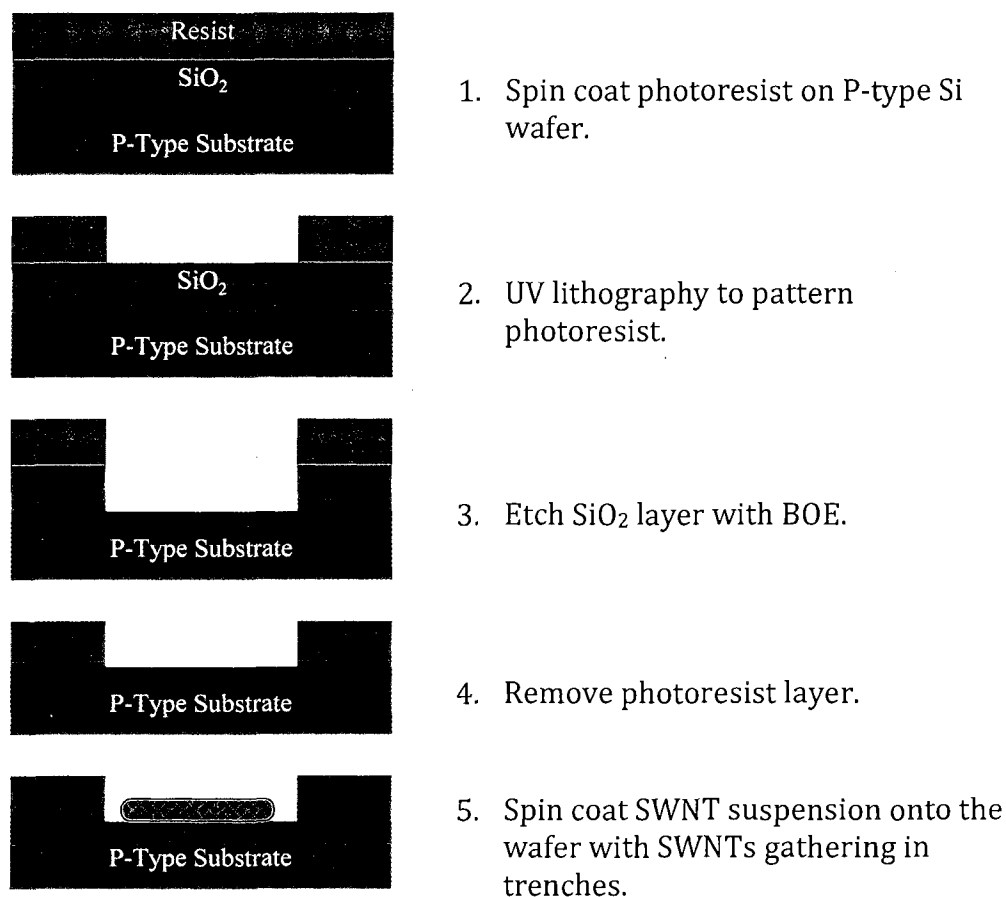


#### **4.1.2 Spin Coating into SiO<sub>2</sub> Trenches without Photoresist**

The next procedure tested was adjusted slightly from the previous process. A photoresist layer is spin coated on top of a Si wafer. The photoresist layer is patterned to remove trenches of different sizes. The SiO<sub>2</sub> layer on top of the Si wafer is then etched to match the pattern in the photoresist. The remaining photoresist is removed with acetone. A suspension of SWNTs is spin coated on top of the SiO<sub>2</sub> layer. The aqueous solution spins off the top surface of the SiO<sub>2</sub> layer

and only gathers in the trenches. The water from the suspension is then evaporated out, leaving only aggregated SWNTs in the trenches. The process is detailed in Table 4.3 below.

Table 4.3: Spin Coating into SiO<sub>2</sub> Trenches without Photoresist

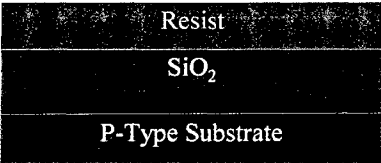
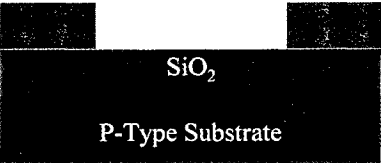
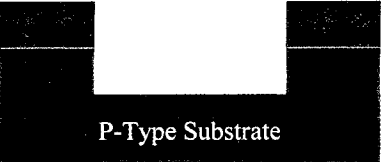
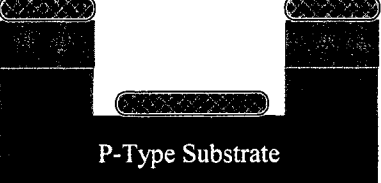
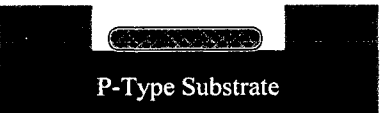


#### **4.1.3 Spin Coating into SiO<sub>2</sub> Trenches with Lift-Off**

The last procedure tested was a hybrid of the two previous processes. As before, a photoresist layer is spin coated on top of a Si wafer. The photoresist layer is patterned to remove trenches of different sizes. The SiO<sub>2</sub> layer on top of the Si wafer is then etched to match the pattern in the photoresist. A suspension of

SWNTs is spin coated on top of the photoresist. The aqueous solution covered the entire wafer with a small layer of suspended SWNTs. The water from the suspension is then evaporated out, leaving only aggregated SWNTs. Because the trenches are deeper than the flat surface and contain more SWNT solution, the water in the trenches should take longer to evaporate out. The water will pull radially from outside the trench towards the trench during evaporation, causing the SWNTs around the trench to be accumulated inside the trench. After evaporation, the wafer is placed in acetone and agitated to remove the photoresist in a lift-off procedure. The photoresist removes the unwanted SWNTs located outside of the wells. The process is detailed in Table 4.4 below.

Table 4.4: Spin Coating into SiO<sub>2</sub> Trenches with Lift-Off

 <p>Resist SiO<sub>2</sub> P-Type Substrate</p>	Spin coat Shipley 1827 photoresist on P-type Si wafer.
 <p>SiO<sub>2</sub> P-Type Substrate</p>	UV lithography to pattern the photoresist.
 <p>P-Type Substrate</p>	Etch SiO <sub>2</sub> layer with BOE.
 <p>P-Type Substrate</p>	Spin coat SWNT suspension onto the wafer.
 <p>P-Type Substrate</p>	Lift-off photoresist layer, removing unwanted SWNTs.

#### 4.2 Mask Design

UV lithography is the standard pattern creation and transfer process for semiconductors and other microelectronic devices. UV lithography utilizes polymers that change solubility when exposed to UV light called photoresist. By controlling the areas on the photoresist that get exposed to light, patterned areas of the photoresist can become soluble. Using photoresist as a coating on top of a wafer or other substrate allows areas of the photoresist to be removed in a controlled pattern, allowing access to the substrate below. Complex designs and

structures can be made by repeating the process, building patterns on top of patterns. To control the areas of the photoresist that get exposed to light, a mask is used. In a mask, light is passed through a clear piece of glass or plastic with an opaque coating. The opaque coating blocks the light from passing, so light only travels through the clear sections to reach the photoresist layer on the wafer as demonstrated in Figure 4.1 below.

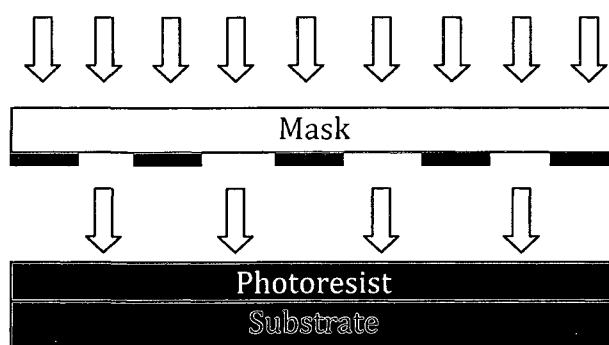


Figure 4.1: UV Lithography

Thin film masks are made of clear plastic with black ink printed on the surface to block the light while chrome masks are made of glass with a chrome layer used to block the light. Thin film masks can be printed on transparency sheets with an ink jet printer that is able to make very small ink droplets. Most thin film masks have a limited feature size, with 10  $\mu\text{m}$  to 15  $\mu\text{m}$  being the smallest available for this study. The thin film mask used in this study was printed at the University of Illinois printing facilities. Chrome masks can be made with a much smaller feature size. Most chrome masks are patterned with an electron beam (E-beam). E-beam lithography is able to achieve feature sizes in the nm range. The E-beam available at the I/M has a feature size of 40 nm. The chrome mask used in this

study was fabricated in-house at the IfM. The two masks were used in this study were designed with LEdit® v9.0 software. A thin film mask was used to create groups of  $15 \mu\text{m}^2$  wells. A chrome mask was used to create groups of trenches of various sizes.

#### **4.2.1 Wells**

The first feasibility experiment in this study created groups of wells,  $15\mu\text{m}^2$ , in a photoresist layer. To design a mask, the 100 mm wafer (diameter is 100 mm) was first broken down into 60 cells of  $10 \text{ mm}^2$ . This would allow the final wafer to be broken into smaller pieces that could be imaged or characterized in various metrology instruments. Markers were added to the mask so the processed wafer would have identifying characteristics to show where the wafer could be broken into the smaller cells. The identifying marks also allow for quicker post processing verification. Without any markers on the wafer, finding a small group of  $15 \mu\text{m}^2$  wells becomes tedious and time consuming. Figure 4.2 shows the layout of the  $10 \text{ mm}^2$  cells in gray and markers in black on the 100 mm wafer in blue.

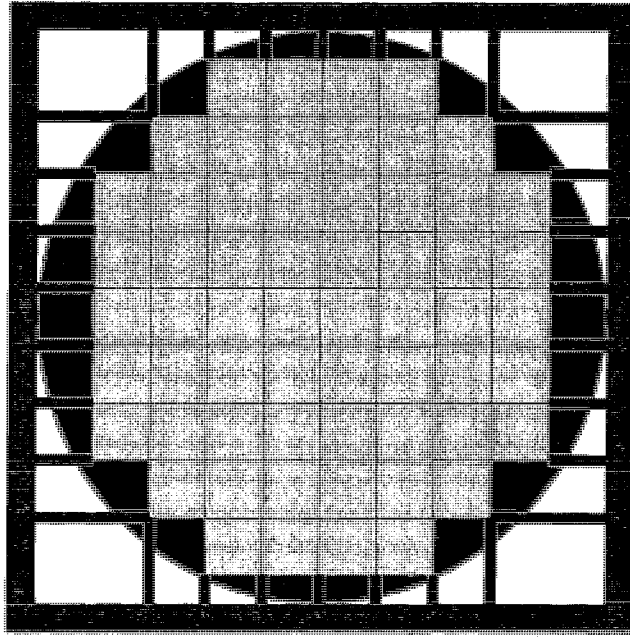


Figure 4.2: LEdit Mask Marking Cells of  $15\mu\text{m}^2$  Wells

Each cell contains an array,  $12 \times 12$ , of  $15\ \mu\text{m}^2$  squares. The spacing between each square is  $20\ \mu\text{m}$ , so the entire array only occupies  $400\ \mu\text{m}^2$ . This allows plenty of space between the groups of wells when the wafer is split into smaller pieces. The array of squares from the mask is shown in Figure 4.3 below.

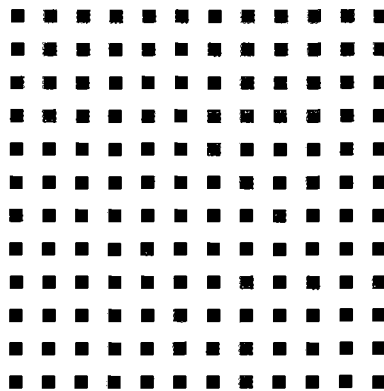


Figure 4.3: LEdit Mask of Single Cell of  $15\ \mu\text{m}$  Wells

This mask design allows for many samples to be created from a single processing. In a single batch, 8,640 wells could be distributed over the surface of the wafer. The large samples would reduce the impact from imperfect fabrication processing or contamination. The final printed mask is shown below in Figure 4.4.

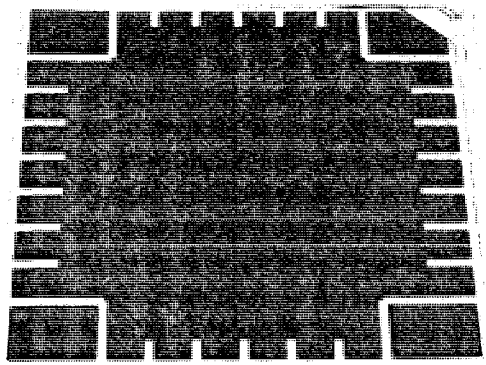


Figure 4.4: Printed Thin Film Mask

#### **4.2.2 Trenches**

The second mask used in this study created trenches instead of wells. The trenches varied in size, with many being smaller than the 15  $\mu\text{m}$  feature size of a thin film mask. To achieve these smaller features, a chrome mask was designed. The 100 mm wafer was separated into cells as before, with the cells being 20  $\text{mm}^2$ . Groups of trenches were in the center of each cell, occupying 12.7  $\text{mm}^2$ . As before, layout markers were added to the mask. Alignment markers were also added to the mask. A third mask was created to add contact pads on the end of each trench and to properly align the second mask on the wafer, markers must be added. The

alignment markers consisted of two rectangles,  $60\ \mu\text{m} \times 500\ \mu\text{m}$ . The mask layout is shown below in Figure 4.5.

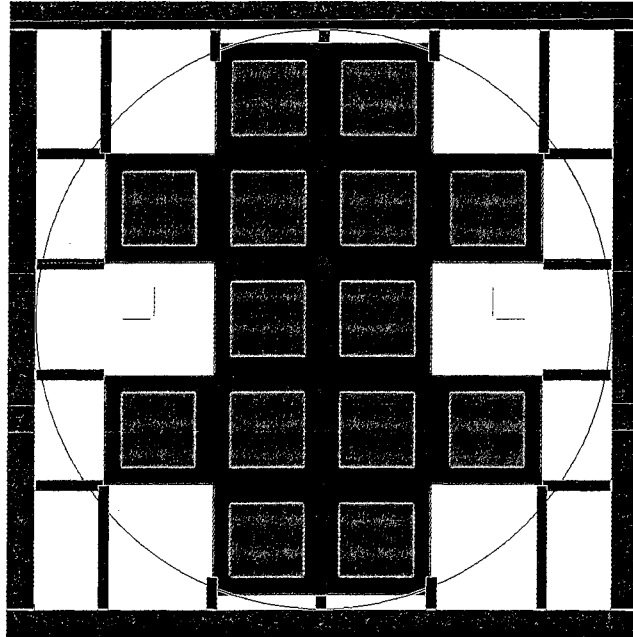


Figure 4.5: LEdit Mask Marking Cells with Trenches

The green squares show the space occupied by the groups of trenches. The red squares show the full cell with spacing. The alignment markers are midway on the wafer at both the right and left sides. The groups of trenches consist of repeating columns of trenches. Each column contains 15 of each of the 12 trench sizes, sequentially from the largest to smallest, grouped first by width, then length. The different trench sizes are listed in Table 4.5 with width and length defined as in Figure 4.6 below.

Table 4.5: Trench Dimensions in Mask Design

Length ( $\mu\text{m}$ )	Width ( $\mu\text{m}$ )
20	2,4
30	2,4
50	2,4
90	2,4
30	8
50	8
90	8
170	8

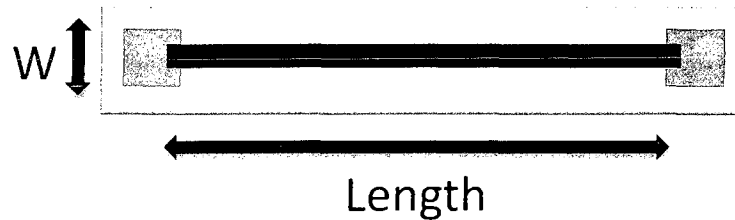


Figure 4.6: Trench Diagram with Dimensions Marked

Figure 4.6 shows the trench dimensions with gray square end points for contact pads. The trenches consisted only of the blue component of Figure 4.6. The gray squares can be created with a third mask as referenced to above. This study did not use the third mask for reason that will be detailed later. In a single cell, 20 columns are placed side by side with  $450\ \mu\text{m}$  spacing between each column. This mask layout, like the thin film mask, allows for many samples to be created quickly.

### **4.3 Procedure Specifications**

All fabrication procedures were performed at the I/M at Louisiana Tech University. Each fabrication step is detailed below with all of the known process

and equipment parameters and settings. The processes are explained in chronological order of fabrication. The only process that is omitted is making SWNT suspensions as that was detailed above.

### **4.3.1 Lithography**

All lithography fabrication occurred in one of the two cleanrooms at the I/M. All lithography used Shipley 1827 photoresist. When spin coated on top of the wafer, the photoresist layer formed has a thickness of 2.7  $\mu\text{m}$ . The spin coater is programmed to ramp to 500 rpm in 2 seconds and stay at that speed for another 2 seconds. Then the spinner is ramped to 4000 rpm in 4 seconds and stays at that speed for 40 seconds. This creates a flat, even surface across the wafer. The wafer is then soft baked on a hotplate at 115°C for 90 seconds. This removes excess water from the resist and hardens it some for the exposure process. Especially with the thin film exposure, the thin film is placed directly on top of the photoresist layer. Hardening the resist prevents any deformation in the layer as well as preventing any of the resist from sticking to the film when it is removed.

The lithography processes using a thin film mask were performed on a Vision EV420 dual-side mask aligner in the class 1000 cleanroom. The EV420 was operated in low vacuum contact mode with a separation of 20  $\mu\text{m}$  and exposure time of 20 seconds. The processes using a chrome mask were performed on a similar mask aligner in the class 100 cleanroom. The mask aligner operated in low vacuum, soft contact mode with a separation of 15  $\mu\text{m}$  and exposure time of 12 seconds.

After exposure, the wafer is developed in a solution of MIF 319 with mild agitation for 30 seconds. The developer removes the exposed areas of the photoresist layer. The procedure is done in steps of 10 seconds, examining the wafer under a microscope each time to determine when the all of the wanted areas were removed without overdeveloping. When the wafer is removed from the developer, it is rinsed in deionized water and blown dry with nitrogen. After the wafer has been fully developed, it is again placed on a hotplate at 115° C for 5 minutes for a hard bake. The hard bake removes all excess moisture from developing and rinsing. The hard bake also stiffens the photoresist, making it stronger for the following processes.

#### **4.3.2 SiO<sub>2</sub> Etching**

After a pattern has been made in the photoresist layer, the photoresist can function as a mask for processing on the substrate. The Si wafers used all contain a 200 nm oxide layer (SiO<sub>2</sub>) on top of the wafer. The patterned photoresist layer acts as a protective coating on the SiO<sub>2</sub> layer. The wafer is placed in a buffered-oxide etch (BOE) solution. BOE is a solution consisting of ammonium fluoride (NH<sub>4</sub>F) and hydrofluoric acid (HF) in a 6:1 ratio by volume added to deionized water. The NH<sub>4</sub>F acts as a buffer to slow down the etching process. Even diluted HF etches the oxide layer too quickly to have precise control. The I/M provides a premade BOE solution because of the dangers of working with HF. Even diluted concentrations of HF can be deadly when in contact with skin. The BOE etch available etches at a rate of  $\approx 1$  nm per second. HF is an isotropic etch, etching the same in all directions regardless of the crystalline plane. The tradeoff to being

isotropic, HF will cause undercutting, or etching part of the oxide layer that is covered with photoresist. The result will be a trench of a slightly larger size. Trenches were etched in SiO<sub>2</sub> using BOE for two different lengths of time. The first wafer of trenches was placed in the BOE solution for 3 minutes while the second wafer was etched for 5 minutes.

#### **4.3.3 Spin Coat SWNT Solution**

Because the SWNT is mostly water, the solution spins off the wafer very easily. Spin coating required a very slow speed, less than 5 rpm. The same results can be achieved with dipping the wafer in a bath of suspended SWNTs and removing it face up. Any slight tilting of the wafer causes the solution to slide off. Covering the entire wafer with SWNTs is of no concern for the fabrication processes that include a lift-off step.

#### **4.3.4 Evaporation**

Evaporation was performed on a hot plate in open air in the clean room. Different temperature settings were experimented with to determine how the evaporation rate would affect the final SWNT structure. Temperatures below 117° C had very little evaporation. After 45 minutes, no visible amount of water evaporated from the SWNT suspension. At a temperature of 117° C, complete evaporation occurred in 30 minutes. Increasing the temperature to 120° C reduced the time of evaporation to 15 minutes with no apparent change to the final SWNT film shape or structure. It was hypothesized that slower evaporation rates would allow more SWNTs to be drawn into the wells or trenches, but there was no evidence to support the idea.

#### **4.3.5 Lift-Off**

All lift-off procedures were performed with acetone. The wafer was submerged in a Petri dish of acetone and agitated with a swirling motion by hand. No sonication device was tested. The lift-off procedure occurred quickly with all visible traces of the photoresist layer removed in under 1 minute.

### **4.4 Results**

Not all of the fabrication processes achieved a SWNT structure. Images were taken in mid process to verify that each stage was performed correctly. The results are divided into each of the three fabrication processes tested in this study. The results are also analyzed. If the results varied from the suggested ideal given in the first section above, a hypothesis as to why the variance is given.

#### **4.4.1 Photoresist Wells**

The first fabrication methodology tested created wells in the layer of photoresist. Optical images were taken of the developed photoresist after 20 seconds, shown below in Figure 4.7.

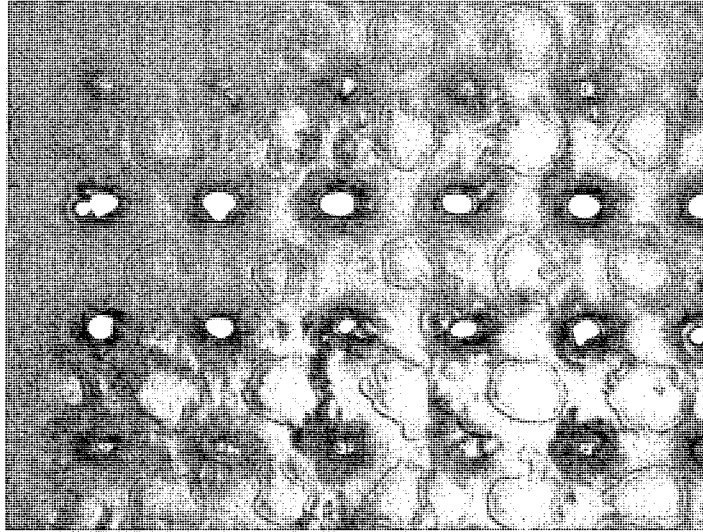


Figure 4.7:  $15\ \mu\text{m}^2$  Wells After Developing for 20 seconds

The wells are not completely removed from the photoresist layer. Longer development is needed. The image also reveals the wells are not square as printed in the mask. This is due to the limitations of the thin film mask. The mask is not able to block out the light strictly along the line, so the light that gets through is more circular in nature. After further developing for a full 60 seconds, the resulting wells are shown in Figure 4.8.

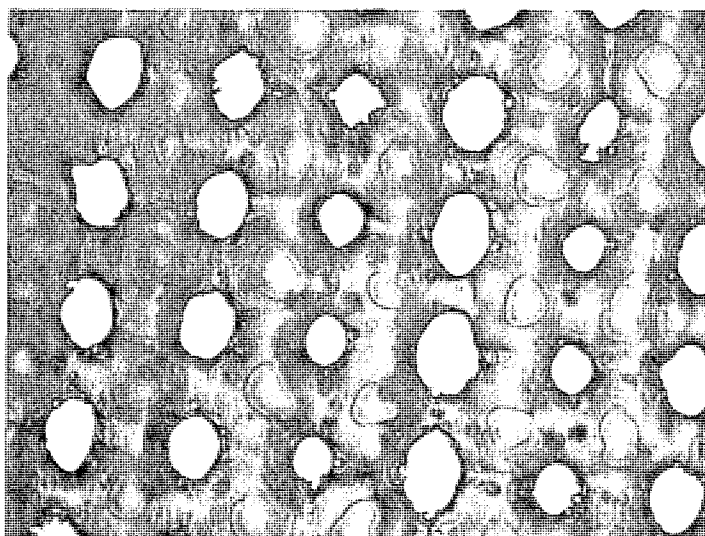


Figure 4.8:  $15 \mu\text{m}^2$  Wells After Developing for 60 seconds.

The wells areas are completely removed. The wells are not uniform in size, again due to the nature of a thin film mask. The photoresist does have clearly defined wells on the scale of  $15 \mu\text{m}^2$ , so continued fabrication is possible. Using the above photoresist wells, the results from fabricating SWNT pads are shown in Figures 4.9 – 4.13 below.



Figure 4.9: SWNT Pad Structures

Figure 4.9 shows resulting SWNT pads with a high correlation to the well shapes. The pads are not perfect squares. The lift-off process cannot cause precise breaks at the edges of the well, resulting in pads that overlap the area of the well.



Figure 4.10: SWNT Pads with Incomplete Fill

Figure 4.10 shows SWNT pads with an incomplete fill. The lift-off process not only can leave extra SWNT material as in Figure 4.9, but can also remove extra material. The SWNT film outside the well was attached to parts of the film inside the well and removed them when it was removed.

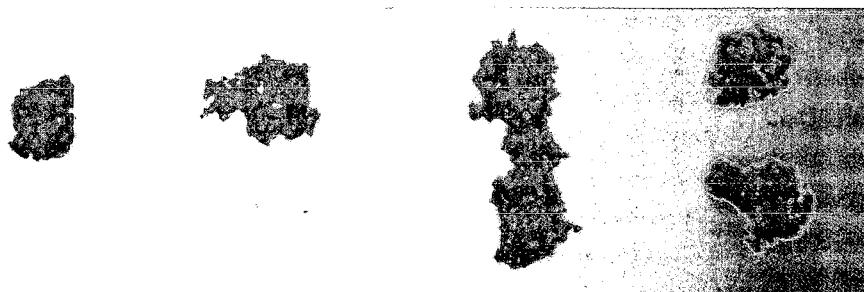


Figure 4.11: SWNT Pad Structures with Incomplete Removal

Figure 4.11 reveals another possible outcome from the lift-off. Adjoining wells are connected by a solid piece of SWNT film that is not removed with the lift-

off. The photoresist layer is removed from underneath the bridging SWNT material without removing the bridge.

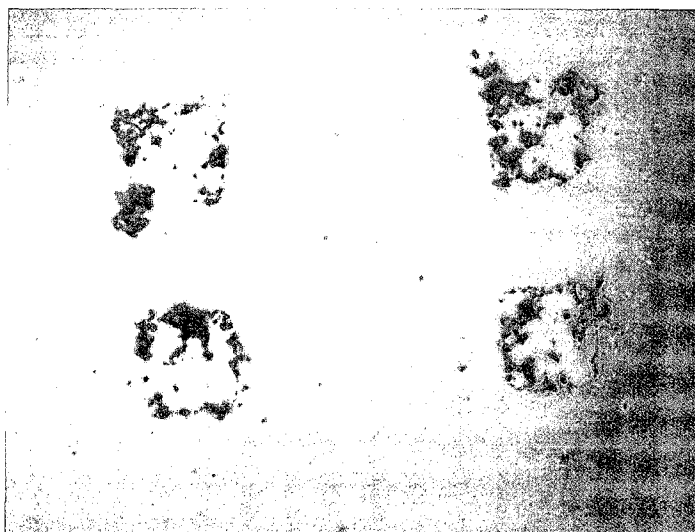


Figure 4.12: SWNT Pads Removed During Lift-Off

Figure 4.12 shows where entire SWNT pads were removed during the lift-off process. Traces of SWNT material around the corners still remain while the majority of the SWNT pad was removed. The corner traces of material show that SWNT material was in the well at one point.

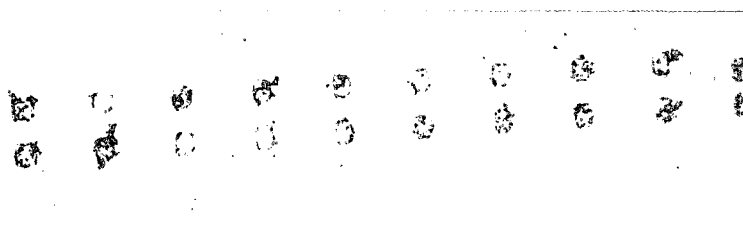


Figure 4.13: Correlation of Well Locations and SWNT Material

Figure 4.13 shows how well the SWNT material correlates with where the wells are located in the photoresist. Although the SWNT pads were mostly removed during the lift-off process, there was a distinct difference between the well areas and the outer surface.

This process, while not perfect, did demonstrate the feasibility of building SWNT structures using photoresist wells to collect SWNTs from suspension and lift-off to remove SWNTs from unwanted areas. Also worth noting, the SWNT structures are firmly attached to the surface of the wafer. Repeated rinsing with deionized water did not wash any of the structures away. This is likely due to a surface attachment with the SWNTs due to van der Waals forces.

#### **4.4.2 SiO<sub>2</sub> Trenches without Photoresist**

Several of the issues revealed in the previous fabrication process were due to limits of the lithography environment. To improve the results, the thin film was replaced with a chrome mask to better control the shape and size of the design pattern. Images were taken of the photoresist after development to verify proper exposure and development. Figure 4.14 shows the resulting trenches developed in photoresist.

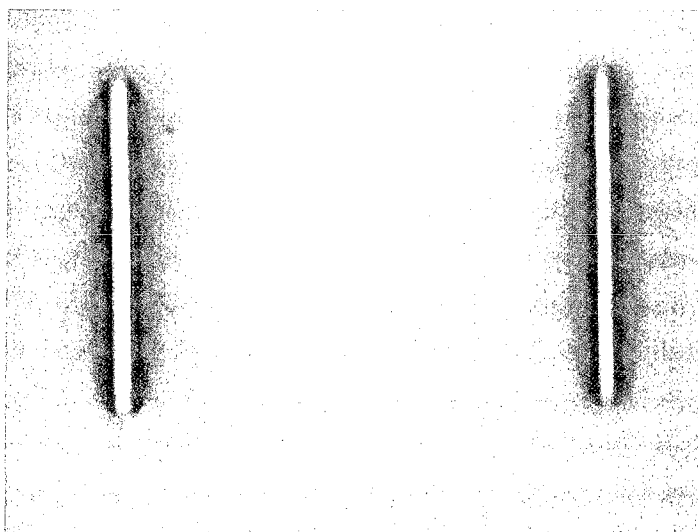


Figure 4.14: Trenches in Photoresist

The trenches have much better shape characteristics compared to the wells from the previous fabrication trial. The shading on the sides of the trenches is characteristic of overdevelopment. The shading is a result of those areas starting to lift off the surface of the wafer because the developer started to remove the sidewalls in the photoresist. The trenches in the photoresist are still adequate for further fabrication. The wafer is placed in the BOE etch to remove an oxide layer. To study the BOE etch, two wafers are fabricated. The first wafer is placed in the BOE solution for 3 minutes and a second wafer is placed in the BOE solution for 5 minutes. After etching, the photoresist layer is removed with acetone and the channels are characterized using a Quesant Qscope atomic force microscope (AFM). The AFM is able to profile each of the trenches to determine width and depth of each to verify the trenches were etched properly in the  $\text{SiO}_2$ . Images obtained from the AFM scan are shown below.

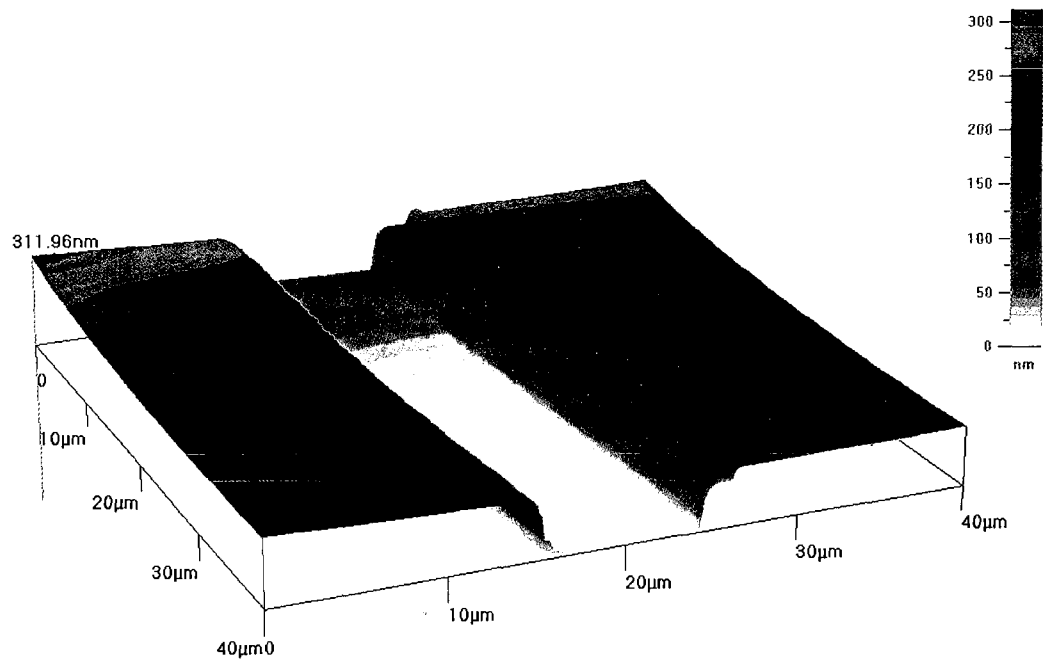


Figure 4.15: AFM Image of 170 μm x 8 μm Trench Etched for 3 Minutes

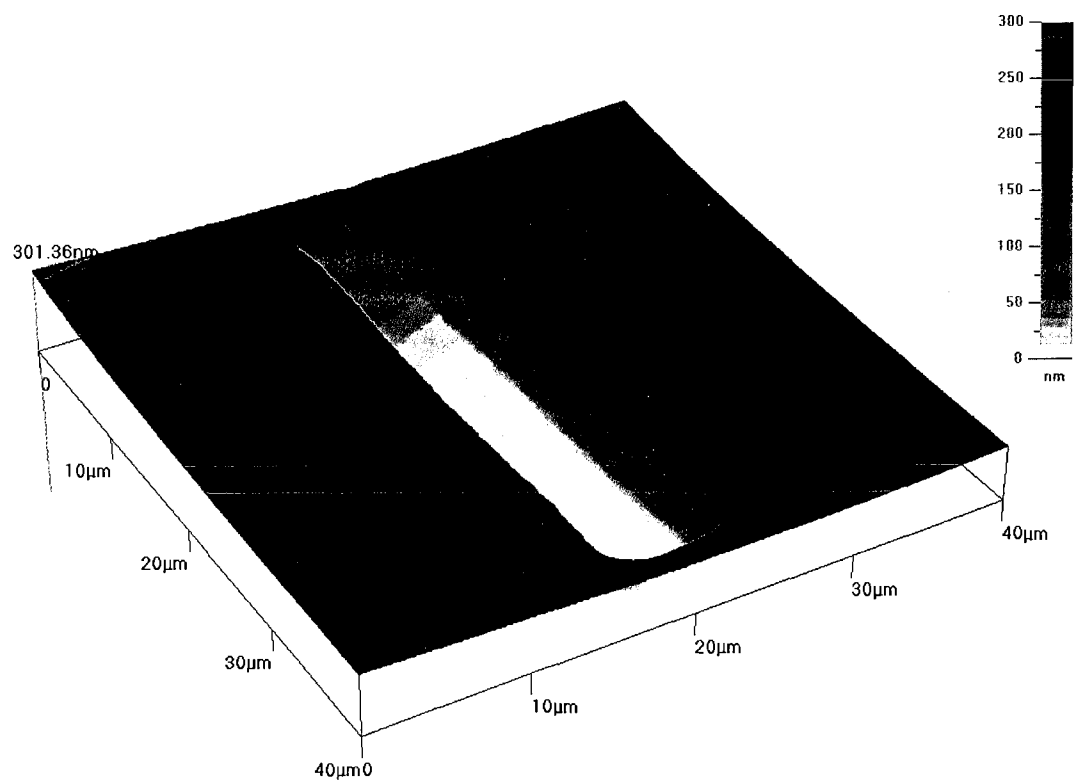


Figure 4.16: AFM Image of 30 μm x 4 μm Trench Etched for 3 Minutes

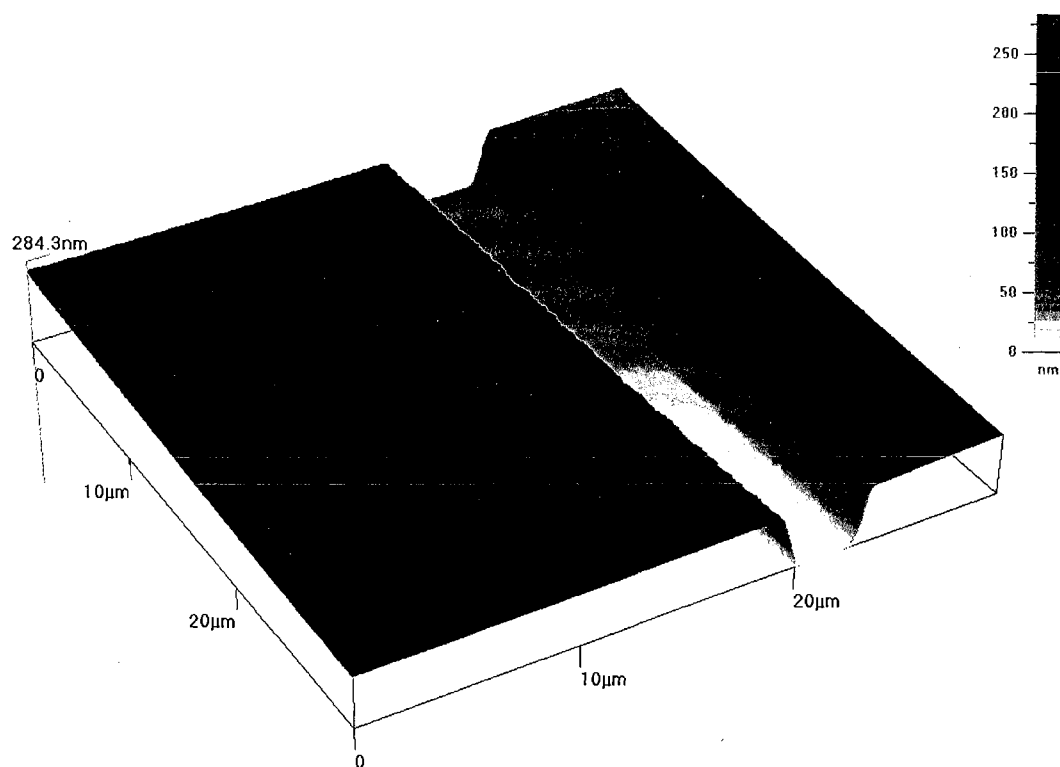


Figure 4.17: AFM Image of 50 μm x 2 μm Trench Etched for 5 Minutes

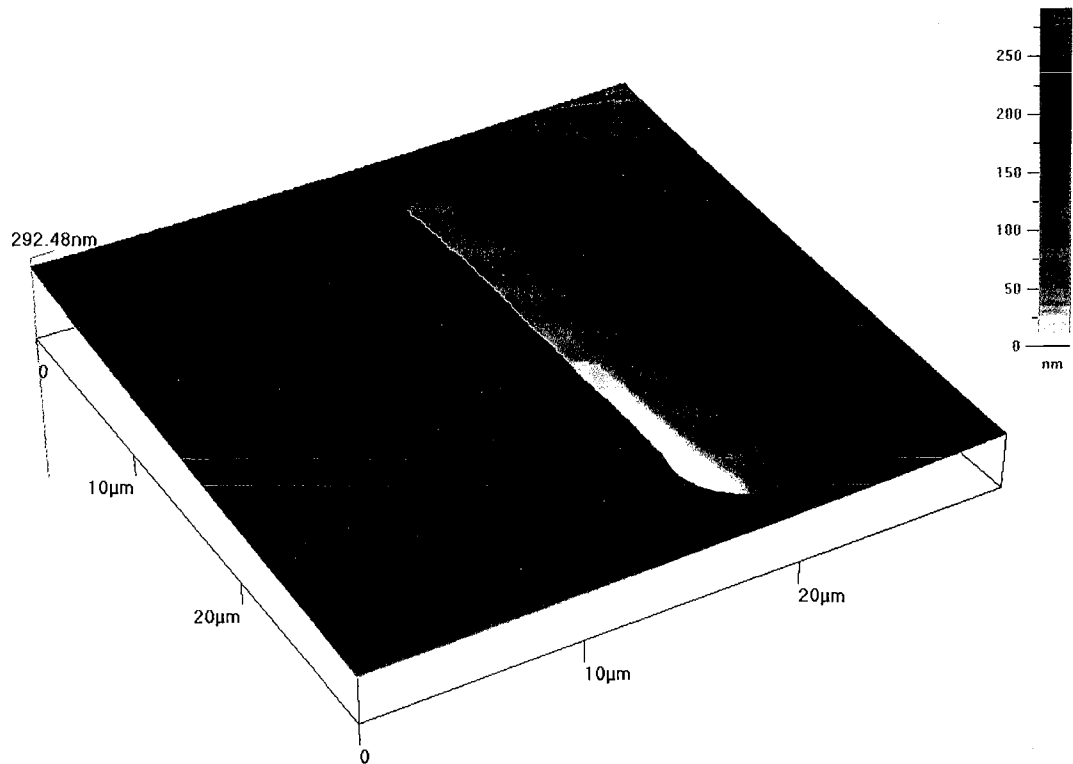


Figure 4.18: AFM Image of 20  $\mu\text{m}$  x 2  $\mu\text{m}$  Trench Etched for 5 Minutes

The AFM scans show the resulting trenches etched in oxide correlate well with the desired channel sizes. More detailed measurements can be obtained from cross section images. The width and depth of each trench size was measured and is listed below in Table 4.6.

Table 4.6: SiO<sub>2</sub> Trench Measurements with AFM

Shape (LxW) ( $\mu\text{m}$ )	3 min BOE Etch		5 min BOE Etch	
	Width ( $\mu\text{m}$ )	Depth (nm)	Width ( $\mu\text{m}$ )	Depth (nm)
170 x 8	9.43	184	11.01	189
90 x 8	9.87	178	11.08	187
50 x 8	11.88	180	11.05	187
30 x 8	11.77	178	11.10	186
90 x 4	6.57	178	6.23	187
50 x 4	7.36	176	6.63	179
30 x 4	6.19	177	7.07	178
20 x 4	7.5	181	7.8	186
90 x 2	4.5	172	4.6	179
50 x 2	4.7	187	4.27	179
30 x 2	4.3	180	4.1	181
20 x 2	4.2	183	3.22	176

When researchers use an AFM to measure the width of a channel, the shape of the AFM tip must be considered. A triangular tip AFM will give measurements that are slightly off because the tip cannot precisely follow the shape of the channel. The trenches all have a similar depth, showing that the BOE had adequate time to fully etch the thickness of the SiO<sub>2</sub> layer. The average depth for the 3 minute etch is 179.5 nm while the average for the 5 minute etch is 182.8 nm. The width measurements show that a significant amount of undercut occurred. The smallest trench width was measured at 3.22  $\mu\text{m}$  while most of the 2  $\mu\text{m}$  trenches all measured at over 4  $\mu\text{m}$ . The 4  $\mu\text{m}$  width trenches all measured between 6-7  $\mu\text{m}$  and most of the 8  $\mu\text{m}$  trenches measure 11  $\mu\text{m}$ . The results do indicate three distinct widths and the undercut on each size is about the same, 2-3  $\mu\text{m}$ .

The fabrication of SWNT structures in this study did not require precise trench size, so the undercut detected here is not a hindrance. However, when attempts were made to spin coat the SWNT suspension on the wafer with fabricated

trenches, none of the suspension would stay on the surface of the wafer. The solution would quickly slide off the surface and no residual would remain.  $\text{SiO}_2$  is a hydrophobic surface that repels water. Any aqueous solution immediately beads up instead of laying on the surface. So the SWNT suspension could not deposit any SWNTs in the trenches because the surface caused the solution to bead up and slip off the surface. This issue was not noticed in the previous fabrication process because the photoresist is not hydrophobic to the same extent as  $\text{SiO}_2$ . There are no images to show in this case because there were no resulting SWNT structures.

#### **4.4.3 $\text{SiO}_2$ Trenches with Lift-Off**

The lithography processing of the last fabrication method improved upon the first trial. The chrome mask achieved much more accurate shape characteristics. The oxide layer posed a problem in the second trial. In the third fabrication trial, the above two methods are combined to form a hybrid process. Keeping the photoresist layer after the BOE etch and utilizing it to remove any unwanted SWNT material will add several secondary benefits. The photoresist layer is less hydrophobic, causing the SWNT suspension to lay better on the surface of the wafer, thereby improving coverage and deposition of SWNTs. The photoresist layer also adds thickness to the depth of the trenches. Increasing the thickness should reduce the amount of SWNT material connecting the desired SWNT structures in the trench with the SWNTs on the surface. This should also improve the shape characteristics of the SWNT because sharper edges should be possible with lift-off. The results should show a reduction in some of the structure anomalies noticed in

the first fabrication process. Etching the SiO<sub>2</sub> trenches can also improve the surface wetting from the first process. When only the photoresist was used as a form to hold the SWNT solution, the aqueous solution had to lie on a SiO<sub>2</sub> layer that is very hydrophobic. By etching the SiO<sub>2</sub>, the solution will now lie on a Si layer that is not hydrophobic. Trenches will also increase the surface area for the SWNTs to attach with van der Waals forces to reduce the SWNT structures that are completely removed with lift-off.

Trenches are fabricated as in the previous methodology. After the BOE etch, the photoresist layer is not removed. With the photoresist layer, the trench sizes could not be characterized with the AFM because the AFM tip cannot accurately profile softer materials like photoresist. There is a profilometer at the I/M that can profile channels with photoresist. However, the equipment is not capable of profiling channels smaller than 5 μm. So no measurements were made of this batch of trenches. The SWNT suspension was spin coated on the wafer and evaporated. The photoresist was removed with acetone in lift-off. The resulting SWNT structures are pictured below.

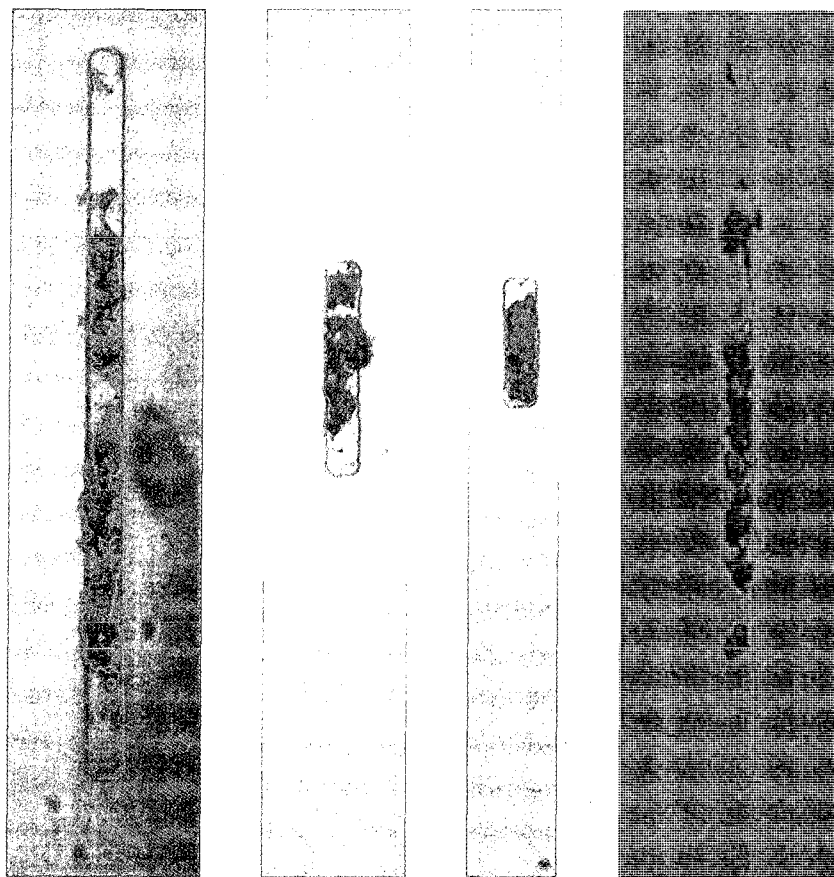


Figure 4.19: SWNT Structures in 8  $\mu\text{m}$  Width Trenches

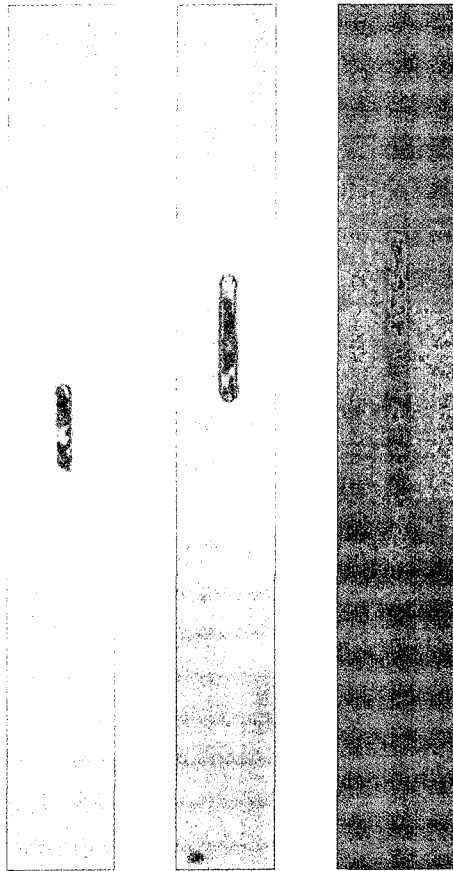


Figure 4.20: SWNT Structures in 4  $\mu\text{m}$  Width Trenches

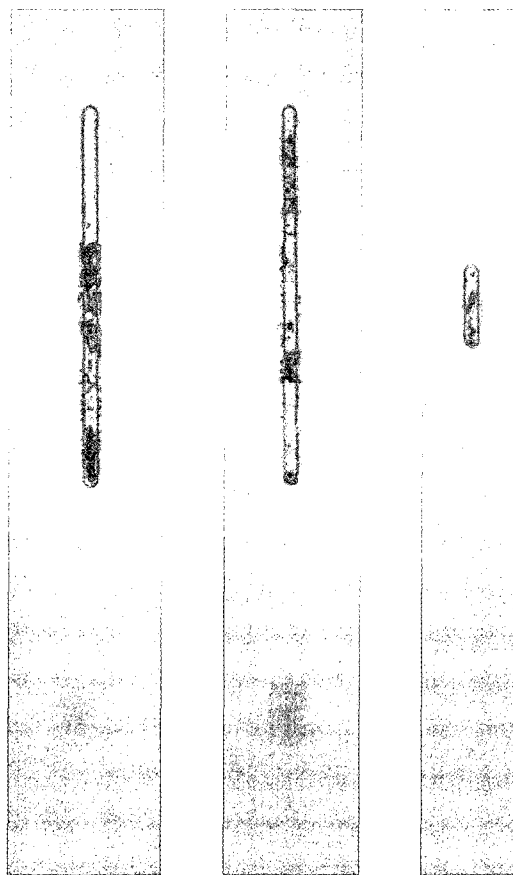


Figure 4.21: SWNT Structures in 2  $\mu\text{m}$  Width Trenches

Although the trenches were not completely filled with SWNTs, the resulting structures have a highly controlled shape matching the trench. There is little to no SWNT material outside of the trenches. Figure 4.22 shows two rows of trenches to show how well the unwanted SWNT material was removed from outside the trenches.

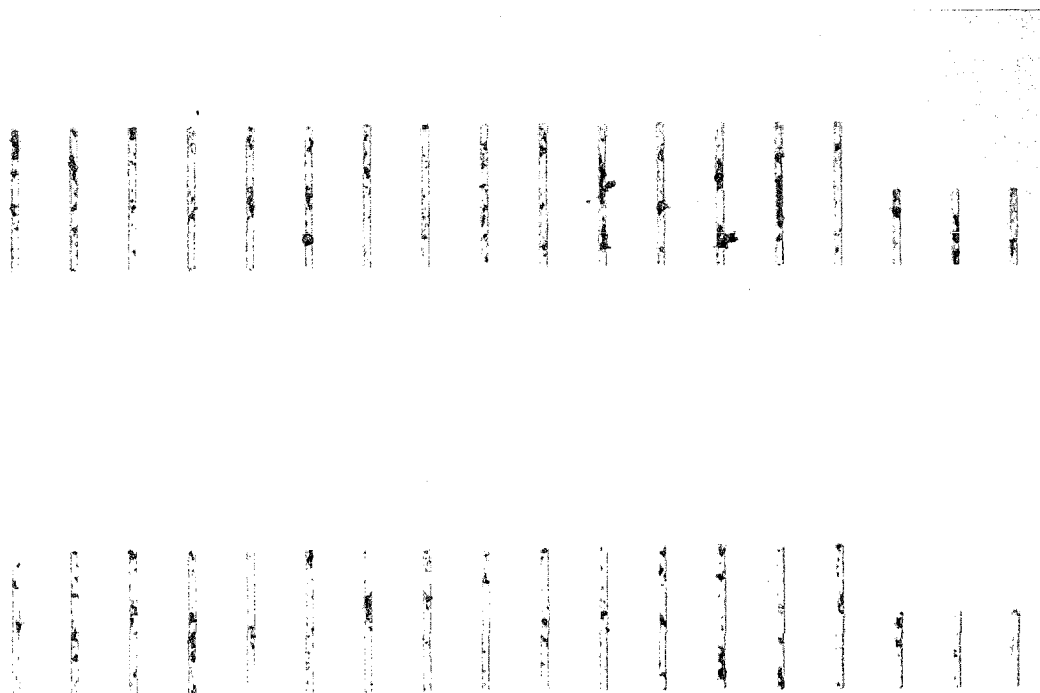


Figure 4.22: Two Rows of SWNTs in Trenches

There are virtually no SWNTs outside of the trenches. There are two spots in the top row where the SWNTs in the trench remained attached to SWNTs outside of the trench after lift-off. Comparing the resulting SWNT structures of the different trench sizes, the 8  $\mu\text{m}$  and 4  $\mu\text{m}$  trench widths had a higher fill rate compared to the 2  $\mu\text{m}$  trenches. All trench widths had samples that were partially filled but only the 8  $\mu\text{m}$  and 4  $\mu\text{m}$  widths had samples that were mostly (> 75%) filled. The shorter length trench lengths also had a higher percentage of being mostly filled. The higher fill rate in the shorter trenches is probably due to a greater percentage of them being completely covered by the SWNT suspension during spin coating as opposed to the longer trenches. The longer trenches may have had areas where the suspension beaded up and failed to deposit any SWNTs.

There was no trench size that was never filled, so all of the trench sizes test could potentially be completely filled by making adjustments to the fabrication process.

#### **4.5 Conclusion**

While perfect structures were not able to be fabricated, the results show the potential of this fabrication method to create controlled SWNT structures. Using standard lithography processes, SWNT structures can be fabricated in any location or orientation without tedious individual manipulation. The fabrication methodology demonstrated could allow SWNTs to be integrated into current microelectronic devices without using any new tooling or fabrication techniques. Building SWNTs using this technique is much quicker than using other lbl self-assembly techniques. Building SWNT films using lbl requires as much as 30 minutes for each layer. Building films of even 10 layers can be time consuming. Spin coating the SWNT suspension and evaporating out the water achieves a similar result in less time.

## CHAPTER 5

### CHARACTERIZATION

The purpose of this study was to develop a fabrication method to incorporate SWNTs into microelectronic devices. A method to fabricate SWNT structures has been demonstrated, but those structures must be verified as usable for microelectronic devices. For the SWNT structures to be used as electrical connections in microelectronic devices, they must have a high conductivity or low resistance. The resistances of the SWNT structures in this study were determined with IV characterization.

The SWNT structures were also studied to determine if the devised fabrication methodology resulted in orienting the SWNTs in any direction. The orientation of SWNTs in a sample can be determined by looking at the Raman spectroscopy.

#### **5.1 IV Characterization**

SWNT thin films comprised of SWNTs and polyelectrolytes fabricated by lbl self-assembly have been characterized before. Thin films comprised of SWNTs and PDDA had a measured resistance of 22.k $\Omega$  [17]. The resistance for films of SWNTs and PEI measured as 66.6 M $\Omega$  [15]. Because the SWNT structures

fabricated in this study are of a similar composition, the measured resistance should be in a similar range.

### **5.1.1 Results**

An IV curve for the SWNT structures was characterized with a Keithley probe station. The probe station automatically changes the source voltage while recording the supply current. Currents are measured for a range of voltages and plotted. Because the trenches were not completely filled with SWNTs from end to end, contact pads could not be fabricated on ends of the trench to connect to the probe station. To make contact with the SWNT structures, small probes that can fit inside the trench were used. The smallest probes available had a point diameter of 2  $\mu\text{m}$ . Measurements were made on the longest filled trench with a width of 8  $\mu\text{m}$ . Probes were adjusted to make direct contact with the fabricated SWNT structure. Smaller trenches were avoided to ensure the probe would not make contact with the substrate. The resulting IV curve is shown in Figure 5.1.

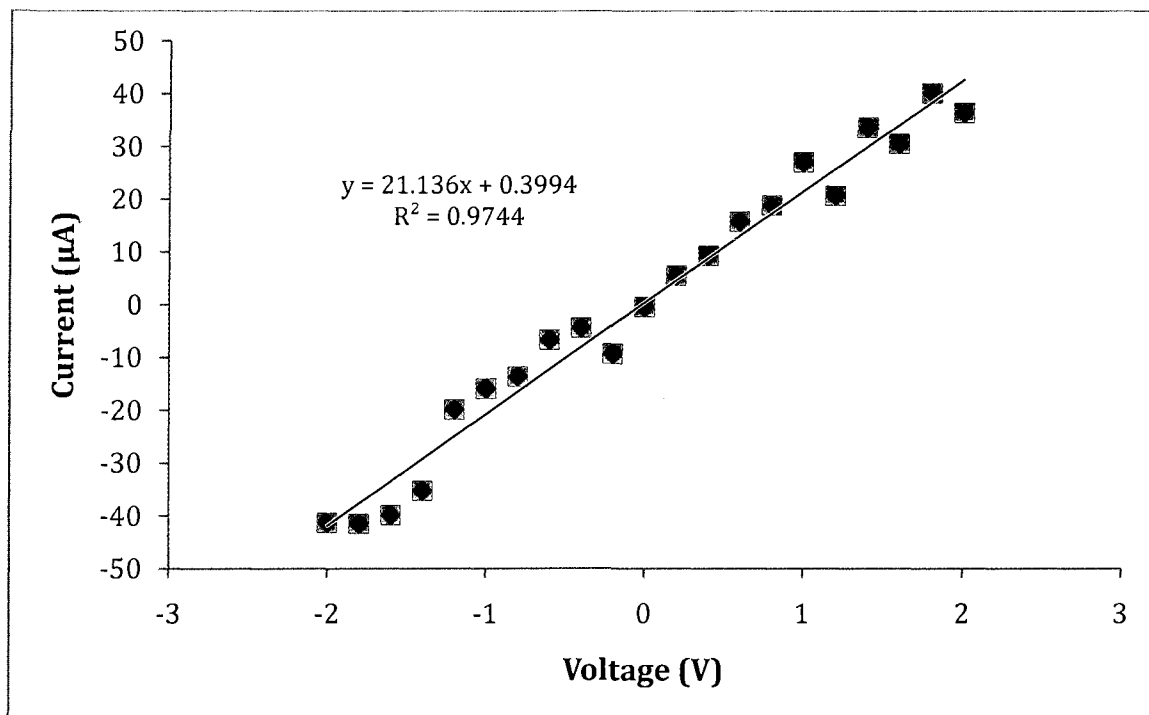


Figure 5.1: IV Characterization of SWNT Wire

The slope of the resulting plot relates to conductance or the inverse of resistance as shown in Equation 5.1.

$$\frac{v}{i} = \frac{1}{R} \quad (5.1)$$

A linear regression is applied to the measured data with the resulting equation and correlation  $R^2$  value also shown in Figure 5.1. The inverted slope equates to 47.3 k $\Omega$ . The resistance may appear high, but it does corroborate well with data from other studies with similar materials. One factor causing the high resistance is due to the polyelectrolyte material in the SWNT structure. The coefficient of determination,  $R^2$ , for a linear fit to the data is 0.9693 which shows the data fits to a linear trend very well. The SWNT wire behaves similarly to an ohmic

contact or metal wire. This verifies the SWNT structure could potentially be used as a replacement material for metal contacts in microelectronic devices.

## **5.2 Raman Characterization**

When a sample is irradiated with light, light is scattered. Most of the scattered light is elastically scattered. Elastically scattered light contains the same energy as the incident light and therefore has the same wavelength and frequency. Some of the scattered light is inelastically scattered. The inelastic scattering causes a change in energy level and a shift in the wavelength and frequency from the incident light. The inelastic scattered light is termed Raman scattering. Raman spectroscopy studies this specific scattering in a sample. Raman scattering can be caused by vibration or rotation energies of a sample, although vibration energies are typically those studied by Raman [104]. In SWNTs, the C-C bond is detected with Raman spectroscopy by a peak in the Raman shift range of  $1520 - 1600 \text{ cm}^{-1}$  [105].

When Raman spectroscopy is used on a crystalline source, the Raman scatter will be polarized because all of the vibrations will be symmetric. Using this knowledge, several studies have used polarized Raman spectroscopy to determine the orientation of SWNTs [106-108]. Polarized Raman can be utilized in different modes HH, VV, HV, or VH. In HH mode, both the incident and scattered light are horizontal to the sample. In VV mode, both the incident and scattered light are vertical to the sample. In HV mode, the incident light is horizontal while the scattered light is vertical to the sample. In VH mode, the incident light is vertical while the scattered light is horizontal to the sample. The samples in this study

were characterized with Raman in HH, VV, and HV modes. Only three of the four modes is needed to determine orientation in any direction [108].

### **5.2.1 Equipment List**

Raman spectroscopy equipment is not available at the I/M, so the samples in this study were sent to Viktor Hadjiev at the Texas Center for Superconductivity at the University of Houston (T<sub>c</sub>SUH) for analysis. The samples were studied with a Horiba Jobin Yvon T6400 Raman spectrometer.

### **5.2.2 Results**

The samples are first characterized with Raman spectroscopy to verify the material gives the characteristic peaks of SWNTs at 1520 – 1600 cm<sup>-1</sup>. The resulting graph is shown below in Figure 5.2.

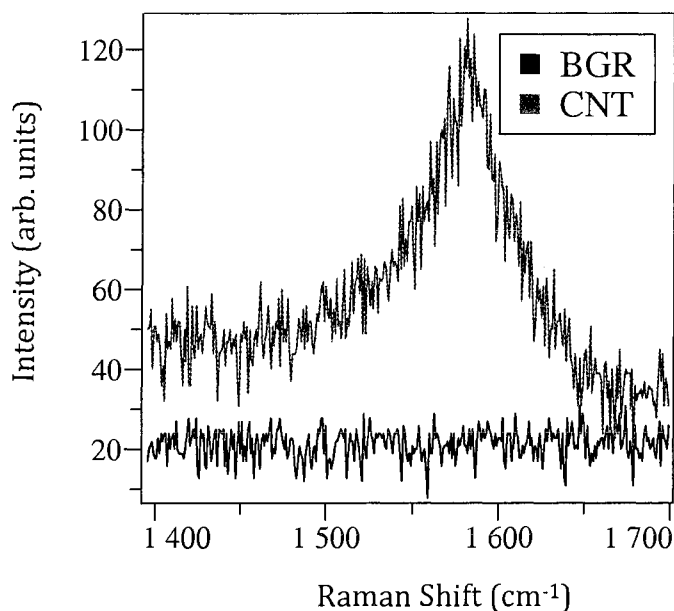


Figure 5.2: Raman Spectroscopy of SWNT Sample

The green line shows the Raman spectra from the sample with the characteristic peaks for SWNTs. The red line shows the background noise scattering from the substrate and PSS material. This verifies the SWNTs in the structure will give the expected Raman scatter.

In order to determine if the SWNTs are oriented in a specific direction, Raman spectroscopy is performed over the entire SWNT structure in polarized mode. Each mode will test a different orientation. If there are SWNTs oriented in the tested orientation, the spectra will have a peak. A map can be created by collecting the intensity of the spectra at multiple points in the structure like a 2D array. An intensity map is made of the entire SWNT structure in HH, VV, and HV modes. Those maps are overlaid with an optical image of the same structure and shown below in Figure 5.3.

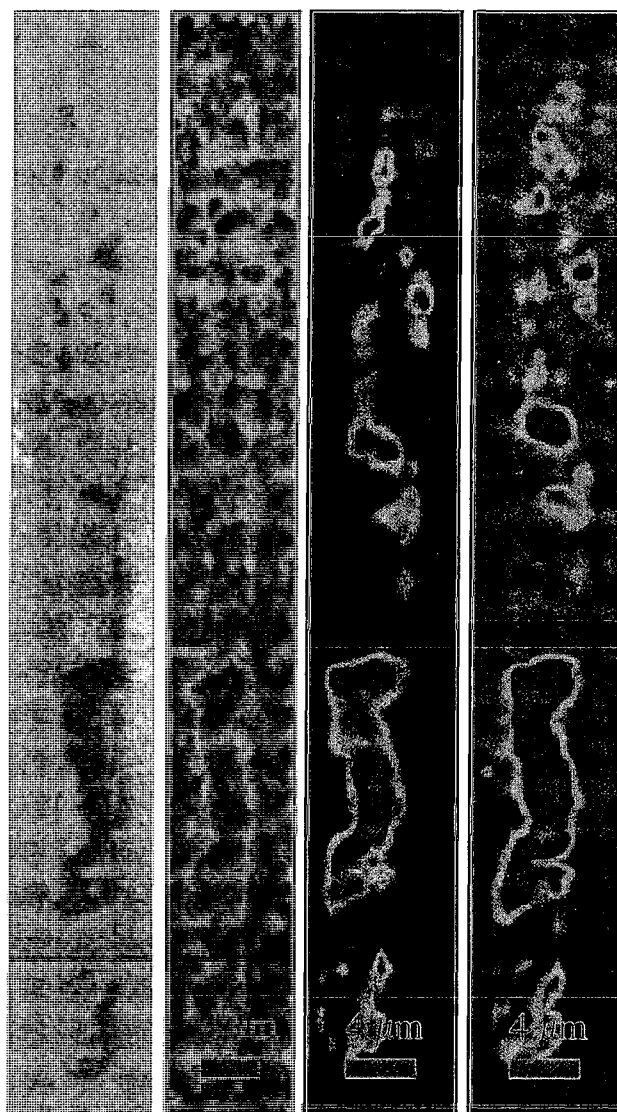


Figure 5.3: Optical and Raman Images Left to Right HV, VV, HH Mode

The Raman spectroscopy of each mode resulted in a map of similar intensity. These results show there are SWNTs oriented in all directions equally. There is no specific direction of orientation in our SWNT structures.

### **5.3 Conclusion**

Although our SWNT structures did not display any specific orientation, they did show electrical characteristics that show their potential for microelectronic devices. The measured resistance for the SWNT structure was higher than currently used metal contacts in semiconductor devices. Some suggestions for improving the conductivity of the SWNT structure will be given in the next chapter. The high current densities possible with SWNTs should keep the conductivity of the SWNT structures high as the structure size is reduced to the nano scale. The purpose of this study was to develop a fabrication methodology that can be used to incorporate SWNTs into microelectronic devices. The IV characterization verified the SWNTs behave as ohmic contacts, the desired behavior for metal contacts in a microelectronic device.

## CHAPTER 6

### CONCLUSIONS AND FUTURE WORK SUGGESTIONS

#### 6.1 Research Conclusion

CNTs have been one of the most exciting and studied discoveries of the early 90s. Their unique shape, size, and properties make them ideal for a wide variety of uses and applications. Companies, universities, and national laboratories across the globe have invested incredible amounts of time and money towards understanding CNTs and trying to figure out how best to apply their unique characteristics to solve problems of today. One field sticks out from the rest when looking at the possible applications for CNTs, microelectronic devices. CNTs, specifically SWNTs, have electrical characteristics that cannot be found in other materials on the same scale. The high current densities show great potential for nano scaled electrical contacts. Semiconducting SWNTs show the promise of one day being able to fabricate single molecule transistors. This study has detailed the current state of CNT technology. Both manufacturing and direct manipulation methodologies were reviewed. Synthesis methods were compared and found to be inadequate for directly incorporating into current semiconductor manufacturing. Direct manipulation failed to scale for mass manufacturing. A new methodology for fabricating SWNT structures utilizing SWNTs in suspension was proposed and

studied. SWNTs were suspended in an aqueous solution using lbl self-assembly. Polyelectrolytes PSS and PAH were self-assembled onto the sidewalls of individual SWNTs to disperse. Because the suspension uses lbl, the polyelectrolytes are non-covalently bonded so the process can be completely reversed. Using the suspension of SWNT+PSS, SWNT structures were fabricated on a  $\mu\text{m}$  scales using the same technology and principle tooling as current semiconductor manufacturing. The shape and location of the SWNT structures could be precisely controlled on a Si wafer. The SWNT structures were then characterized with IV measurements and Raman spectroscopy. IV characterization revealed the SWNT structures behave as ohmic contacts with a resistance of 47.3 k $\Omega$ . The Raman spectroscopy showed the SWNTs in the SWNT structure were randomly oriented.

## **6.2 Future Suggestions**

No work can ever be exhaustive and cover all possibilities. The results from this study are very promising and hopeful. However, there is always striving to improve and better the obtained results. After delving into the world of CNTs and completing this study, the author has several recommendations for future improvement on the fabrication and characterization of these SWNT structures.

### **6.2.1 Fabrication**

The fabrication results were very promising, building SWNT structures of the desired shape at the desired locations. However, the trenches were not completely filled with SWNTs. Completely filled structures are necessary for future application. There are a few options to try in future work.

1. Coat the trenches and possibly the surface of the substrate with a very hydrophilic material such as  $\text{TiO}_2$ . This would reduce the wetting angle and should improve the deposition of SWNTs into the desired structures.
2. Repeat the spin coating and evaporation of SWNT solution. Adding extra opportunities for SWNTs to be deposited into the desired structures should increase the fill rate.
3. Add a thickening agent to the SWNT suspension. A thicker suspension would spin coat more evenly over the surface of the substrate, allowing a better coating of SWNTs. However, the thickening agent added could not hinder the electrical characteristics of the final SWNT structure.
4. Perform an image analysis before the lift-off stage to compare with the SWNTs in the trench afterwards. This will help determine how much of the empty trenches were filled and removed during lift-off compared to how many of the empty trenches were never filled.

### **6.2.2 Heat treatment**

The conductivity of the SWNT structures fabricated was not as high as pure SWNTs due to the polymers added from the suspension. If the polyelectrolytes are removed from the structures, the electrical characteristics should improve. The easiest way to remove the polymers from the structures is to burn them off. Polyelectrolytes melt and the SWNTs are stable even at very high temperatures. A heat treatment was referenced in this study where the conductivity of a SWNT thin film with PDDA was improved from 0.045 mS (22.2 k $\Omega$ ) to 2.29 mS (437  $\Omega$ ) when

heated to 300° C [17]. Applying a similar heat treatment to SWNT structures fabricated with spin coating would be an interesting study.

### **6.2.3 Raman Spectroscopy**

Another factor that affects the electrical conductivity of the fabricated SWNT structures is the makeup of SWNTs in the structure. Purchased SWNTs were used; however, there was no characterization on the purchased SWNTs determining what percentage of the SWNTs were metallic vs semiconducting. If the majority of the SWNTs used in the fabrication of these structures were semiconducting, replacing the SWNTs with metallic SWNTs would dramatically improve the conductivity. Raman spectroscopy could be utilized to determine what type of SWNTs compose the SWNT structures.

### **6.2.4 Three or Four Probe Measurements**

The measurement used to characterize the SWNTs was a two probe technique to plot current vs voltage. This method is an accurate methodology to create an IV curve for a desired element. However, the length of the structure being analyzed affects the final graph. In the same way, a long wire will have a higher resistance compared to a short one. To get a better material characteristic, a three or four probe technique can be used to get the conductivity of the material rather than the conductance of the structure. This data would be more useful for comparing between different materials and structures.

## REFERENCES

- [1] S. Iijima, "Helical microtubules of graphitic carbon," *Nature*, vol. 354, no. 6348, pp. 56-58, 1991.
- [2] NEC. "Tests Verify Carbon Nanotube Enable Ultra High Performance Transistor," 2/23/2009; <http://www.nec.co.jp/press/en/0309/1901.html>.
- [3] J. C. Miller, and D. L. Harris, "Carbon Nanotube Patent Landscape, The," *Nanotechnology Law & Business*, vol. 3, pp. 427, 2006.
- [4] P. Harris, *Carbon Nanotubes and Related Structures*, New York: Cambridge, 1999.
- [5] P. M. Ajayan, "Nanotubes from Carbon," *Chem Rev*, vol. 99, no. 7, pp. 1787-1800, 1999.
- [6] J. Kong, H. T. Soh, A. M. Cassell, C. F. Quate, and H. Dai, "Synthesis of individual single-walled carbon nanotubes on patterned silicon wafers," *Nature*, vol. 395, no. 6705, pp. 878-881, 1998.
- [7] M. S. Dresselhaus, G. Dresselhaus, and P. C. Eklund, *Science of Fullerenes and Carbon Nanotubes*, San Diego: Academic Press, 1996.
- [8] J. W. G. Wildoer, L. C. Venema, A. G. Rinzler, R. E. Smalley, and C. Dekker, "Electronic structure of atomically resolved carbon nanotubes," *Nature*, vol. 391, no. 6662, pp. 59-62, 1998.
- [9] P. L. McEuen, "Single-wall carbon nanotubes," *Physics World*, vol. 13, no. 6, pp. 31-36, 2000.
- [10] J. Kong, C. Zhou, A. Morpurgo, H. T. Soh, C. F. Quate, C. Marcus, and H. Dai, "Synthesis, integration, and electrical properties of individual single-walled carbon nanotubes," *Applied Physics A: Materials Science and Processing*, vol. 69, no. 3, pp. 305-308, 1999.
- [11] A. J. Hart, B. O. Boskovic, A. T. H. Chuang, V. B. Golovko, J. Robertson, B. F. G. Johnson, and A. H. Slocum, "Uniform and selective CVD growth of carbon nanotubes and nanofibres on arbitrarily microstructured silicon surfaces," *Nanotechnology*, vol. 17, no. 5, pp. 1397-1403, 2006.

- [12] R. Martel, T. Schmidt, H. R. Shea, T. Hertel, and P. Avouris, "Single-and multi-wall carbon nanotube field-effect transistors," *Applied Physics Letters*, vol. 73, pp. 2447, 1998.
- [13] A. Rochefort, and P. Avouris, "Electron interference effects on the conductance of doped carbon nanotubes," *Journal of Physical Chemistry A*, vol. 104, no. 44, pp. 9807-9811, 2000.
- [14] P. G. Collins, M. S. Arnold, and P. Avouris, "Engineering carbon nanotubes and nanotube circuits using electrical breakdown," *Science*, vol. 292, no. 5517, pp. 706-709, 2001.
- [15] M. Palumbo, K. U. Lee, B. T. Ahn, A. Suri, K. S. Coleman, D. Zeze, D. Wood, C. Pearson, and M. C. Petty, "Electrical investigations of layer-by-layer films of carbon nanotubes," *Journal of Physics D-Applied Physics*, vol. 39, no. 14, pp. 3077, 2006.
- [16] J. H. Rouse, and P. T. Lillehei, "Electrostatic assembly of polymer/single walled carbon nanotube multilayer films," *Nano Letters*, vol. 3, no. 1, pp. 59-62, 2003.
- [17] W. Xue, and T. Cui, "Characterization of layer-by-layer self-assembled carbon nanotube multilayer thin films," *Nanotechnology*, vol. 18, no. 14, pp. 145709, 2007.
- [18] Intel. "Intel Demonstrates Industry's First 32nm Chip and Next-Generation Nehalem Microprocessor Architecture," 3/2/2008; [http://www.intel.com/pressroom/archive/releases/20070918corp\\_a.htm](http://www.intel.com/pressroom/archive/releases/20070918corp_a.htm).
- [19] E. Stern, G. Cheng, J. F. Klemic, E. Broomfield, D. Turner-Evans, C. Li, C. Zhou, and M. A. Reed, "Methods for fabricating Ohmic contacts to nanowires and nanotubes," *Journal of Vacuum Science & Technology B: Microelectronics and Nanometer Structures*, vol. 24, pp. 231, 2006.
- [20] H. T. Soh, C. F. Quate, A. F. Morpurgo, C. M. Marcus, J. Kong, and H. Dai, "Integrated nanotube circuits: Controlled growth and ohmic contacting of single-walled carbon nanotubes," *Applied Physics Letters*, vol. 75, no. 5, pp. 627-629, 1999.
- [21] P. Avouris, T. Hertel, R. Martel, T. Schmidt, H. R. Shea, and R. E. Walkup, "Carbon nanotubes: Nanomechanics, manipulation, and electronic devices," *Applied Surface Science*, vol. 141, no. 3-4, pp. 201-209, 1999.
- [22] M. H. Yang, K. B. K. Teo, W. I. Milne, and D. G. Hasko, "Carbon nanotube Schottky diode and directionally dependent field-effect transistor using asymmetrical contacts," *Applied Physics Letters*, vol. 87, pp. 253116, 2005.

- [23] Z. Chen, J. Appenzeller, J. Knoch, Y. Lin, and P. Avouris, "The role of metal-nanotube contact in the performance of carbon nanotube field-effect transistors," *Nano Letters*, vol. 5, no. 7, pp. 1497-1502, 2005.
- [24] Z. Chen, W. Hu, J. Guo, and K. Saito, "Fabrication of nanoelectrodes based on controlled placement of carbon nanotubes using alternating-current electric field," *Journal of Vacuum Science & Technology B: Microelectronics and Nanometer Structures*, vol. 22, pp. 776, 2004.
- [25] A. P. Graham, G. S. Duesberg, R. Seidel, M. Liebau, E. Unger, F. Kreupl, and W. Honlein, "Towards the integration of carbon nanotubes in microelectronics," *Diamond and Related Materials*, vol. 13, no. 4-8, pp. 1296-1300, 2004.
- [26] Y. F. Hsiou, Y. J. Yang, L. Stobinski, W. Kuo, and C. D. Chen, "Controlled placement and electrical contact properties of individual multiwalled carbon nanotubes on patterned silicon chips," *Applied Physics Letters*, vol. 84, pp. 984, 2004.
- [27] W. Steinhögl, G. Schindler, G. Steinlesberger, and M. Engelhardt, "Size-dependent resistivity of metallic wires in the mesoscopic range," *Int. J. Mod. Phys. B Phys Rev B*, vol. 66, pp. 075414, 1989.
- [28] M. Olek, J. Ostrander, S. Jurga, H. Mohwald, N. Kotov, K. Kempa, and M. Giersig, "Layer-by-layer assembled composites from multiwall carbon nanotubes with different morphologies," *Nano Letters*, vol. 4, no. 10, pp. 1889-1895, 2004.
- [29] A. A. Mamedov, N. A. Kotov, M. Prato, D. M. Guldi, J. P. Wicksted, and A. Hirsch, "Molecular design of strong single-wall carbon nanotube/polyelectrolyte multilayer composites," *Nature Materials*, vol. 1, no. 3, pp. 190-194, 2002.
- [30] H. Kong, P. Luo, C. Gao, and D. Yan, "Polyelectrolyte-functionalized multiwalled carbon nanotubes: preparation, characterization and layer-by-layer self-assembly," *Polymer*, vol. 46, no. 8, pp. 2472-2485, 2005.
- [31] M. Sato, and M. Sano, "van der Waals layer-by-layer construction of a carbon nanotube 2D network," *Langmuir*, vol. 21, no. 24, pp. 11490-11494, 2005.
- [32] H. Paloniemi, M. Lukkarinen, T. Aaritalo, S. Areva, J. Leiro, M. Heinonen, K. Haapakka, and J. Lukkari, "Layer-by-layer electrostatic self-assembly of single-wall carbon nanotube polyelectrolytes," *Langmuir*, vol. 22, no. 1, pp. 74-83, 2006.
- [33] B. I. Yakobson, M. P. Campbell, C. J. Brabec, and J. Bernholc, "High strain rate fracture and C-chain unraveling in carbon nanotubes," *Computational Materials Science*, vol. 8, no. 4, pp. 341-348, 1997.

- [34] Z. Jin, K. P. Pramoda, G. Xu, and S. H. Goh, "Dynamic mechanical behavior of melt-processed multi-walled carbon nanotube/poly (methyl methacrylate) composites," *Chemical Physics Letters*, vol. 337, no. 1-3, pp. 43-47, 2001.
- [35] M. F. Yu, O. Lourie, M. J. Dyer, K. Moloni, T. F. Kelly, and R. S. Ruoff, "Strength and breaking mechanism of multiwalled carbon nanotubes under tensile load," *Science*, vol. 287, no. 5453, pp. 637, 2000.
- [36] M. S. Dresselhaus, *Carbon nanotubes: synthesis, structure, properties, and applications*: Springer, 2001.
- [37] W. A. De Heer, A. Chatelain, and D. Ugarte, "A carbon nanotube field-emission electron source," *Science*, vol. 270, no. 5239, pp. 1179, 1995.
- [38] S. Fan, M. G. Chapline, N. R. Franklin, T. W. Tomblor, A. M. Cassell, and H. Dai, "Self-oriented regular arrays of carbon nanotubes and their field emission properties," *Science*, vol. 283, no. 5401, pp. 512, 1999.
- [39] G. Che, B. B. Lakshmi, E. R. Fisher, and C. R. Martin, "Carbon nanotubule membranes for electrochemical energy storage and production," *Nature*, vol. 393, no. 6683, pp. 346-349, 1998.
- [40] S. M. Lee, and Y. H. Lee, "Hydrogen storage in single-walled carbon nanotubes," *Applied Physics Letters*, vol. 76, pp. 2877, 2000.
- [41] C. Liu, Y. Y. Fan, M. Liu, H. T. Cong, H. M. Cheng, and M. S. Dresselhaus, "Hydrogen storage in single-walled carbon nanotubes at room temperature," *Science*, vol. 286, no. 5442, pp. 1127, 1999.
- [42] R. Martel, T. Schmidt, H. R. Shea, T. Hertel, and P. Avouris, "Single- and multi-wall carbon nanotube field-effect transistors," *Applied Physics Letters*, vol. 73, no. 17, pp. 2447, 1998.
- [43] A. Rubio, D. Sanchez-Portal, E. Artacho, P. Ordejon, and J. M. Soler, "Electronic states in a finite carbon nanotube: A one-dimensional quantum box," *Physical Review Letters*, vol. 82, no. 17, pp. 3520-3523, 1999.
- [44] A. Bachtold, P. Hadley, T. Nakanishi, and C. Dekker, "Logic Circuits with Carbon Nanotube Transistors," 5545, 2001, pp. 1317-1320.
- [45] A. Rochefort, M. Di Ventra, and P. Avouris, "Switching behavior of semiconducting carbon nanotubes under an external electric field," *Applied Physics Letters*, vol. 78, no. 17, pp. 2521, 2001.
- [46] T. W. Ebbesen, and P. M. Ajayan, "Large-scale synthesis of carbon nanotubes," *Nature*, vol. 358, no. 6383, pp. 220-222, 1992.

- [47] S. Iijima, and T. Ichihashi, "Single-shell carbon nanotubes of 1-nm diameter," *Nature* 363, vol. 603, pp. 605, 1993.
- [48] D. S. Bethune, C. H. Kiang, M. S. De Vries, G. Gorman, R. Savoy, J. Vazquez, and R. Beyers, "Cobalt-catalysed growth of carbon nanotubes with single-atomic-layer walls," *Nature*, vol. 363, no. 6430, pp. 605-607, 1993.
- [49] M. Yu, M. J. Dyer, G. D. Skidmore, H. W. Rohrs, X. Lu, K. D. Ausman, J. R. Von Ehr, and R. S. Ruoff, "Three-dimensional manipulation of carbon nanotubes under a scanning electron microscope," *Nanotechnology*, vol. 10, no. 3, pp. 244-252, 1999.
- [50] E. G. Gamaly, and T. W. Ebbesen, "Mechanism of carbon nanotube formation in the arc discharge," *Mater. Sci. Eng. B Phys Rev B*, vol. 52, pp. 2083, 1993.
- [51] C. Journet, W. K. Maser, P. Bernier, A. Loiseau, M. L. de la Chapelle, S. Lefrant, P. Deniard, R. Lee, and J. E. Fischer, "Large-scale production of single-walled carbon nanotubes by the electric-arc technique," *Nature*, vol. 388, no. 6644, pp. 756-758, 1997.
- [52] J. Liu, A. G. Rinzler, H. Dai, J. H. Hafner, R. K. Bradley, P. J. Boul, A. Lu, T. Iverson, K. Shelimov, and C. B. Huffman, "Fullerene pipes," *Science*, vol. 280, no. 5367, pp. 1253, 1998.
- [53] A. Thess, R. Lee, P. Nikolaev, H. Dai, P. Petit, J. Robert, C. Xu, Y. H. Lee, S. G. Kim, and A. G. Rinzler, "Crystalline ropes of metallic carbon nanotubes," *Science*, vol. 273, no. 5274, pp. 483, 1996.
- [54] C. Ducati, I. Alexandrou, M. Chhowalla, G. A. J. Amaratunga, and J. Robertson, "Temperature selective growth of carbon nanotubes by chemical vapor deposition," *Journal of Applied Physics*, vol. 92, no. 6, pp. 3299, 2002.
- [55] S. Hofmann, B. Kleinsorge, C. Ducati, A. C. Ferrari, and J. Robertson, "Low-temperature plasma enhanced chemical vapour deposition of carbon nanotubes," *Diamond and Related Materials*, vol. 13, no. 4-8, pp. 1171-1176, 2004.
- [56] N. R. Franklin, Y. Li, R. J. Chen, A. Javey, and H. Dai, "Patterned growth of single-walled carbon nanotubes on full 4-inch wafers," *Applied Physics Letters*, vol. 79, no. 27, pp. 4571, 2001.
- [57] J. Cheng, X. Zhang, Z. Luo, F. Liu, Y. Ye, W. Yin, W. Liu, and Y. Han, "Carbon nanotube synthesis and parametric study using CaCO<sub>3</sub> nanocrystals as catalyst support by CVD," *Materials Chemistry and Physics*, vol. 95, no. 1, pp. 5-11, 2006.

- [58] Y. Kobayashi, H. Nakashima, D. Takagi, and Y. Homma, "CVD growth of single-walled carbon nanotubes using size-controlled nanoparticle catalyst," *Thin Solid Films*, vol. 464-465, pp. 286-289, 2004.
- [59] T. Kato, G. H. Jeong, T. Hirata, and R. Hatakeyama, "Structure control of carbon nanotubes using radio-frequency plasma enhanced chemical vapor deposition," *Thin Solid Films*, vol. 457, pp. 2-6.
- [60] J. Liu, X. Li, A. Schrand, T. Ohashi, and L. Dai, "Controlled Syntheses of Aligned Multi-Walled Carbon Nanotubes: Catalyst Particle Size and Density Control via Layer-by-Layer Assembling," *Chemistry of Materials*, vol. 17, no. 26, pp. 6599-6604, 2005.
- [61] B. Zheng, Y. Li, and J. Liu, "CVD synthesis and purification of single-walled carbon nanotubes on aerogel-supported catalyst," *Applied Physics A: Materials Science and Processing*, vol. 74, no. 3, pp. 345-348, 2002.
- [62] R. T. K. Baker, P. S. Harris, R. B. Thomas, and R. J. Waite, "Nucleation and growth of carbon deposits from the nickel catalyzed decomposition of acetylene.," *Journal of Catalysis*, vol. 26, no. 1, pp. 51-62, July, 1972.
- [63] A. Oberlin, M. Endo, and T. Koyama, "Filamentous growth of carbon through benzene decomposition.," *Journal of Crystal Growth*, vol. 32, no. 3, pp. 335-349, March, 1976.
- [64] P. A. Tesner, E. Y. Robinovich, I. S. Rafalkes, and E. F. Arefieva, "Formation of carbon fibers from acetylene," vol. 8, no. 4, pp. 435-42, 1970.
- [65] G. G. Tibbetts, "Why are carbon filaments tubular?," *Journal of Crystal Growth* vol. 66, no. 3, pp. 632-638, May, 1984.
- [66] M. Su, B. Zheng, and J. Liu, "A scalable CVD method for the synthesis of single-walled carbon nanotubes with high catalyst productivity" *Chemical Physics Letters*, vol. 322, no. 5, pp. 321-326, May, 2000.
- [67] Z. Y. Juang, I. P. Chien, J. F. Lai, T. S. Lai, and C. H. Tsai, "The effects of ammonia on the growth of large-scale patterned aligned carbon nanotubes using thermal chemical vapor deposition method," *Diamond and Related Materials*, vol. 13, no. 4-8, pp. 1203-1209, 2004.
- [68] S. Li, Z. Yu, G. Gadde, P. J. Burke, and W. C. Tang, "Carbon nanotube growth for GHz devices," vol. 1, pp. 256-258 vol.2.
- [69] Z. Y. Juang, J. F. Lai, C. H. Weng, J. H. Lee, H. J. Lai, T. S. Lai, and C. H. Tsai, "On the kinetics of carbon nanotube growth by thermal CVD method," *Diamond and Related Materials*, vol. 13, pp. 2140-2146, 2004.

- [70] NEC. "NEC Concludes First Carbon Nanotube Patent License Agreement in U.S. with Southwest NanoTechnologies, Inc.," 3/09/2009; <http://www.nec.co.jp/press/en/0608/0301.html>.
- [71] M. Lundstrom, "APPLIED PHYSICS: Enhanced: Moore's Law Forever?," *Science*, vol. 299, no. 5604, pp. 210-211, January 10, 2003, 2003.
- [72] L. Peters, "Making a Carbon Nanotube Ring Oscillator," *Semiconductor International*, vol. 29, no. 9, pp. 57-60, 2006.
- [73] T. Hertel, R. Martel, and P. Avouris, "Manipulation of individual carbon nanotubes and their interaction with surfaces," *Journal of Physical Chemistry B*, vol. 102, no. 6, pp. 910-915, 1998.
- [74] S. J. Tans, M. H. Devoret, H. Dai, A. Thess, R. E. Smalley, L. J. Geerligs, and C. Dekker, "Individual single-wall carbon nanotubes as quantum wires," *Nature*, vol. 386, no. 6624, pp. 474-477, 1997.
- [75] S. J. Tans, M. H. Devoret, R. J. A. Groeneveld, and C. Dekker, "Electron-electron correlations in carbon nanotubes," *Nature*, vol. 394, no. 6695, pp. 761-764, 1998.
- [76] S. J. Tans, A. R. M. Verschueren, and C. Dekker, "Room-temperature transistor based on a single carbon nanotube," *Nature*, vol. 393, no. 6680, pp. 49-52, 1998.
- [77] K. Bubke, H. Gnewuch, M. Hempstead, J. Hammer, and M. L. H. Green, "Optical anisotropy of dispersed carbon nanotubes induced by an electric field," *Applied physics letters*, vol. 71, pp. 1906, 1997.
- [78] K. Yamamoto, S. Akita, and Y. Nakayama, "Orientation and purification of carbon nanotubes using ac electrophoresis," *Journal of Physics D-Applied Physics*, vol. 31, no. 8, pp. 34, 1998.
- [79] Y. Zhang, A. Chang, J. Cao, Q. Wang, W. Kim, Y. Li, N. Morris, E. Yenilmez, J. Kong, and H. Dai, "Electric-field-directed growth of aligned single-walled carbon nanotubes," *Applied physics letters*, vol. 79, pp. 3155, 2001.
- [80] X. Q. Chen, T. Saito, H. Yamada, and K. Matsushige, "Aligning single-wall carbon nanotubes with an alternating-current electric field," *Applied physics letters*, vol. 78, pp. 3714, 2001.
- [81] M. Dipasquale, F. Gatti, D. Ricci, D. Caviglia, and E. Di Zitti, "Assembly of carbon nanotubes onto arrays of microfabricated test patterns for the design of nanoelectronic devices," vol., pp. 550-552.

- [82] Y. Lvov, K. Ariga, I. Ichinose, and T. Kunitake, "Assembly of multicomponent protein films by means of electrostatic layer-by-layer adsorption," *J. Am. Chem. Soc.*, vol. 117, no. 22, pp. 6117-6123, 1995.
- [83] R. B. Dhullipudi, T. A. Dobbins, S. R. Adiddela, Z. Zheng, R. A. Gunasekaran, Y. M. Lvov, and R. Tittsworth, "Noncovalent Functionalization of Single Walled Carbon Nanotubes Using Alternate Layer-By-Layer Polyelectrolyte Adsorption for Nanocomposite Fuel Cell Electrodes," *Materials Research Society Symposium Proceedings* vol. 837, p. 109.
- [84] M. Zhang, Y. Yan, K. Gong, L. Mao, Z. Guo, and Y. Chen, "Electrostatic Layer-by-Layer Assembled Carbon Nanotube Multilayer Film and Its Electrocatalytic Activity for O<sub>2</sub> Reduction," *Langmuir*, vol. 20, no. 20, pp. 8781-8785, 2004.
- [85] J. Liu, M. J. Casavant, M. Cox, D. A. Walters, P. Boul, W. Lu, A. J. Rimerberg, K. A. Smith, D. T. Colbert, and R. E. Smalley, "Controlled deposition of individual single-walled carbon nanotubes on chemically functionalized templates," *Chemical Physics Letters*, vol. 303, no. 1-2, pp. 125-129, 1999.
- [86] Y. Wang, D. MasPOCH, S. Zou, G. C. Schatz, R. E. Smalley, and C. A. Mirkin, "Controlling the shape, orientation, and linkage of carbon nanotube features with nano affinity templates," *Proceedings of the National Academy of Sciences*, vol. 103, no. 7, pp. 2026-2031, 2006.
- [87] L. H. Dubois, and R. G. Nuzzo, "Synthesis, structure, and properties of model organic surfaces," *Annual review of physical chemistry*, vol. 43, no. 1, pp. 437-463, 1992.
- [88] I. D. Rosca, F. Watari, M. Uo, and T. Akasaka, "Oxidation of multiwalled carbon nanotubes by nitric acid," *Carbon*, vol. 43, no. 15, pp. 3124-3131, 2005.
- [89] M. A. Chappell, A. J. George, K. M. Dontsova, B. E. Porter, C. L. Price, P. Zhou, E. Morikawa, A. J. Kennedy, and J. A. Steevens, "Surfactive stabilization of multi-walled carbon nanotube dispersions with dissolved humic substances," *Environmental Pollution*, 2008.
- [90] M. Bratcher, B. Gersten, H. Ji, and J. Mays, "Study in the dispersion of carbon nanotubes," vol. 706, pp. 323-330.
- [91] M. F. Islam, E. Rojas, D. M. Bergey, A. T. Johnson, and A. G. Yodh, "High weight fraction surfactant solubilization of single-wall carbon nanotubes in water," *Nano Letters*, vol. 3, no. 2, pp. 269, 2003.
- [92] V. C. Moore, M. S. Strano, E. H. Haroz, R. H. Hauge, R. E. Smalley, J. Schmidt, and Y. Talmon, "Individually suspended single-walled carbon nanotubes in various surfactants," *Nano Letters*, vol. 3, no. 10, pp. 1379-1382, 2003.

- [93] C. A. Dyke, and J. M. Tour, "Unbundled and highly functionalized carbon nanotubes from aqueous reactions," *Nano Letters*, vol. 3, no. 9, pp. 1215-1218, 2003.
- [94] Y. F. Zhu, Z. Chan, J. D. Wang, S. Lei, and L. Ji, "Influence of electric field on dispersion of carbon nanotubes in liquids," *Journal of dispersion science and technology*, vol. 27, no. 3, pp. 371-375, 2006.
- [95] Z. Yue-Feng, Z. Chan, W. Jing-Dong, S. Lei, and L. Ji, "Influence of Electric Field on Dispersion of Carbon Nanotubes in Liquids," *Journal of Dispersion Science and Technology*, vol. 27, no. 3, pp. 371 - 375, 2006.
- [96] R. Chevious, and T. A. Dobbins, "Aqueous Suspension of Single-walled Carbon Nanotubes using Polystyrene sulfonate Surfactant," *Louisiana Annual Conference*, 2005.
- [97] A. Kuznetsova, I. Popova, J. T. Yates, M. J. Bronikowski, C. B. Huffman, J. Liu, R. E. Smalley, H. H. Hwu, and J. G. Chen, "Oxygen-containing functional groups on single-wall carbon nanotubes: NEXAFS and vibrational spectroscopic studies," *Journal of the American Chemical Society*, vol. 123, no. 43, pp. 10699-10704, 2001.
- [98] P. Hummel, and T. A. Dobbins, "NEXAFS Study of HNO<sub>3</sub> and HCl Acid Treatment for Micromanufacturing-Friendly Functionalization of CNTs," *Louisiana Annual Conference*, 2005.
- [99] S. Banerjee, T. Hemraj-Benny, S. Sambasivan, D. A. Fischer, J. A. Misewich, and S. S. Wong, "Near-Edge X-ray Absorption Fine Structure Investigations of Order in Carbon Nanotube-Based Systems†," *J. Phys. Chem. B*, vol. 109, no. 17, pp. 8489-8495, 2005.
- [100] S. Banerjee, T. Hemraj-Benny, M. Balasubramanian, D. A. Fischer, J. A. Misewich, and S. S. Wong, "Ozonized single-walled carbon nanotubes investigated using NEXAFS spectroscopy," *Chemical Communications*, vol. 2004, no. 7, pp. 772-773, 2004.
- [101] A. G. Rinzler, J. Liu, H. Dai, P. Nikolaev, C. B. Huffman, F. J. Rodriguez-Macias, P. J. Boul, A. H. Lu, D. Heymann, and D. T. Colbert, "Large-scale purification of single-wall carbon nanotubes: process, product, and characterization," *Applied Physics A: Materials Science & Processing*, vol. 67, no. 1, pp. 29-37, 1998.
- [102] M. LaPedus, "More gloom: iSuppli cuts IC forecast," *EE Times*, <http://www.eetimes.com/showArticle.jhtml?articleID=212501066>, [4/12/09, 2008].

- [103] P. Hummel, and T. A. Dobbins, "Controlled Placement of Single-walled Carbon Nanotubes by Spin Coating into Photoresist Cavities," *MRS Fall*, 2007.
- [104] B. Schrader, D. Bougeard, and W. InterScience, *Infrared and Raman spectroscopy: methods and applications*: VCH Weinheim, 1995.
- [105] M. S. Dresselhaus, and P. C. Eklund, "Phonons in carbon nanotubes," *Advances in Physics*, vol. 49, no. 6, pp. 705-814, 2000.
- [106] V. G. Hadjiev, S. Arepalli, P. Nikolaev, S. Jandl, and L. Yowell, "Enhanced Raman microprobe imaging of single-wall carbon nanotubes," *nanotechnology*, vol. 15, no. 5, pp. 562-567, 2004.
- [107] T. Chatterjee, C. A. Mitchell, V. G. Hadjiev, and R. Krishnamoorti, "Hierarchical polymer-nanotube composites," *Advanced Materials*, vol. 19, no. 22, pp. 3850, 2007.
- [108] T. Liu, and S. Kumar, "Quantitative characterization of SWNT orientation by polarized Raman spectroscopy," *Chemical Physics Letters*, vol. 378, no. 3-4, pp. 257-262, 2003.